TIRF and its application to protein adsorption

Electrostatics and Orientation

Promotor: dr. J. Lyklema,
hoogleraar in de Fysische en Kolloïdchemie

Co-promotor: dr.ir. J.M. Kleijn, universitair docent
bij de vakgroep Fysische en Kolloïdchemie

M.A. Bos

TIRF and its application to protein adsorption

Electrostatics and Orientation

Proefschrift
ter verkrijging van de graad van doctor
in de landbouw- en milieuwetenschappen
op gezag van de rector magnificus,
dr. C.M. Karssen,
in het openbaar te verdedigen
op woensdag 1 juni 1994
des namiddags te vier uur in de Aula
van de Landbouwuniversiteit te Wageningen.

CIP DATA KONINKLIJKE BIBLIOTHEEK, DEN HAAG

Bos, M.A.

TIRF and its application to protein adsorption :
Electrostatics and Orientation / M.A. Bos. -
[S.l. : s.n.]
Thesis Wageningen. - With ref. - With summary in Dutch.
ISBN 90-5485-255-0
Subject headings: protein adsorption / TIRF /
colloid chemistry.

Chapter 5 accepted for publication in Colloids and Surfaces B: Biointerfaces

Stellingen

(1)

In tegenstelling tot hetgeen Margalit en Vasquez beweren, is de Totale Interne Reflectie Fluorescentie (TIRF) techniek wel degelijk geschikt om conformatie en oriëntatie van eiwitten aan vaste oppervlakken te bestuderen.

Margalit, R., and Vasquez, R.P., **1990**, *J. Protein Chem.*, 9, 105-108

Hlady, V., and Andrade, J.D., **1989**, *Colloids Surfaces*, 42, 85-96

Dit proefschrift.

(2)

Bij het kwalitatief meten van geadsorbeerde hoeveelheden met TIRF wordt in het algemeen ten onrechte geen rekening gehouden met de oriëntatie van de geadsorbeerde moleculen.

Dit proefschrift.

(3)

Het aanpassingsvermogen van eiwitten op een veranderende omgeving tijdens het adsorptieproces wordt bij de interpretatie van adsorptieresultaten veelal onderschat.

Dit proefschrift, hfdst 5.

(4)

De ene Martin Bos is de andere niet.

(5)

Volgens de definitie die de IUPAC geeft van een polymeer is een *gedenatureerd* eiwit wel een polymeer.

IUPAC, *Pure Appl. Chem.*, **1974**, 40, 479

vgl. C.M. Wijmans (1994) proefschrift LUW, stelling 9

(6)

Er zijn drie condities met betrekking tot de werkomgeving om tot een goed proefschrift te komen, te weten; wetenschappelijke kwaliteit, een goede infrastructuur en een goede werksfeer, waarvan de volgorde niet noodzakelijkerwijs de hierboven weergegevene behoeft te zijn.

(7)

In het kader van het Onderzoeksprogramma Biosensoren zijn AIO-onderzoeksprojecten gehonoreerd met een fundamenteel-wetenschappelijke doelstelling. Het is daarom merkwaardig dat de verlengingsaanvragen voor de laatste twee jaar werden beoordeeld door de Stichting Technische Wetenschappen op grond van utilisatie-aspecten.

(8)

Een vergaande integratie van de alternatieve geneeswijzen en de moderne geneeskunst zal menig patient ten goede komen.

(9)

Het onbezoldigd aanstellen van vrouwelijke AIO's is in strijd met de doelstelling van het emancipatiebeleid van de Landbouwuniversiteit.

(10)

Kunst is een wetenschap. Wetenschap is een vorm van kunst.

Stellingen behorende bij het proefschrift "TIRF and its application to protein adsorption. Electrostatics and Orientation" van Martin Bos, Landbouwuniversiteit Wageningen, 1 juni 1994.

Voorwoord

Na vier jaar hard werken en doorzetten kan ik nu eindelijk zeggen *het is af !* Ik ben zelf zeer content met het proefschrift zoals dat nu voor U ligt. Het is echter niet door mij alleen tot stand gekomen. Velen hebben een bijdrage aan dit proefschrift geleverd. Een aantal personen wil ik in het bijzonder vernoemen.

Allereerst mijn co-promotor. Beste Mieke, jouw inspiratie, vakkennis, ondersteuning en gezelligheid heeft mij zeer geholpen tijdens mijn promotie onderzoek. Vooral de manier waarop je, ondanks de bevalling van een tweeling, mijn manuscripten hebt gecorrigeerd, heeft op mij een diepe indruk achtergelaten. Bedankt en ik wens je alle succes toe in je verdere wetenschappelijke carrière. Beste Hans, ik wil jouw bedanken voor de vrijheid waarin ik mijn onderzoek kon uitvoeren. Vooral jouw overzicht en de kritische commentaren bij de verschillende hoofdstukken kwamen goed van pas. Ik wens je veel succes met de afronding van deel twee van FICS.

Willem Norde en Herman van Leeuwen wil ik bedanken voor de ondersteuning vanuit hun vakgebied welke heeft bijgedragen aan mijn boekje.

Het werk van de doctoraalstudenten Luc Schlangen, Laetitia Ingen Housz, Annelore de Nijs en Thekla Werkhoven heeft ook een belangrijke bijdrage aan het onderzoek geleverd. Ik vond het zeer plezierig om met jullie samen te werken ondanks de moeilijke vragen waar ik soms niet direct een antwoord op kon bedenken.

I am grateful to Hideo Matsumura, Zameer Shervani and Alphonso Anusiem for collaborating with them in different research projects performed in our department. They gave me a different view on the Dutch culture.

Erna Rouwendal wil ik bedanken voor de vele adsorptie isothermen en de voltammetrie experimenten die ze heeft uitgevoerd en Marcel Giesbers voor de reflectometer experimenten die hij gemeten heeft.

De adviezen van Arie van Hoek waren een goede hulp bij het aanschaffen van de optische apparatuur.

De mensen van de fijn mechanische werkplaats, Henny van Beek, Louis Verhagen en Aardt van Wijk, zullen wel vaak gedacht hebben "*daar heb je hem ook weer*" als ik weer eens kwam om een cel of iets anders te laten maken. Gelukkig waren de problemen vakkundig en snel opgelost.

Ramun Kho (Akzo Arnhem) wil ik bedanken voor zijn wiskundige bijdrage ter verkrijging van de orientatie distributies en de leden van de gebruikerscommissie van de STW voor het meedenken aan het project.

Ik hoop dat de kamergenoten van de laatste jaren, Jaap Dijt en Remco Fokkink, mijn aanwezigheid net zo prettig hebben ervaren als ik hun aanwezigheid. Niet alleen het flipperen maar ook de dagelijkse gang van zaken en de discussies zorgden voor een gezellige en prettige omgeving om in te werken. In dit licht moet ik ook de mensen van het secretariaat noemen. Het gelach dat regelmatig door hun deur sijpelde (en nog sijpelt) is daar een voorbeeld van. Daarnaast hebben ze ook voor de minder leuke dingen een oor, ondanks hun drukke werkzaamheden. Josie Zeevat, Yvonne Toussaint, Wil Kleijne en Bert Bouman; ga zo door !

De grafische aspecten van dit proefschrift zijn door Gert Buurman op een uiterst nauwkeurige wijze uitgewerkt. Zijn kijk op optiek is dan ook op de omslag te zien. Gert bedankt voor je hulp en het leuke idee.

Zonder mijn ouders was ik er niet geweest en was dit proefschrift nooit verschenen.

Anja voor jouw was het schrijven van mijn proefschrift niet altijd even gemakkelijk. Een humeurige Martin was niet altijd te genieten en bovendien kwam ik niet altijd aan de huishoudelijke taken toe. Je bent voor mij een grote steun geweest, ook al heb ik dat niet altijd laten blijken. Beschouw dit boekje dan ook een beetje het jouwe.

Ik hoop dat sommige mensen van de vakgroep zich niet tekort voelen gedaan door hun hier niet met naam te noemen. Echter voor mij is de manier waarop wij met z'n allen de vakgroep vormen en met elkaar omgaan een voorbeeld voor hoe het in elke werkkring zou moeten. Hieronder vallen ook de "vergaderingen", de weddenschappen, de feestjes, het volleyballen en ga zo maar door. Deze laatste vijf jaar zal ik niet gauw vergeten.

Bedankt allemaal.

Martin

CONTENTS

Chapter 1

Introduction

1.1. General Introduction

Exposure of an aqueous protein solution to a solid surface often results in accumulation of protein molecules at the solid-liquid interface. The tendency of proteins to spontaneously adsorb is important for many disciplines, including medical sciences, biomedical engineering, biotechnology and life sciences. Applications of protein adsorption involve immobilisation of enzymes, protein separation, stabilization of dispersions like emulsions, lotions and foams, fouling of equipment and corporal devices, immunoassays and biosensors.

Protein adsorption can be undesirable. Examples of this are the thrombus development on cardiovascular implant materials [Vroman and Leonard, 1991; Willems *et al.*, 1991], plaque formation on teeth [White, 1991], and fouling of heat exchangers, membranes, ship hulls, food processing units, etc. [Norde and Lyklema, 1991]. In other cases protein adsorption is beneficial and can/must be controlled. Development of drug delivery systems and biosensors for in vivo monitoring of glucose in blood, and the use of proteins in immunoassays and diagnostic tests are examples involving controlled protein adsorption [Rechnitz, 1988; Yamasaki *et al.*, 1989].

One result of the research on protein adsorption was the development of new, in situ, experimental techniques. These new techniques (among which ellipsometry, infrared reflection spectroscopy, calorimetry, circular dichroism spectroscopy, Raman spectroscopy and fluorescence spectroscopy) gave information on the kinetics of protein adsorption, the conformations and the activities of adsorbed proteins. Over the past years special attention has been given to the orientation of adsorbed protein molecules, especially in ways to determine the orientation of adsorbed protein molecules by developing new methods and/or techniques [Kozarac *et al.*, 1988; Margalit and Vasquez, 1990; Fraaije *et al.*, 1990; Pachence *et al.*, 1990; Reipa *et al.*, 1993]. In this thesis it is tried to measure the orientation of adsorbed protein molecules with the optical technique Total Internal

Reflection Fluorescence (TIRF). Therefore it is necessary to explain what protein conformations are, what the process of adsorption determines, why it is important to know the orientation of adsorbed protein molecules and how we try to obtain the orientation of adsorbed protein molecules.

1.2. Protein structure

Protein molecules are natural polymers of circa twenty different amino acids which are linked to each other to form a linear polypeptide chain. Two of the three bonds in a peptide unit are free to rotate; the C-N bond is fixed due to its partial double bond character (see figure 1.1). The number of possible conformations of a polypeptide chain, the combinations between ϕ and ψ allowed, can be represented in a so-called Ramachandran plot [Ramachandran and Sasisekharan, 1968].

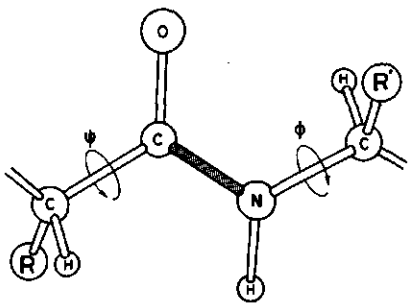

Figure 1.1. *Structure of a peptide unit in a polymer chain. Two (ψ and ϕ) of the three bonds are free to rotate; the other one is fixed. R and R' represent amino acid side groups [Norde and Lyklema, 1991].*

The amino acid side groups can be uncharged, acidic or basic resulting in the amphoteric character of proteins. Furthermore, the side groups vary in polarity. Some of them are hydrophobic, others are hydrophilic. Proteins are complex structures, made up of one or more polypeptide chains. The sequence of the amino acids in the polypeptide chain is called the *primary* structure [Creighton, 1983]. The *secondary* structure is concerned with orderly twists or bends in the polypeptide backbone, recurring in one dimension as α-helices or β-sheets. The way in which these twists or bends fold together in space and the way the side groups arrange themselves in space is called the *tertiary* structure. *Quartenary* structure is present only when a protein consists of more than one polypeptide chain, as it is related

to interchain interactions. The combined secondary, tertiary and quartenary structure is called the conformation of a protein. Globular proteins adopt their native conformation spontaneously under physiological conditions, resulting in high packing densities. The most relevant inter- and intramolecular interactions determining the conformation of a protein molecule in solution are [Tanford, 1961; Creighton, 1983; Andrade, 1985; Norde, 1986]:

electrostatic interactions: coulombic interactions in which the charged side groups of the polypeptide chain (mostly present at the exterior of the molecule) and ions are involved (in the interior of the protein molecule the charges tend to be compensated); dipolar interactions involving parts of the protein molecule (e.g. the peptide bonds have a dipolar character) and water molecules.

hydrogen bonds involving groups of the protein molecule and water molecules;

hydrophobic interactions resulting in a tendency to bury the hydrophobic residues in the interior of the protein molecule, so that they are shielded from the water;

covalent binding between two cysteine amino acids forming a disulphide linkage.

Altering the environment of a protein molecule might induce conformational changes due to the fact that the inter- and intramolecular interactions are affected. Offering a surface onto which the protein can adsorb also belongs to this category.

1.3. Protein adsorption

1.3.1. Fundamentals

The tendency of proteins to accumulate at interfaces is determined by many variables among which the pH, ionic strength, temperature, the properties of the protein molecules, the nature of the solvent and other molecules and ions in the medium. Whatever the mechanism (and kinetics) of protein adsorption are, the process will occur only if the Gibbs energy G of the system decreases:

$$\Delta_{ads}G = \Delta_{ads}H - T\Delta_{ads}S < 0 \qquad (1.1)$$

where H, S and T refer to the enthalpy, entropy and absolute temperature and Δ_{ads} indicates the change of the thermodynamic function of state resulting from the adsorption process.

The process is complicated, involving 1) transport of the protein molecules toward the surface, 2) attachment at the surface, 3) structure rearrangements in the adsorbed protein layer and the outer sorbent layer, 4) detachment from the surface and 5) transport away from the surface. In figure 1.2 these five sub-processes are presented schematically.

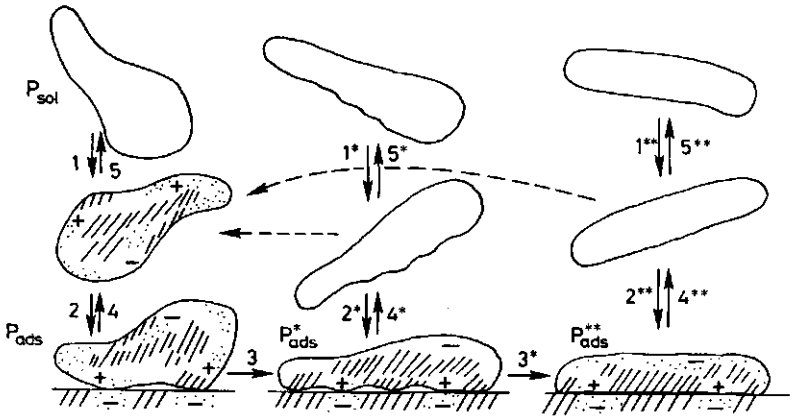

Figure 1.2. *A schematic representation of the adsorption process as described by Norde [1992]. For explanation of the numbers see the text.*

The process is determined by a delicate balance of interactions between protein molecules and the adsorbent, which are different for various classes of proteins. Over the past 20 years it became clear that these interactions can be categorized as follows [Norde, 1986; Shirahama *et al.*, 1990; Arai and Norde, 1990a; Norde *et al.*, 1991]:

1. *Electrostatic interactions*

Electrostatic interactions are mainly due to the electrostatic attraction or repulsion between protein and the interface. The charge of the protein is the result of the dissociation of amino acids on the periphery of the molecule and might be homogeneously or non-homogeneously distributed over the protein molecule. Any inhomogeneous charge distribution, leading to a dipole moment, can also contribute to the electrostatic interaction. Furthermore, ion incorporation into the adsorption layer plays a role

because it leads to screening of the electrostatic interactions [Fraaije *et al.*, 1991a,b,c].

2. *Hydrophobic interactions*

Dehydration of hydrophobic patches of both the protein and the sorbent surface promotes protein adsorption. Through dehydration a large number of water molecules gain entropy because they are no longer "bound" to the protein or the surface. The more hydrophobic the surface, the higher the promotion of protein adsorption. The adsorption affinity and the adsorbed amounts also depend on the hydrophobicity of the protein. This interaction is very important and often overrules the other interactions.

3. *Structural stability*

The conformation of a globular protein molecule in solution is dominated by the hydrophobic interactions in the interior of the molecule over the intra-molecular electrostatic repulsion in the periphery of the molecule and the loss of entropy upon folding. In the presence of a surface the interior of the protein molecule can prevent itself from hydration in an alternative way: exposing its hydrophobic interior to the surface by unfolding. This unfolding will be promoted by stronger electrostatic repulsion between the charges on the surface of the adsorbed protein. Unfolding of the adsorbed protein will increase the surface area occupied by the protein and the entropy of the protein and will lower the electrostatic repulsion between like charges in the adsorbed protein. The degree of unfolding at the surface also depends on the characteristics of the sorbent; a hydrophobic surface promotes unfolding, whereas a hydrophilic surface inhibits it.

Although all three sorts of interactions generally play a role in the adsorption process, for each individual protein the contributions of each of these interactions to the adsorption process can be different. Recently, a kind of "classification" was introduced in terms of the structural stability of the protein molecules, the so-called "hard" and "soft" proteins [Arai and Norde, 1990a,b; Norde *et al.*, 1991]. For the "hard" proteins the structural changes upon adsorption are negligible and the driving forces for adsorption are the dehydration of hydrophobic interfaces and electrostatic interactions. These proteins adsorb on all hydrophobic surfaces irrespective of the charge of the surface and do not adsorb on hydrophilic surfaces unless there is electrostatic attraction. In contrast, "soft" proteins unfold partially upon adsorption. They tend to adsorb on all surfaces irrespective of the electrostatic interactions between the surface and the protein, due to a gain in conformational entropy during adsorption.

1.3.2. Techniques used for studying protein adsorption

When protein adsorption takes place it takes a certain time before the adsorbed amount and the protein concentration in solution reach their equilibrium values (figure 1.3a). The kinetics of adsorption is an important subject of many protein adsorption studies, for instance when competition between proteins is studied [Lundström and Elwing, 1991; Arai and Norde, 1990b; Norde *et al.*, 1991; Elgersma *et al.*, 1991]. When the equilibrium adsorption values are determined as a function of the equilibrium protein concentration in solution an adsorption isotherm is obtained. Measurement of an adsorption isotherm is the starting point of most protein adsorption studies. By measuring adsorption isotherms under several experimental conditions one tries to determine which of the in section 1.3.1 mentioned interactions play a role in the adsorption process. The adsorption isotherm depends on the experimental conditions such as the pH, the ionic strength, the charge of the adsorbent surface and on the nature of the protein and gives information on the affinity of the protein for the surface. If the initial slope is steep, the isotherm is called "high affinity".

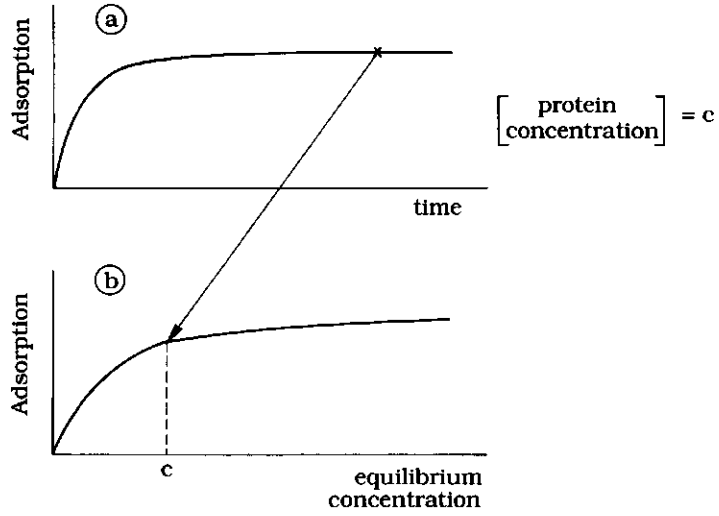

Figure 1.3. a) *The adsorption for a protein with concentration c followed in time.* ***b)*** *The amount adsorbed as a function of the equilibrium concentration.*

At high concentrations the adsorbed amount often reaches a plateau value, called Γ_{plat}. Then the surface is saturated with protein molecules. The plateau value depends on the experimental conditions mentioned above, the

conformation of the adsorbed molecules, the affinity of the proteins for the surface and the surface coverage-dependent lateral interactions. The shape of the protein adsorption isotherm is often described in terms of an a Langmuir gas adsorption isotherm, but for most proteins the irreversibility of protein adsorption against dilution shows that one of the premises for the applicability of the Langmuir isotherm equation is not fulfilled.

Over the past decades technology has provided new experimental and theoretical strategies for studying protein adsorption. Research on the kinetics of protein adsorption has motivated the development of a number of in situ methods for determining rates of adsorption and adsorbed amounts; examples include reflection infrared spectroscopy [Brash, 1969; Lee, 1974], ellipsometry [Vroman, 1969; Elwing *et al.*, 1987a,b], streaming potential measurements [Norde and Rouwendal, 1991], reflectometry [Norde *et al.*, 1991; Norde and Anusiem, 1992] and Total Internal Reflection Fluorescence [Burghardt and Axelrod, 1983; Hlady *et al.*, 1985; Gölander *et* al., 1990]. Experiments to determine conformations and activities of adsorbed proteins have involved applications of nuclear magnetic resonance [Cantor and Schimmel, 1980; Wüthrich, 1986], Raman and infrared spectroscopy [Cantor and Schimmel, 1980], fluorescent probes [Hlady, 1989], calorimetry [Norde, 1985] and transmission circulair dichroïsm (CD) [Norde *et al.*, 1986; Norde and Favier, 1992; Kondo *et al.*, 1991]. The latter two techniques give information on the fraction of ordered secondary structure (α-helix and β-sheet) in a protein. Norde and Favier [1992] found a decrease in α-helix content for lysozyme and bovine serum albumin upon adsorption. The α-helix decrease was shown to increase with decreasing native state stability and with decreasing protein concentration in the bulk. Similar results were obtained by Kondo *et al.* [1991] for the adsorption of albumin on silica particles.

Fluorescence spectroscopy has also provided direct information on the structures of proteins in the adsorbed state. Over the past years, Total Internal Reflection Fluorescence (TIRF) has been used to study conformational changes in adsorbed molecules [Watkins, 1977; Beisinger and Leonard, 1980; Burghardt and Axelrod, 1983]. Van Wagenen *et al.* [1982] found that albumin and γ-globulin undergo significant conformational changes upon adsorption onto hydrophilic glass. The principle of TIRF is that a light beam is totally reflected at an interface between two media 1 and 2 if the refractive index of medium 1, n_1, is higher than the refractive index of medium 2, n_2, and if the angle of incidence θ_i

exceeds the critical angle. Due to interference of the incident and reflected light beam a standing wave is generated in the optical rarer medium. When medium 2 consists of a solution of fluorescent molecules that absorb at the wavelenght of the incident light, the molecules in the evanescent field will fluorescence, especially molecules which are adsorbed. Based on this principle, TIRF has been used in this thesis to obtain information on the orientation of adsorbed molecules.

1.4. Orientation of adsorbed proteins

As many proteins have an extended form (ellipsoidal or globular) the term orientation is often used to refer to the arrangement of a protein molecule with repect to the solid surface or interface. The protein molecule is belonging to the class of "hard" proteins. For example, the orientation of an adsorbed ellipsoidal protein molecule can be with its long axis situated parallel to the surface ("side-on") or normal to the surface ("end-on"). The orientation of adsorbed protein molecules not only determines the amount adsorbed, but also whether or not the active site of the protein molecule, if any, is exposed to the solution. In figure 1.4 adsorbed protein molecules (enzymes, falling into the class of the "hard" proteins) with different orientations are drawn. In the first orientation of the molecule, left hand side of the picture, the active site of the enzymes is oriented to the solution, making it possible for substrates to react. On the right hand side of the picture the same enzymes are drawn with the same molecular conformation but in a complete different orientation. It is clear that in the latter case the substrate molecules cannot attach and start the enzyme reaction.

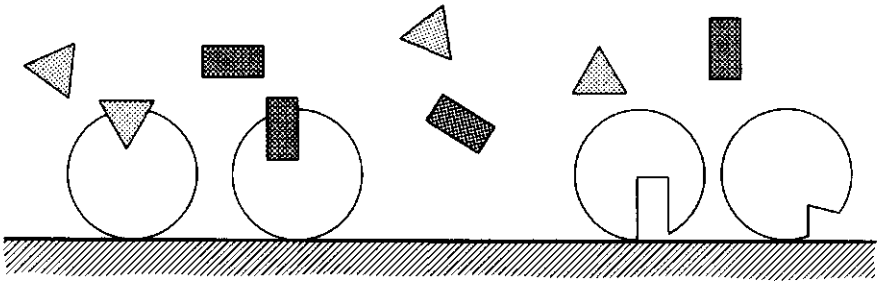

Figure 1.4. *Adsorbed protein molecules having the same conformation but with different orientations (schematic).*

The orientation of adsorbed proteins plays an important role in the effectivity and the development of immunoassays and diagnostic tests. One can imagine that if the orientation of an antibody (or enzyme) is not the right one, no recognition of the antigen (or substrate) occurs. Therefore, either much research is done to develop methods to adsorb antibodies and enzymes in the proper orientation or in ways to steer the adsorption process.

In the development of biosensors knowledge and insight into the adsorption process and the orientation of the adsorbed proteins molecules on inorganic materials play essential roles. A biosensor is a device incorporating a biological sensing element (selector) either intimately connected to or integrated within a transducer. A schematic model of a biosensor is drawn in figure 1.5. The selector part (often consisting of proteins) is responsible for the selectivity and sensitivity of the biosensor. Binding of species from the solution to the selector molecules (molecular recognition) results in a change in a physical or chemical parameter such as refractive index or charge. This change will be converted into an electrical signal by the detector.

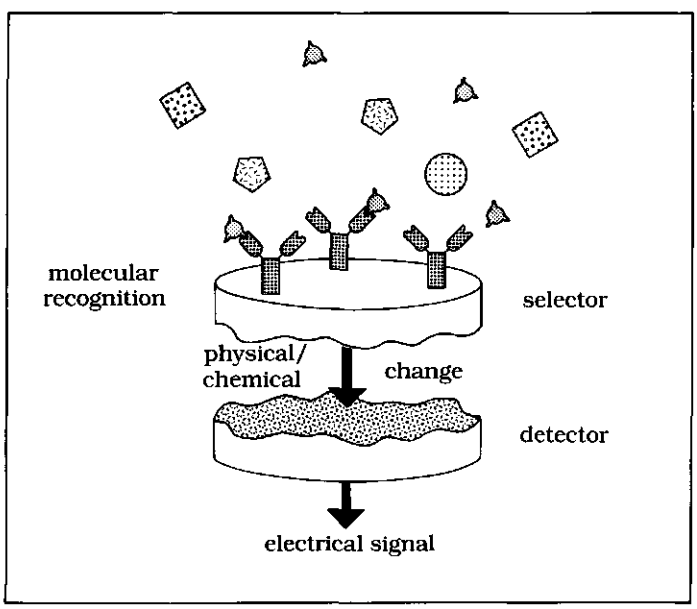

Figure 1.5. *A schematic model of a biosensor.*

If proteins are used as the selector molecules in a biosensor, the adsorbed protein molecules should have the right orientation (see figure 1.4) in order to obtain a high sensitivity and selectivity. But even if proteins are not used as the selector molecules, protein adsorption might still be of importance for the proper functioning of the biosensor device. The substrate to be detected might be a protein, and/or fouling of the biosensor by undesired adsorption of proteins (always present in biological environments) occurs.

Techniques for studying the orientation of adsorbed molecules are attenuated total reflection infrared spectroscopy, X-ray Photoelectron Spectroscopy, Total Internal Reflection Fluorescence (TIRF) and atomic force microscopy. Margalit and Vasquez [1990] used X-Ray Photoelectron Spectroscopy for studying the orientation of adsorbed protein on aluminium and indium tinoxide surfaces. They have found that a myoglobin derivative (a penta-amineruthenium group was attached to a specific histidine) is preferentially oriented along the Ru-Fe axis of the myoglobin with the Ru the furthest away from the substrate.

TIRF can provide information on adsorbed molecules. By changing the polarization of the incident light beam it is possible to change the direction of the electrical field vector of the evanescent field. By measuring the fluorescence as a function of the polarization of the incident light beam gives information on the orientation. Thompson *et al.* [1984] used this method for determining the order in supported layers of fluorescent-labelled phospholipids. In 1986 the theory for determining the spatial and orientational distributions of fluorophores with TIRF was described by Thompson and Burghardt [1986]. Fraaije *et al.* [1990] conducted TIRF orientation measurements on adsorbed cytochrome *c* molecules using the haem group (porphyrin ring) as an intrinsic fluorescent label. They made a start to elaborate the theory for a special case: for the porphyrin ring system, where two transition dipole moments are lying perpendicular to one another.

A method developed more recently for studying protein adsorption is Atomic Force Microscopy (AFM). With this technique it is possible to monitor the sorbent surface with its adsorbed molecules, providing information on the structure of the adsorbed layer. Unfortunately, the cantilever tip gives rise to destruction of the adsorbed layer if the applied force is too high, especially when biological systems are observed [Lea *et al.*, 1992]. Furthermore, the resolution of the apparatus is too small to study the

orientation of a single protein molecule. In the near future these problems will be overcome, making AFM a serious candidate for studying the orientation of adsorbed protein molecules.

1.5. Outline of this thesis

The central theme of this thesis is the orientation of adsorbed proteins and how to influence the adsorption process and the orientation of adsorbed proteins by applying an external potential to the sorbent surface.

Until now only average orientation angles or possible combinations of average angles and widths of orientation distributions for adsorbed molecules have been found, due to lack of information from measurements and incomplete theory. Therefore in **chapter 2** of this thesis the theory for orientation measurements with Total Internal Reflection Fluorescence (TIRF) based on the principles described by Thompson and Burghardt [1986] and Fraaije *et al.* [1990] will be extended in general terms and elaborated especially for porphyrin and cytochrome *c* molecules. It will be shown that in order to obtain complete orientation distributions, it is necessary to measure not only the intensity but also the polarization of the fluorescence as a function of the polarization angle of the incident light. Using the Maximum Entropy Method (MEM) the orientation distribution can be reconstructed. In the last section of this chapter the influence of the rotational mobility of the adsorbed molecules on the orientation measurements is evaluated.

In **chapter 3** the experimental techniques used in this thesis will be discussed. In the first section of this chapter the set-up, the flow cell and the data handling of the TIRF measurements will be explained. In the second section the set-up of the optical technique reflectometry and reflectivity calculations made for the solution/indium tinoxide/silicon layer system will be explained. Finally, the method of applying potentials at the sorbent surface will be discussed and some relevant characteristics of the indium tinoxide films will be presented.

Chapter 4 presents a study of the adsorption behaviour of tetramethylpyridinium porphyrin (H_2TMPyP) on silica. It will be shown that it is possible to obtain the orientation distribution of adsorbed molecules with TIRF and that the orientation of adsorbed tetramethylpyridinium porphyrin molecules depends on the solution concentration.

In **chapter 5** the adsorption behaviour of various proteins as a function of an externally imposed interfacial potential is the subject of study. On the basis of the results the relative importance of electrostatic interactions in the process of protein adsorption will be discussed.

Experiments concerning the adsorption behaviour of native and porphyrin cytochrome *c* molecules are described and discussed in **chapter 6**. The orientation of adsorbed porphyrin cytochrome *c* molecules, the influence of an applied potential and the structural stability of the protein will be evaluated.

Finally, in **chapter 7** this work is summarized and the most important conclusions and some perspectives of the TIRF method for orientation measurements are given.

Chapter 2

Determination of the orientation distribution of adsorbed chromophores using TIRF

Theory

2.1. Introduction

More than 275 years ago Newton discovered the phenomenon of total internal reflection of light at the interface between glass and vacuum or air. He observed that light falling too oblique on the interface was not travelling from the glass into the optical rarer medium but was totally reflected into the air. His explanation was that the light, if it goes out into the vacuum, is "attracted" back by the optically denser medium. He suggested that the path of the light ray is "a parabola with the vertex in the rarer medium" [Newton, 1717].

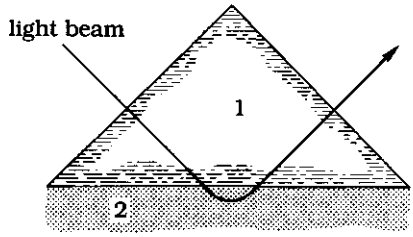

Figure 2.1. *Visualisation of the phenomenon of total internal reflection according to Newton [1717]. The refractive index of medium 1 is larger than that of medium 2.*

We now know that this explanation and picture are incorrect; the light is not propagated in the manner shown. Total internal reflection is (just like refraction) in fact caused by the difference in the speed of light in the two media. Due to interference of the incident and reflected ray a standing wave, normal to the reflecting interface, is established in the denser medium and there is an evanescent non-propagating electromagnetic field in the optical rarer medium (also called the evanescent wave), of which the amplitude decays exponentially with distance from the surface [Harrick, 1965].

In the first half of the twentieth century total internal reflection was utilised in many areas, most of them involving the development of optics and/or optical components. A good review has been given by Harrick [1967]. In the fifties and sixties total internal reflection was used in Internal Reflection Spectroscopy (IRS). IRS is a technique which records the absorption spectrum of sample material that is in contact with an optical denser, but transparent, medium by measuring the wavelength dependence of the reflectivity of the interface by introducing light into the denser medium. At first IRS was used to study surfaces and thin films that play an important role in e.g. catalysis, oxidation and electrode reactions. Another important application of IRS is the measurement of optical constants of dielectrics and metals. As a result of the work with thin films the nature of total internal reflection was better understood and IRS came into general usage. Later, IRS spectra were also obtained from adsorbed protein molecules [Brash, 1969; Lee, 1974]. The amount of adsorbed protein could be determined by measuring the absorption near 1650 cm^{-1} and 1550 cm^{-1}, being the characteristic frequencies of the amide bonds present in all proteins. Unfortunately, water absorbs strongly in this region and therefore had to be excluded from the samples. Recently, a book dealing with IRS has been written by Mirabella [1993].

At the end of the sixties and the beginning of the seventies a new technique based on total internal reflection was developed. This technique exploits the fluorescent properties of adsorbed molecules and is called Total Internal Reflection Fluorescence (TIRF). One of the first people using TIRF to study protein adsorption was Watkins [1977], but it took to the beginning of the eighties before the potential of this technique for studying protein and polymer adsorption was more generally recognised.

In the last ten years many papers dealing with TIRF have been published. They can be classified in four categories by the kind of information obtained. The first category is the adsorption/desorption behaviour of (macro)molecules, especially proteins. As a substrate quartz, [Burghardt, 1981] or polymer surfaces are used [Anderson, 1987; Lok *et al.*, 1982a,b; Hasegawa, 1992; Cheng, 1986]. Also Fluorescence Recovery After Photobleaching (TIRFRAP) experiments in which the molecules are bleached by an evanescent wave, giving information on lateral mobility of adsorbed molecules and exchange with molecules in solution, can be placed in this category [Burghardt, 1981; Thompson, 1981].

Secondly, important information can be obtained from the fluorescence spectra of adsorbed molecules. Differences between the

emission spectra of adsorbed molecules and molecules in solution can result e.g. from changes in the environment of the fluorescent group, from energy transfer between adsorbed neighbours or quenching by surface groups. In this way information on interactions between biological cells on a glass surface was obtained [Gingell *et al.*, 1987]. In case the fluorescent group resides in the interior of the molecule, information on conformational rearrangements can be obtained [Hlady *et al.*, 1985].

A third and an important application of TIRF is the determination of concentration profiles of adsorbed molecules. By gradually decreasing the angle of incidence the penetration depth of the evanescent wave can be increased (see section 2.2), so that fluorophores, situated at longer distances from the surface, will be excited more strongly. Analysis of the fluorescence signal as a function of the angle of incidence gives the concentration profile perpendicular to the surface. This is mainly done for adsorbed flexible polymers making use of fluorescent labels [Allain *et al.*, 1982; Ausseré *et al.*, 1985; Reichert *et al.*, 1987; Caucheteux *et al.*, 1990]. For adsorbed proteins the concentration profile cannot be determined because of the small size of protein molecules: 3-20 nm. The penetration depth depends on the wavelength of the incident light beam and can be varied between 50-200 nm.

Finally, TIRF can provide information on the orientation of adsorbed molecules. By changing the polarization angle of the incident light beam it is possible to change the direction of the electrical field vector of the evanescent field. As a result the interaction between the evanescent field and the absorption transition dipole moment of the molecules is changed. By measuring the fluorescence as a function of the polarization of the incident light beam information on the orientation can be obtained. This method was first used by Thompson *et al.* [1984] to detect the order in supported layers of fluorescent-labelled phospholipids. Two years later a theoretical description for the measurement of spatial and orientational distributions of fluorophores, with one transition dipole moment, near planar dielectric interfaces using TIRF was given [Thompson and Burghardt, 1986]. Fraaije *et al.* [1990] conducted TIRF orientation measurements on adsorbed cytochrome *c* molecules using the haem group (porphyrin ring) as an intrinsic fluorescent label. A start was made to elaborate the theory for this special case: in the porphyrin ring system two transition dipole moments are present perpendicular to one another. Because the theory was still incomplete, until now no orientation distribution functions have been obtained, but only average orientation angles or possible combinations of

average angles and widths of distributions for adsorbed molecules have been found.

In this chapter we will extend the theory for orientation measurements with TIRF based on the principles described by Thompson and Burghardt [1986] and Fraaije *et al.* [1990]. First the evanescent field will be described in some detail, followed by the theory for orientation measurements on adsorbed fluorophores in general terms and applied to the special case of porphyrins. It will be shown for the first time that in order to obtain complete orientation distributions, it is necessary to measure not only the *intensity* of the fluorescence as a function of the polarization angle of the incident light, but also its *polarization*. Using the Maximum Entropy Method (MEM), orientation distribution functions can be reconstructed. In the last section of this chapter the influence of the mobility of the adsorbed molecules on the orientation measurements will be evaluated.

2.2. The evanescent field; principle of TIRF

The phenomenon of total internal reflection is illustrated in figure 2.2. A light beam striking an interface between two media 1 and 2 with refractive indices n_1 and n_2 is totally reflected if $n_1 > n_2$ and if the angle of incidence θ_i exceeds the critical angle, θ_c, defined by $\theta_c = \arcsin(n_2/n_1)$. Due to interference of the incident and reflected light beam a standing wave is generated in the optical rarer medium.

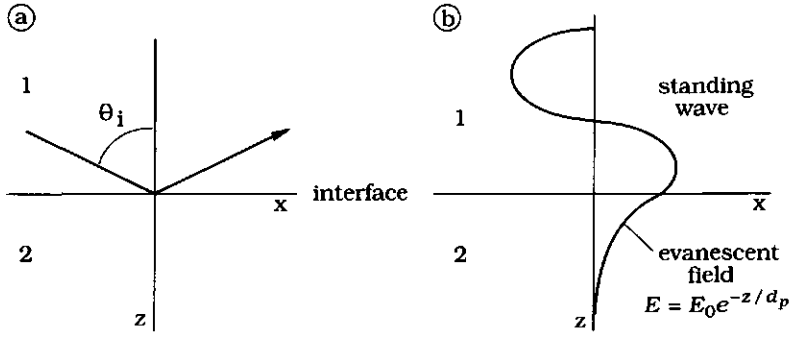

Figure 2.2. a) *An incoming light beam is totally internally reflected at an interface; the optical density of medium 1 higher is than that of medium 2.* ***b)*** *Due to interference, a standing wave is generated giving rise to an evanescent wave in medium 2.*

According to the laws of Maxwell the amplitude of this standing wave cannot abruptly go to zero at the interface [Harrick, 1967]. As a result an electromagnetic field exists in the rarer medium beyond the reflecting interface. This electromagnetic field has the same frequency as the standing wave and is called "evanescent wave". Its electric field amplitude decays exponentially with distance from the surface :

$$E(\Psi) = E_0(\Psi)e^{-z/d_p} \tag{2.1}$$

in which Ψ is the polarization angle of the incident light beam and d_p is called the penetration depth. $E_0(\Psi)$ is the electric field amplitude at the interface (z = 0). The direction of the electrical field vector $\vec{E}$ in the evanescent field is given by the x-, y- and z-components of $\vec{E}_0(\Psi)$:

$$\vec{E}_0(\Psi) = \begin{pmatrix} E_x \\ E_y \\ E_z \end{pmatrix} = \begin{pmatrix} \varepsilon_x \cos\Psi \\ \varepsilon_y \sin\Psi \\ \varepsilon_z \cos\Psi \end{pmatrix} \tag{2.2}$$

with [Harrick, 1967]

$$\varepsilon_x = \frac{2\cos\theta_i \sqrt{\sin^2\theta_i - (n_2/n_1)^2}}{\sqrt{(n_2/n_1)^4\cos^2\theta_i + \sin^2\theta_i - (n_2/n_1)^2}} \tag{2.3a}$$

$$\varepsilon_y = \frac{2\cos\theta_i}{\sqrt{1-(n_2/n_1)^2}} \tag{2.3b}$$

$$\varepsilon_z = \frac{2\cos\theta_i \sin\theta_i}{\sqrt{(n_2/n_1)^4\cos^2\theta_t + \sin^2\theta_i - (n_2/n_1)^2}} \tag{2.3c}$$

From equations (2.2) and (2.3) we can see that the direction of the electric field vector of the evanescent field is dependent on the polarization angle (Ψ) of the incident light beam. Defining the xz-plane as the plane of incidence (see figure 2.2a), ε_y (= $E_\perp$) represents the electric field amplitude of the evanescent field for the TE (transverse electric) polarization mode of the incident beam, in which $\vec{E}$ is perpendicular to the plane of incidence and E_x and E_z are zero. For the TM (transverse magnetic) polarization mode the electric field amplitude is given by $E_{//} = \left(|\varepsilon_x|^2 + |\varepsilon_z|^2\right)^{1/2}$. Now $\vec{E}$ lies in the plane of incidence and E_y is zero.

The penetration depth, defined as the distance over which the electric field amplitude falls off to e^{-1} of its value at the surface, is given by

$$d_p = \frac{\lambda_0}{2\pi n_1 \sqrt{\left(\sin^2 \theta_i - (n_2/n_1)^2\right)}} \tag{2.4}$$

where λ_0 is the wavelenght of the incident light beam in vacuum (≈ air). It is worth mentioning that if the rarer medium is non-absorbing, there is no net flow of energy into the rarer medium.

When medium 2 consists of a solution of fluorescent molecules that absorb at the wavelenght of the incident light, the molecules in the evanescent field will fluoresce. In the case of adsorption and not too high bulk concentrations, most of the fluorescence intensity will be caused by molecules in the adsorption layer. This is the principle of TIRF experiments.

2.3. Determination of the orientation of adsorbed fluorophores

2.3.1. General

Fluorescence from a molecule is a two-photon process. First a photon is absorbed and the molecule undergoes a transition to an excited electronic and possibly a higher vibronic state. Subsequently, the molecule relaxes in a short time $\left(10^{-15} - 10^{-12}\ \mathrm{s}\right)$ to the lowest excited state, from where fluorescence occurs. The fluorescence process takes place in a few nanoseconds [Feynman *et al.*, 1965; Lakowicz, 1983]. Generally, the total fluorescence emitted from a sample depends in a linear way on the absorption intensity. The absorption intensity per molecule is given by

$$A \sim \left\langle \left(\vec{\mu} \cdot \vec{E}\right)^2 \right\rangle \tag{2.5}$$

where $\vec{\mu}$ represents the direction of the absorption transition dipole moment of the molecule, $\vec{E}$ the electric field component of the excitation light and $\langle\ \rangle$ stands for a time average or an ensemble average.

Of the total fluorescence emitted by the sample, only a part is collected into the detector. The detected fluorescence per molecule depends

on the direction of the emission transition dipole moment, represented by $\vec{\upsilon}$, the direction of detection and on the aperture angle of the detection system [Feynman *et al.*, 1965]. In our TIRF-experiments detection is along the *z*-axis, i.e. perpendicular to the interface. If the aperture angle of the detection system is zero, only the projection of $\vec{\upsilon}$ in the *xy*-plane is "observed". Then the collection efficiency f is

$$f(\vec{\upsilon}) \sim \left(\upsilon_x^2 + \upsilon_y^2\right) \tag{2.6}$$

while the collection efficiencies for fluorescence polarized parallelly to the plane of incidence $f_{//}$ and perpendicularly to that plane, $f_{\perp}$, are given by:

$$f_{//} \sim \upsilon_x^2 \quad \text{and} \quad f_{\perp} \sim \upsilon_y^2 \tag{2.6a},$$

respectively. If the aperture angle is non-zero the situation is somewhat different. Then also fluorescence from the *z*-component υ_z of the emission dipole moment $\vec{\upsilon}$ is detected and

$$f(\vec{\upsilon}) \sim \left(\upsilon_x^2 + \upsilon_y^2\right) + (1-\gamma)\upsilon_z^2 \tag{2.7}$$

The parameter γ is the so-called dichroic factor. The relation between γ and the aperture angle of the detection system is given by Burghardt and Thompson [1984]. The "extra" detected fluorescence is equally polarized along the *x*- and *y*-axis [Axelrod, 1979; Burghardt and Thompson, 1984], resulting in the following expressions for $f_{//}$ and $f_{\perp}$:

$$f_{//} \sim \upsilon_x^2 + \tfrac{1}{2}(1-\gamma)\upsilon_z^2 \quad \text{and} \quad f_{\perp} \sim \upsilon_y^2 + \tfrac{1}{2}(1-\gamma)\upsilon_z^2 \tag{2.7a}$$

The total detected fluorescence F can now be written as

$$F(\vec{\mu}, \vec{\upsilon}) = C\left\langle \left(\vec{\mu} \cdot \vec{E}\right)^2 f(\vec{\upsilon}) \right\rangle \tag{2.8}$$

The constant C in equation (2.8) incorporates the magnitudes of the absorption and emission dipole moments, the quantum yield, the surface concentration of fluorophores, the intensity of the evanescent field, and properties of the detection system. The directions of the absorption and

emission dipoles of a molecule, $\vec{\mu}$ and $\vec{\nu}$, depend of course on the orientation Ω of that molecule; $\langle\ \rangle$ denotes an average over all orientations:

$$\langle x \rangle \equiv \int_{\Omega} N(\Omega)\, x\, d\Omega \tag{2.9}$$

with $N(\Omega)$ the normalized orientation distribution function. In the present treatment it is assumed that the orientations of the molecules do not change on the time scale of fluorescence (10^{-9} s). For molecules in solution the rotation diffusion time scale is in the order of 0.1 ns. This time scale will be much lower for molecules which are adsorbed on a surface and therefore this assumption seems to be justified. Another assumption is that energy transfer between the molecules is negligible. To the influence of the mobility of adsorbed molecules we will come back later (section 2.3.4). Furthermore, one should keep in mind that the orientation distribution function of the fluorescent groups only gives information on the orientation of the complete adsorbed molecules if the fluorescent group is firmly anchored in the molecule and if the molecule does not undergo any conformational changes upon adsorption.

The direction of the electric field vector of the evanescent field, $\vec{E}$, can be varied in a simple way by changing the polarization angle Ψ of the incident light beam (see equation (2.2)). Equation (2.8) can be rewritten as

$$F(\Psi) = C \int_{\Omega} N(\Omega) \left(\vec{E}(\Psi) \cdot \vec{\mu}(\Omega) \right)^2 f\left(\vec{\nu}(\Omega)\right)\, d\Omega \tag{2.10}$$

The dependence on the polarization angle Ψ of the incident light has been made explicit to emphasize that by measuring F at different polarization angles a transformation of $N(\Omega)$ into a function of Ψ is obtained. To reconstruct $N(\Omega)$ it is necessary to measure not only the intensity, but also the polarization of the fluorescence (i.e. both $F_{//}(\Psi)$ and $F_{\perp}(\Psi)$). In the next section this will be explained.

2.3.2. Orientation measurements on porphyrins and cytochrome c

For TIRF studies on the adsorption of cytochrome *c* molecules, the haem can be used as an intrinsic fluorescent label, provided that the central Fe atom is removed (or replaced by, e.g., Zn or Sn) [Vanderkooi and

Erecinska, 1975; Vanderkooi *et a l.*, 1976]. As the three-dimensional structure of cytochrome *c* is known in detail from X-ray diffraction studies [Dickerson *et al.*, 1971], the orientation of the haem relative to the remainder of the molecule is known. In chapter 6 we will come back to the subject of structure and structure stability of the protein and of its free base derivate (i.e. the protein without Fe).

In figure 2.3 the structure of the free base porphyrin ring is shown. Contrary to the metal porphyrins, there are distinct *X*- and *Y*- symmetry axes. By definition the molecular *X*-axis passes through the two central protons [Gouterman and Stryer, 1962].

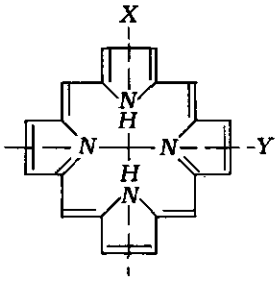

Figure 2.3. *The structure of the free base porphyrin ring with the molecular X- and Y-axis.*

The structure has a characteristic four-banded visible absorption spectrum (see figure 2.4a). *Q*-bands represent absorption along two transition dipole moments oriented in the plane of the ring along the molecular *X*- and *Y*-axes [Gouterman and Stryer, 1962; Vanderkooi and Erecinska, 1975; Vanderkooi *et al.*, 1976].

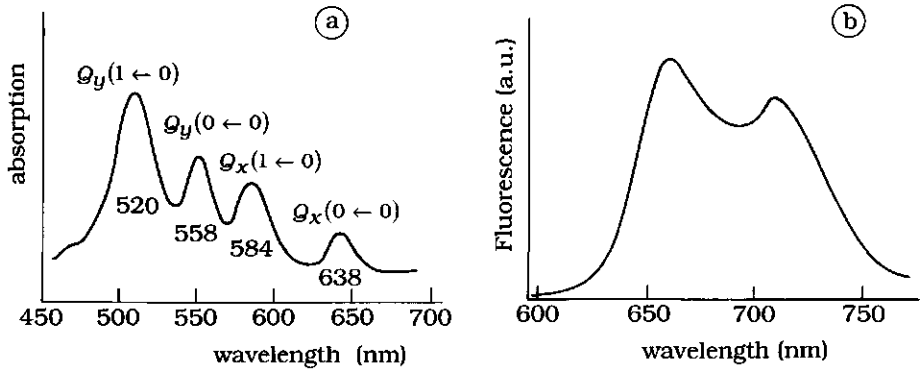

Figure 2.4. a) *Absorption spectrum of a porphyrin ring (H_2TMPyP). The Q-bands stem from excitation along the two transition dipole moments in the plane of the ring, which have a different absorption energy.* ***b)*** *Emission spectrum a porphyrin ring (H_2TMPyP).*

These two transition dipole moments, of which the directions are given by the vectors $\vec{\mu}_x$ and $\vec{\mu}_y$, have a slightly different absorption energy due to the presence of the two protons on opposite pyrrole rings (but the environment of the porphyrin might also play a role). The protons can move over to the other pair of opposite pyrrole rings, resulting in an exchange of the orientations of the molecular *X*- and *Y*-axes, and thus of $\vec{\mu}_x$ and $\vec{\mu}_y$. This tautomeric process (time scale microseconds [Janson and Katz, 1979]) is much slower than the absorption and emission process (time scale nanoseconds [Gouterman and Stryer, 1962; Vanderkooi and Erecinska, 1975]). Emission takes place along two transition dipole moments $\vec{\upsilon}_x$ and $\vec{\upsilon}_y$ parallel to the absorption dipole moments. The emission spectrum is shown in figure 2.4b. The absorption and emission bands are of a composite nature [Gouterman and Stryer, 1962], i.e. depending on the wavelength and band width of the excitation light absorption takes place partly along $\vec{\mu}_x$ and partly along $\vec{\mu}_y$, and depending on the detection wavelength and band width, the detected emission stems partly from $\vec{\upsilon}_x$ and partly from $\vec{\upsilon}_y$.

We now introduce a new orthogonal coordinate system $x'y'z'$ to describe the absorption and emission transition dipole moments in the porphyrin ring system. In this coordinate system the $x'y'$-plane corresponds to the plane in which the transition dipole moments are situated, i.e. the plane of the ring. In figure 2.5 the relation between the new coordinate system $x'y'z'$ and the laboratory coordinate system xyz is shown. In figure 2.5 the absorption and emission dipole moments are in the $x'y'$-plane on the molecular *X*- and *Y*-axis. As mentioned before, the tautomeric process results in a continuing exchange of the orientations of these molecular axes. Therefore the *X*- and *Y*-axis and the transition dipole moments $\vec{\mu}_x$, $\vec{\mu}_y$, $\vec{\upsilon}_x$ and $\vec{\upsilon}_y$ do not have fixed orientations in the molecule. However, we can define two auxiliary vectors $\vec{\xi}$ and $\vec{\eta}$ which do have fixed orientations in the molecule, representing the directions of the molecular axes. It is reasonable to assume that half of the time (or for half of the ensemble of molecules) the direction of the molecular *X*-axis (and of $\vec{\mu}_x$ and $\vec{\upsilon}_x$) is given by $\vec{\xi}$ and the direction of the molecular *Y*-axis (and of $\vec{\mu}_y$ and $\vec{\upsilon}_y$) by $\vec{\eta}$ and for the rest of the time (or for the other half of the ensemble) just the other way around. The directions of $\vec{\xi}$ and $\vec{\eta}$ in the laboratory coordinate system xyz are defined by three orientation angles θ, ϕ and α : θ is the angle between the z'-axis and the z-axis (i.e. the angle between the (normal of the) porphyrin ring and the (normal of the) interface); ϕ is the angle between the x'-axis and the x-axis (the x'-axis is taken parallel to the

interface, i.e. in the xy-plane); α is the angle between $\vec{\xi}$ and the x'-axis, which is equal to the angle between $\vec{\eta}$ and the y'-axis.

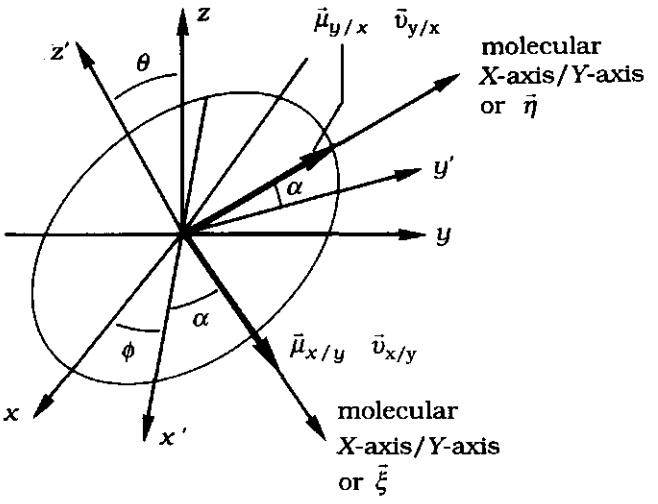

Figure 2.5. *The porphyrin plane in which the transition dipole moments are situated along the molecular X- and Y-axes. Their directions are defined by the three orientation angles α, ϕ, and θ. For explanation see the text.*

This transformation of coordinates results in the following expressions for $\vec{\xi}$ and $\vec{\eta}$ in the laboratory coordinate system :

$$\vec{\xi} = \begin{pmatrix} \cos\phi\cos\alpha - \cos\theta\sin\phi\sin\alpha \\ \sin\phi\cos\alpha + \cos\theta\cos\phi\sin\alpha \\ \sin\theta\sin\alpha \end{pmatrix} \tag{2.11a}$$

$$\vec{\eta} = \begin{pmatrix} -\cos\phi\sin\alpha - \cos\theta\sin\phi\cos\alpha \\ -\sin\phi\sin\alpha + \cos\theta\cos\phi\cos\alpha \\ \sin\theta\cos\alpha \end{pmatrix} \tag{2.11b}$$

The orientation distribution of the porphyrin rings at the interface is given by a function $N(\theta,\phi,\alpha)$, which is normalized so that

$$\int_{\theta=0}^{\pi}\int_{\phi=0}^{2\pi}\int_{\alpha=0}^{2\pi} N(\theta,\phi,\alpha)\sin\theta\, d\alpha\, d\phi\, d\theta = 1 \tag{2.12}$$

As stated before, depending on the wavelength and the band width of excitation in the *Q*-band area of the spectrum, absorption takes place partly along $\vec{\mu}_x$ (this fraction is called r_x) and partly along $\vec{\mu}_y$ (fraction r_y). The detected fluorescence is partly due to emission along $\vec{v}_x$ (fraction q_x) and partly due to emission along $\vec{v}_y$ (fraction q_y). So the measured fluorescence signal consists of four contributions $F(\vec{\mu}_x, \vec{v}_x)$, $F(\vec{\mu}_x, \vec{v}_y)$, $F(\vec{\mu}_y, \vec{v}_x)$ and $F(\vec{\mu}_y, \vec{v}_y)$ with relative intensities $r_x q_x$, $r_x q_y$, $r_y q_x$ and $r_y q_y$, respectively. The expression for the parallelly polarized component of the fluorescence signal $F_{//}$ is

$$F_{//} = r_x q_x F_{//}(\vec{\mu}_x, \vec{v}_x) + r_x q_y F_{//}(\vec{\mu}_x, \vec{v}_y) + r_y q_x F_{//}(\vec{\mu}_y, \vec{v}_x) + r_y q_y F_{//}(\vec{\mu}_y, \vec{v}_y) \tag{2.13}$$

in which, in line with equation (2.8) :

$$F_{//}(\vec{\mu}_x, \vec{v}_x) = C\left\langle (\vec{\mu}_x \cdot \vec{E})^2 f_{//}(\vec{v}_x) \right\rangle \tag{2.14a}$$

$$F_{//}(\vec{\mu}_y, \vec{v}_x) = C\left\langle (\vec{\mu}_y \cdot \vec{E})^2 f_{//}(\vec{v}_x) \right\rangle \tag{2.14b}$$

$$F_{//}(\vec{\mu}_x, \vec{v}_y) = C\left\langle (\vec{\mu}_x \cdot \vec{E})^2 f_{//}(\vec{v}_y) \right\rangle \tag{2.14c}$$

$$F_{//}(\vec{\mu}_y, \vec{v}_y) = C\left\langle (\vec{\mu}_y \cdot \vec{E})^2 f_{//}(\vec{v}_y) \right\rangle \tag{2.14d}$$

By taking for all four contributions to $F_{//}$ the same proportionality constant *C*, we implicitely assume that the magnitudes of the absorption dipole moments along the molecular *X*-axis and *Y*-axis are equal and also that the magnitudes of the emission dipole moments $\vec{v}_x$ and $\vec{v}_y$ are the same. Because of the distinct *X*-*Y* symmetry in the porphyrin ring this is not entirely true. Furthermore, an asymmetric environment of the porphyrin ring, like in cytochrome *c*, in which the porphyrin ring is situated at one side of the molecule, might result in larger differences in the magnitudes of the transition dipole moments. (In fact, then the magnitude of each individual transition dipole moment will also depend on the tautomeric form in which the porphyrin exists at a particular moment.) However, from the fact that the absorption bands as well as the emission bands in the spectra of free base porphyrins and free base cytochrome *c* have a composite character [Gouterman an Stryer, 1962; Vanderkooi and Erecinska, 1975] it can be concluded that the differences in magnitude between $\vec{\mu}_x$ and $\vec{\mu}_y$, and

also between $\vec{v}_x$ and $\vec{v}_y$ are small: otherwise mixing would not occur. Making use of the reasonable assumption that for half of the ensemble $\vec{\mu}_x = \vec{v}_x = \vec{\xi}$ and $\vec{\mu}_y = \vec{v}_y = \vec{\eta}$, and for the other half of the molecules $\vec{\mu}_x = \vec{v}_x = \vec{\eta}$ and $\vec{\mu}_y = \vec{v}_y = \vec{\xi}$, we can write:

$$F_{//}(\vec{\mu},\vec{v}) = \frac{1}{2}\left\{r_x q_x F_{//}\left(\vec{\xi},\vec{\xi}\right) + r_x q_y F_{//}\left(\vec{\xi},\vec{\eta}\right) + r_y q_x F_{//}\left(\vec{\eta},\vec{\xi}\right) + r_y q_y F_{//}(\vec{\eta},\vec{\eta})\right\} + \frac{1}{2}\left\{r_x q_x F_{//}(\vec{\eta},\vec{\eta}) + r_x q_y F_{//}\left(\vec{\eta},\vec{\xi}\right) + r_y q_x F_{//}\left(\vec{\xi},\vec{\eta}\right) + r_y q_y F_{//}\left(\vec{\xi},\vec{\xi}\right)\right\}$$

or simply:

$$F_{//} = \frac{1}{2}\left\{\left(r_x q_x + r_y q_y\right)\left[F_{//}\left(\vec{\xi},\vec{\xi}\right) + F_{//}(\vec{\eta},\vec{\eta})\right] + \left(r_x q_y + r_y q_x\right)\left[F_{//}\left(\vec{\eta},\vec{\xi}\right) + F_{//}\left(\vec{\xi},\vec{\eta}\right)\right]\right\} \qquad (2.15)$$

Making use of

$$F_{//}\left(\vec{\xi},\vec{\xi}\right) = C\left\langle\left(\vec{\xi}\cdot\vec{E}\right)^2 f_{//}\left(\vec{\xi}\right)\right\rangle \qquad \text{etc.}$$

and the equations (2.11) for $\vec{\xi}$ and $\vec{\eta}$ and (2.7a) for $f_{//}\left(\vec{\xi}\right)$, equation (2.15) can be elaborated into a rather complicated expression with many terms. Fortunately, by assuming that the orientation distribution of the molecules at the interface is isotropic in ϕ, we can simplify the problem. This assumption holds if the interface is isotropic in the x- and y-directions and if the correlation length of local ordening of the molecules along the angle ϕ is much smaller than the dimensions of the illuminated spot (the area of the interface under examination). The orientation distribution function of the molecules $N(\theta,\phi,\alpha)$ is now replaced by a normalized distribution function $N(\theta,\alpha)$ (for an isotropic distribution in ϕ: $N(\theta,\phi,\alpha) = N(\theta,\alpha)/2\pi$). The angle ϕ disappears from the abovementioned complicated equation by integration over ϕ from $\phi = 0$ to $\phi = 2\pi$ and dividing by 2π.

Using

$$\begin{aligned} r_x q_x + r_y q_y &= a \\ r_x q_y + r_y q_x &= b \\ a + b &= 1 \end{aligned} \tag{2.16}$$

we finally arrive at the following expression for $F_{//}$:

$$\begin{aligned} F_{//} = C\Big[&\frac{1}{4}\left\{(2a+1)E_x^2 + (2b+1)E_y^2\right\} - \frac{1}{4}\left\{(\gamma+2a)E_x^2 + (\gamma+2b)E_y^2 - 2E_z^2\right\}\left\langle \sin^2\theta \right\rangle + \\ &+ \frac{1}{8}a\left\{(2\gamma+1)E_x^2 + (2\gamma-1)E_y^2 - 4\gamma E_z^2\right\}\left\langle \sin^4\theta \right\rangle + \\ &+ \frac{1}{4}(b-a)\left\{(2\gamma+1)E_x^2 + (2\gamma-1)E_y^2 - 4\gamma E_z^2\right\}\left\langle \sin^4\theta\cos^2\alpha\sin^2\alpha \right\rangle\Big] \end{aligned} \tag{2.17}$$

in which

$$\left\langle \sin^2\theta \right\rangle = \int_{\theta=0}^{\pi}\int_{\alpha=0}^{2\pi} \sin^2\theta\, N(\theta,\alpha)\sin\theta \;\; da\, d\theta$$

$$\left\langle \sin^4\theta \right\rangle = \int_{\theta=0}^{\pi}\int_{\alpha=0}^{2\pi} \sin^4\theta\, N(\theta,\alpha)\sin\theta \;\; da\, d\theta$$

$$\left\langle \sin^4\theta\sin^2\alpha\cos^2\alpha \right\rangle = \int_{\theta=0}^{\pi}\int_{\alpha=0}^{2\pi} \sin^4\theta\cos^2\alpha\sin^2\alpha\, N(\theta,\alpha)\sin\theta \;\; da\, d\theta$$

In the same way an expression for the component of the fluorescence polarized perpendicularly to the plane of incidence, $F_{\perp}$, can be derived. This equation for $F_{\perp}$ is:

$$\begin{aligned} F_{\perp} = C\Big[&\frac{1}{4}\left\{(2b+1)E_x^2 + (2a+1)E_y^2\right\} \\ &- \frac{1}{4}\left\{(\gamma+2b)E_x^2 + (\gamma+2a)E_y^2 - 2E_z^2\right\}\left\langle \sin^2\theta \right\rangle + \\ &+ \frac{1}{8}a\left\{(2\gamma-1)E_x^2 + (2\gamma+1)E_y^2 - 4\gamma E_z^2\right\}\left\langle \sin^4\theta \right\rangle + \\ &+ \frac{1}{4}(b-a)\left\{(2\gamma-1)E_x^2 + (2\gamma+1)E_y^2 - 4\gamma E_z^2\right\}\left\langle \sin^4\theta\cos^2\alpha\sin^2\alpha \right\rangle\Big] \end{aligned} \tag{2.18}$$

The total detected fluorescence F is

$$F = F_{//} + F_{\perp} = C\Big[E_x^2 + E_y^2 - \frac{1}{2}\Big\{(\gamma+1)\Big(E_x^2 + E_y^2\Big) - 2E_z^2\Big\}\Big\langle \sin^2\theta\Big\rangle + \frac{1}{2}\alpha\gamma\Big(E_x^2 + E_y^2 - 2E_z^2\Big)\Big\langle \sin^4\theta\Big\rangle + \gamma(\mathrm{b}-\mathrm{a})\Big(E_x^2 + E_y^2 - 2E_z^2\Big)\Big\langle \sin^4\theta\cos^2\alpha\sin^2\alpha\Big\rangle\Big] \tag{2.19}$$

Using equation (2.2), the equation for the total detected fluorescence can be rewritten in the form

$$F(\Psi) = C\Big(A + B\cos^2\Psi\Big) \tag{2.20}$$

in which A and B are functions of the components of $\varepsilon_x, \varepsilon_y$ and ε_z (defined by equations (2.3)), the dichroic factor γ, the parameters a and b (defined by equation (2.16)) and the orientation distribution of the molecules at the interface. From this equation it is easily seen that by measuring $F(\Psi)$ only the ratio A/B can be obtained, since the value of the proportionality constant C is unknown (see section 2.3.1).

However, by measuring the components $F_{//}(\Psi)$ and $F_{\perp}(\Psi)$ additional information is obtained. Like for $F(\Psi)$, we can express these components as linear functions of $\cos^2\Psi$:

$$F_{//}(\Psi) = C\Big(A_{//} + B_{//}\cos^2\Psi\Big) \tag{2.20a}$$

$$F_{\perp}(\Psi) = C\Big(A_{\perp} + B_{\perp}\cos^2\Psi\Big) \tag{2.20b}$$

Now three independent parameters (viz. the ratios of $A_{//}$, $A_{\perp}$, $B_{//}$ and $B_{\perp}$) can be determined, from which the values of $\langle\sin^2\theta\rangle$, $\langle\sin^4\theta\rangle$ and $\langle\sin^4\theta\cos^2\alpha\sin^2\alpha\rangle$ can be calculated (see equations 2.17 and 2.18). How to construct the orientation distribution function from these average values (in fact orderparameters), will be explained in section 2.3.3. Since $F_{//}(\Psi)$ and $F_{\perp}(\Psi)$ are linear functions of $\cos^2\Psi$, only four measurements are necessary to extract the maximally obtainable information on the orientation distribution of the molecules, for example $F_{//}(0°)$, $F_{\perp}(0°)$, $F_{//}(90°)$ and $F_{\perp}(90°)$. From equations (2.17) and (2.18), using equations (2.3), it follows that:

$$
\begin{aligned}
F_{//}(0) &= \frac{1}{4}C\Big[(2a+1)\varepsilon_x^2 - \Big\{(\gamma+2a)\varepsilon_x^2 - 2\varepsilon_z^2\Big\}\big\langle\sin^2\theta\big\rangle + \frac{1}{2}a\Big\{(2\gamma+1)\varepsilon_x^2 - 4\gamma\varepsilon_z^2\Big\}\big\langle\sin^4\theta\big\rangle \\
&\quad +(\mathrm{b}-\mathrm{a})\Big\{(2\gamma+1)\varepsilon_x^2 - 4\gamma\varepsilon_z^2\Big\}\big\langle\sin^4\phi\cos^2\alpha\sin^2\alpha\big\rangle\Big] \\
F_{//}(90) &= \frac{1}{4}C\Big[(2b+1)\varepsilon_y^2 - (\gamma+2b)\varepsilon_y^2\big\langle\sin^2\theta\big\rangle + \frac{1}{2}a(2\gamma-1)\varepsilon_y^2\big\langle\sin^4\theta\big\rangle \\
&\quad +(\mathrm{b}-\mathrm{a})(2\gamma-1)\varepsilon_y^2\big\langle\sin^4\theta\cos^2\alpha\sin^2\alpha\big\rangle\Big] \\
F_{\perp}(0) &= \frac{1}{4}C\Big[(2a+1)\varepsilon_x^2 - \Big\{(\gamma+2b)\varepsilon_x^2 - 2\varepsilon_z^2\Big\}\big\langle\sin^2\theta\big\rangle + \frac{1}{2}a\Big\{(2\gamma+1)\varepsilon_x^2 - 4\gamma\varepsilon_z^2\Big\}\big\langle\sin^4\theta\big\rangle \\
&\quad +(b-a)\Big\{(2\gamma-1)\varepsilon_x^2 - 4\gamma\varepsilon_z^2\Big\}\big\langle\sin^4\theta\cos^2\alpha\sin^2\alpha\big\rangle\Big] \\
F_{\perp}(90) &= \frac{1}{4}C\Big[(2a+1)\varepsilon_y^2 - (\gamma+2a)\varepsilon_y^2\big\langle\sin^2\theta\big\rangle + \frac{1}{2}a(2\gamma+1)\varepsilon_y^2\big\langle\sin^4\theta\big\rangle \\
&\quad +(b-a)(2\gamma-1)\varepsilon_x^2\big\langle\sin^4\theta\cos^2\alpha\sin^2\alpha\big\rangle\Big]
\end{aligned}
\tag{2.21}
$$

The values for a and b depend on the excitation and detection wavelengths and band widths applied and can be obtained from polarization spectra [Gouterman and Stryer, 1962].

Polarization spectra describe the polarization of the fluorescence from a molecule as a function of the excitation wavelength (detection wavelength and bandwidth fixed). In figure 2.6 the experimental set-up for measurement of polarization spectra is given. The polarization P is defined as [Cantor and Schimmel, 1980]

$$
P = \frac{I_{//} - I_{\perp}}{I_{//} + I_{\perp}} \tag{2.22}
$$

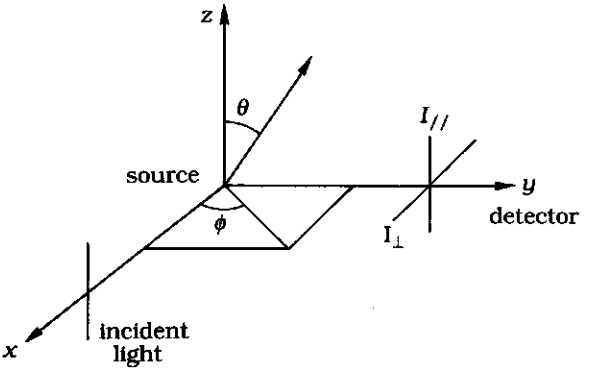

Figure 2.6. *Set-up for determination of polarization spectra. Definition of the parallelly, $I_{//}$, and perpendicularly, $I_{\perp}$, polarized fluorescence intensities.*

In the case of a totally rigid system with the absorption transition dipole moment parallel to the emission transition dipole moment the polarization $P = 1/2$. For a totally rigid system in which the emission transition dipole moment is perpendicular to the absorption transition dipole moment $P = -1/3$. When there is an angle β between the absorption and emission dipole moments, the average angle can be obtained from

$$\langle \cos^2 \beta \rangle = \frac{3P+1}{3-P} \tag{2.23}$$

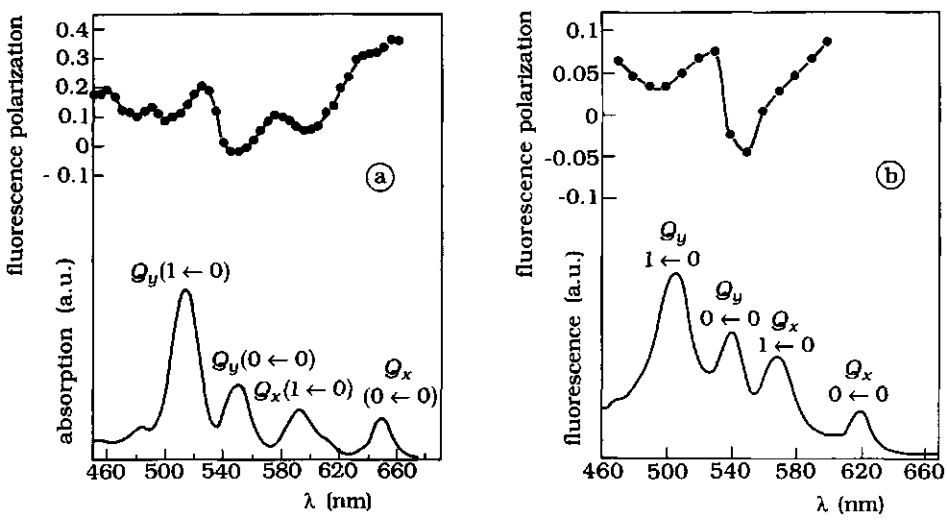

Figure 2.7. *The polarization and absorption spectra of tetraphenylporphyrin and porphyrin cytochrome c.* ***a)*** *Tetraphenylporphyrin (~ 10^{-5} M) in "castor oil"; excitation bandwidth 6.6 nm, the entire emission spectrum was detected [Gouterman and Stryer, 1962].* ***b)*** *Porphyrin cytochrome c in 90% glycerol. Emission 620 nm; excitation slit: 8 nm; emission slit: 10 nm. [Vanderkooi and Erecinska, 1975].*

For tetraphenylporphyrin and for porphyrin cytochrome *c* (the free base derivate of cytochrome *c*) in highly viscous media polarization spectra have been obtained by Gouterman and Stryer [1962] and Vanderkooi and Erecinska [1975]. In figure 2.7 these polarization spectra are shown.

It can be shown [Gouterman and Stryer, 1962] that for the porphyrin ring the average angle between the absorption and emission dipole moment is

$$\langle \cos^2 \beta \rangle = r_x q_x + r_y q_y \tag{2.24}$$

Throughout the present study an excitation wavelength of 514 nm is used (bandwidth 3 nm) (see chapter 3). At this wavelength excitation occurs in the $Q_y(1,0)$ transition band (see figure 2.4a). Both for tetraphenylporphyrin and cytochrome *c* at 514 nm excitation, the polarization $P \approx 0.13$ (see figure 2.7). From this value, using equations (2.23) and (2.24), it is found that $r_x q_x + r_y q_y = a = 0.5$ and therefore $b = 0.5$. The expressions for $F_{//}(0)$, $F_{\perp}(0)$, $F_{//}(90)$ and $F_{\perp}(90)$ now become :

$$F_{//}(0) = \frac{1}{4}C\left[2\varepsilon_x^2 - \left\{(\gamma+1)\varepsilon_x^2 - 2\varepsilon_z^2\right\}\left\langle\sin^2\theta\right\rangle + \frac{1}{4}\left\{(2\gamma+1)\varepsilon_x^2 - 4\gamma\varepsilon_z^2\right\}\left\langle\sin^4\theta\right\rangle\right]$$

$$F_{//}(90) = \frac{1}{4}C\left[2\varepsilon_y^2 - (\gamma+1)\varepsilon_y^2\left\langle\sin^2\theta\right\rangle + \frac{1}{4}(2\gamma-1)\varepsilon_y^2\left\langle\sin^4\theta\right\rangle\right]$$

$$F_{\perp}(0) = \frac{1}{4}C\left[2\varepsilon_x^2 - \left\{(\gamma+1)\varepsilon_x^2 - 2\varepsilon_z^2\right\}\left\langle\sin^2\theta\right\rangle + \frac{1}{4}\left\{(2\gamma-1)\varepsilon_x^2 - 4\gamma\varepsilon_z^2\right\}\left\langle\sin^4\theta\right\rangle\right]$$

$$F_{\perp}(90) = \frac{1}{4}C\left[2\varepsilon_y^2 - (\gamma+1)\varepsilon_y^2\left\langle\sin^2\theta\right\rangle + \frac{1}{4}(2\gamma+1)\varepsilon_y^2\left\langle\sin^4\theta\right\rangle\right] \qquad (2.25)$$

It is a direct consequence of the equality $a = b = 0.5$ that the orientation angle α no longer occurs in the equations for the fluorescence. Therefore, by using an excitation wavelength of 514 nm, only orientation distributions in θ can be determined, i.e. the orientation distribution of the porphyrin plane.

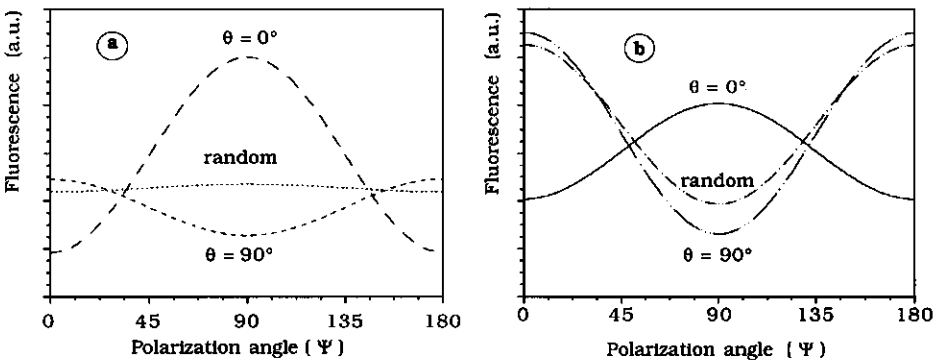

Figure 2.8. *Theoretical curves for the totally detected fluorescence F as a function of the polarization angle Ψ of the incident light beam.* ***a)*** *Sorbent surface is glass.* ***b)*** *Sorbent surface is indium tin oxide (ITO).*

By way of example, in figure 2.8 theoretical curves for F as a function of the polarization angle Ψ of the incident light beam are shown for quartz or indium tin oxide as sorbent surface. In figure 2.8a and 2.8b the curves shown are for the case the porphyrin ring is parallel to the surface ($\theta = 0°$), perpendicular to the surface ($\theta = 90°$) and for a random orientation of the molecules at the surface.

2.3.3. Reconstruction of the orientation distribution function

Generally, from the experimental values obtained for $F_{//}(0°)$, $F_{\perp}(0°)$, $F_{//}(90°)$ and $F_{\perp}(90°)$ the following ensemble averages can be calculated: $\langle \sin^2\theta \rangle$, $\langle \sin^4\theta \rangle$ and $\langle \sin^4\theta \cos^2\alpha \sin^2\alpha \rangle$ (see equations (2.21)). From this limited information it is not possible to obtain the orientation distribution in θ and α exactly. The most convenient thing to do is to expand the orientation distribution function $N(\theta,\alpha)$ into spherical harmonics:

$$N(\theta,\alpha) = \sum_l \sum_m d_{l,m} Y_{l,m}(\theta,\alpha) \qquad (2.26)$$

with

$$Y_{l,m}(\theta,\alpha) = \Theta_{l,m}(\theta)\Phi_m(\alpha)$$

in which

$$\Theta_{l,m}(\theta) = \left\{ \frac{(2l+1)(l-|m|)!}{2(l+|m|)!} \right\}^{\frac{1}{2}} P_l^{|m|}(\cos\theta) \quad \text{and} \quad \Phi_m(\alpha) = \sqrt{\frac{1}{2\pi}}\, e^{-im\alpha}$$

The coefficients $d_{l,m}$ can be obtained from

$$d_{l,m} = \int_0^{\pi} \int_0^{2\pi} N(\theta,\alpha) Y_{l,m}^*(\theta,\alpha) \sin\theta \, d\alpha \, d\theta$$

where $Y_{l,m}^*$ is the complex conjugated of $Y_{l,m}$. In this expansion (equation (2.26)) the terms $\sin^2\theta$, $\sin^4\theta$ and $\sin^4\theta\cos^2\alpha\sin^2\alpha$ stem from the contributions of $Y_{2,0}$, $Y_{4,0}$ and $Y_{4,4} + Y_{4,-4}$. Since only the averages of these terms are known from experiment, only $d_{2,0}$, $d_{4,0}$ and $d_{4,\pm4}$ are obtainable.

In the case of porphyrins and cytochrome *c* the values for both *a* and *b* in equation (2.21) are 0.5 [Gouterman and Stryer, 1962]. This implies that the term $\langle \sin^4\theta \cos^2\alpha \sin^2\alpha \rangle$ disappears from the expressions for the detected fluorescence, resulting in equations (2.25). Now only information on the orientation distribution in θ is obtained. The orientation distribution $N(\theta)$ can be expanded in Legendre polynomials :

$$N(\theta) = \sum_{n=0}^{\infty} c_n P_n(\cos\theta); \tag{2.27}$$

in which

$$P_n(x) = \frac{1}{2^n n!}\left(\left(x^2-1\right)^n\right)^{(n)} \tag{2.28a}$$

and

$$c_n = \left[\frac{(2n+1)}{2}\right]\langle P_n \rangle \tag{2.28b}$$

$\langle P_n \rangle$ are the momenta of the distribution function, the so-called order parameters. The orientation distribution in θ is fully characterized if all the order parameters $\langle P_n \rangle$ are known. As a result of the symmetry in the porphyrin ring there is no difference between $N(\theta)$ and $N(\pi-\theta)$, corresponding to the uneven coefficients c_n in the expansion (2.27) being zero. Experimentally only two order parameters are accessible, i.e. $\langle P_2 \rangle$ and $\langle P_4 \rangle$. $\langle P_2 \rangle$ and $\langle P_4 \rangle$ are given by

$$\langle P_2 \rangle = \frac{1}{2}\left(3\langle \cos^2\theta \rangle - 1\right) \tag{2.29a}$$

$$\langle P_4 \rangle = \frac{1}{8}\left(35\langle \cos^4\theta \rangle - 30\langle \cos^2\theta \rangle + 3\right) \tag{2.29b}$$

which can be calculated from $\langle \sin^2\theta \rangle$ and $\langle \sin^4\theta \rangle$.

One way to get an approximation of $N(\theta)$ from this restricted knowledge of the order parameters is to use the Maximum Entropy Method (MEM), stemming from information theory [Bevensee, 1983]. According to this approach the best guess for the orientation distribution $N(\theta)$ is obtained by maximizing the informational entropy of the distribution:

$$S\{N(\theta)\} = -\int_0^{\pi} N(\theta)\ln\{N(\theta)\}\sin\theta\, d\theta \tag{2.30}$$

with the constraints

$$N(\theta) \geq 0 \tag{2.31a}$$

$$\int_0^{\pi} N(\theta) \sin\theta \, d\theta = 1 \tag{2.31b}$$

and by definition

$$\langle P_2 \rangle = \int_0^{\pi} N(\theta) P_2(\cos\theta) \sin\theta \, d\theta \tag{2.31c}$$

$$\langle P_4 \rangle = \int_0^{\pi} N(\theta) P_4(\cos\theta) \sin\theta \, d\theta \tag{2.31d}$$

Equations (2.31a) and (2.31b) define $N(\theta)$ as a normalized probability function. Equation (2.30) can be maximized using the method of Lagrange multipliers [Levine, 1979]. This method gives the most probable values for $\langle P_n \rangle$, $n \geq 6$. We obtain the smoothest and broadest distribution consistent with the limited data at our disposal. The result is a Maxwell-Boltzmann distribution with ordening energy $U(\theta)$:

$$N(\theta) = \exp(-U(\theta)/kT) = \exp\{\lambda_0 + \lambda_2 P_2(\cos\theta) + \lambda_4 P_4(\cos\theta)\} \tag{2.32}$$

Equation (2.32) can be rewritten as:

$$N(\theta) = N_0 \exp\{\lambda_2 P_2(\cos\theta) + \lambda_4 P_4(\cos\theta)\} \tag{2.33}$$

with the normalization factor N_0 given by

$$\frac{1}{N_0} = \int_0^{\pi} \exp(\lambda_2 P_2(\cos\theta) + \lambda_4 P_4(\cos\theta)) \, d\theta \tag{2.34}$$

Substitution of equations (2.33) and (2.34) for $N(\theta)$ in equations (2.31c) and (2.31d) leads to :

$$\langle P_2 \rangle = \frac{\int_0^{\pi} P_2(\cos\theta) \exp(\lambda_2 P_2(\cos\theta) + \lambda_4 P_4(\cos\theta)) \sin\theta \, d\theta}{\int_0^{\pi} \exp(\lambda_2 P_2(\cos\theta) + \lambda_4 P_4(\cos\theta)) \sin\theta \, d\theta} \tag{2.35a}$$

and

$$\langle P_4 \rangle = \frac{\int_0^{\pi} P_4(\cos\theta)\exp\left(\lambda_2 P_2(\cos\theta) + \lambda_4 P_4(\cos\theta)\right)\sin\theta\, d\theta}{\int_0^{\pi} \exp\left(\lambda_2 P_2(\cos\theta) + \lambda_4 P_4(\cos\theta)\right)\sin\theta\, d\theta} \qquad (2.35b)$$

By fitting λ_2 and λ_4 using a least square method to the experimentally accessible values of $\langle P_2 \rangle$ and $\langle P_4 \rangle$ a unique fit is obtained, i.e. each pair $\{\lambda_2, \lambda_4\}$ defines a unique pair of order parameters $\langle P_2 \rangle$ and $\langle P_4 \rangle$. Considerations on the distribution function obtained in this way show that knowledge of $\langle P_2 \rangle$ essentially gives the width of the distribution, whereas $\langle P_4 \rangle$ provides information on the overall shape of the distribution [Levine, 1979].

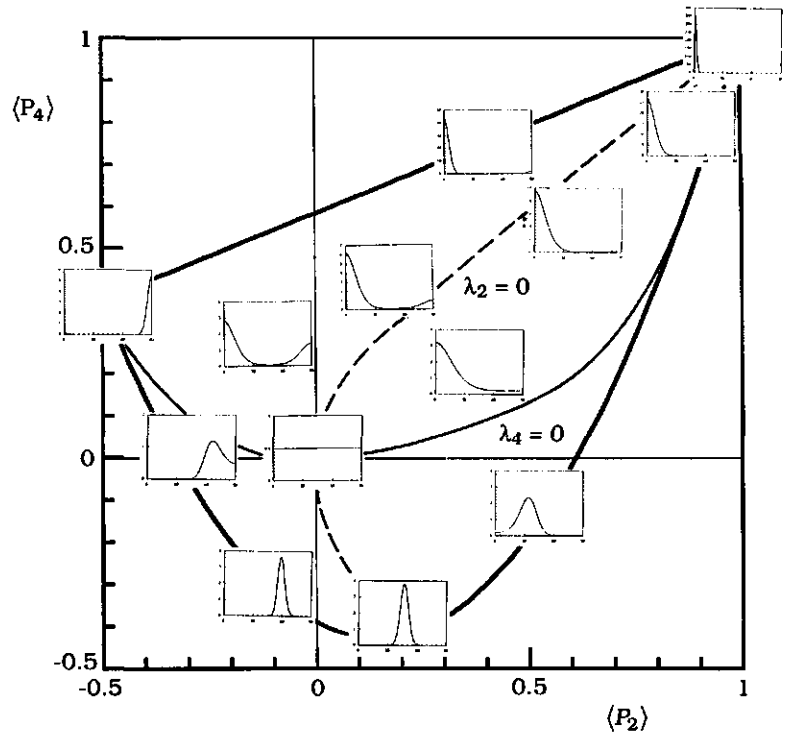

Figure 2.9. *Relation between the nature of the distribution function $N(\theta)$ and the parameters $\langle P_2 \rangle$ and $\langle P_4 \rangle$. The physically realistic combinations of $\langle P_2 \rangle$ and $\langle P_4 \rangle$ are within the area marked by drawn heavy curves. The small figures are the orientation distributions (given between θ = 0° and 90°) corresponding to that particular combination of $\langle P_2 \rangle$ and $\langle P_4 \rangle$.*

In figure 2.9 the shape of the distribution function $N(\theta)$ as a function of the order parameters $\langle P_2 \rangle$ and $\langle P_4 \rangle$ is shown. $\langle P_2 \rangle$ should lie between –0.5 and 1.0 (see equation 2.29a). For a given value of $\langle P_2 \rangle$ the value of $\langle P_4 \rangle$ should lie between upper and lower boundaries because $\langle \cos^4\theta \rangle \leq \langle \cos^2\theta \rangle$ and $\langle \cos^4\theta \rangle \geq \langle \cos^2\theta \rangle^2$. The upper boundary is the line where $\langle \cos^4\theta \rangle = \langle \cos^2\theta \rangle$. The lower boundary is the line where $\langle \cos^4\theta \rangle = \langle \cos^2\theta \rangle^2$; on this line a sharp distribution around the angle $\theta = \arccos\left(\langle \cos^2\theta \rangle^{1/2}\right)$ is found. When $\lambda_4 > 0$ a bimodal distribution is found (having maxima at $\theta = 0$ and $\theta = \pi/2$ and a minimum at some intermediate angle) and for $\lambda_4 < 0$ a distribution with one peak is observed (the distribution exhibits a maximum at some angle θ_m where $0 \leq \theta_m \leq \pi/2$). For $\lambda_4 = 0$ a Gaussian distribution is found. A random distribution is observed for $\lambda_2 = \lambda_4 = 0$, which implies that $\langle P_2 \rangle = \langle P_4 \rangle = 0$.

2.3.4. *Effect of rotational mobility of the adsorbed molecules on the orientation measurements*

One of the assumptions made in the previous sections is that the orientation of the adsorbed molecules does not change on the time scale of fluorescence. This implies that the angle between the absorption transition dipole moment and the emission transition dipole moment does not change during the fluorescence lifetime. If there is any mobility of the adsorbed molecules the total detected fluorescence can be written as

$$F \sim \left\langle \left(\vec{\mu}(\alpha_0, \phi_0, \theta_0) \cdot \vec{E}\right)^2 f\left(\vec{v}(\alpha_t, \phi_t, \theta_t)\right) \right\rangle \qquad (2.36)$$

where the subscript 0 denotes the absorption of electromagnetic radiation on time $t = 0$, and the subscript t denotes the emission of fluorescence at time t. In figure 3.10 rotations corresponding to changes in the angles α, θ and ϕ are shown.

Rotations resulting in a change of orientation angle ϕ do not have any influence on the orientation measurements because of the isotropy in ϕ, which is present at $t = 0$ and at any time t. For changes in angles θ and α, the effect on the orientation measurements is more difficult to assess. Probably the detected fluorescence intensities $F_{//}(\Psi)$ and $F_{\perp}(\Psi)$ will still depend on the orientation distribution in α, contrary to the case that there

is no rotational mobility as described by equations (2.25). Because of this complexity in introducing the mobility in the theoretical equations, we did not work it out any further. We distinguish three time scales on which mobility has different effects on the orientation measurements.

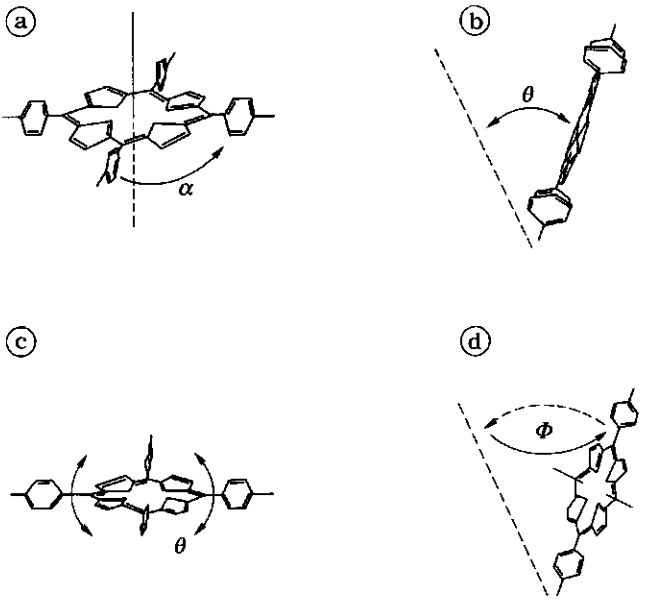

Figure 2.10. *Possible rotations of a porphyrin molecule.* ***a)*** *Rotation in angle α.* ***b)*** *and* ***c)*** *Rotation in angle θ.* ***d)*** *Rotation in angle ϕ.*

These three time scales are: the mobility is much slower that the fluorescence lifetime, the mobility is much faster than the fluorescence lifetime or the mobility is at the same time scale as the fluorescence lifetime. The case that the mobility of the adsorbed molecules is much slower that the fluorescence lifetime has already been worked out in the previous sections.

In the case that the mobility of adsorbed molecules is much faster than the fluorescence lifetime, the orientations of the absorption dipole moment on $t = 0$ and the emission dipole moment at time t are independent of each other and the equation for the total detected fluorescence is given by

$$F \sim \left\langle \left(\vec{\mu}_0 \cdot \vec{E}\right)^2 \right\rangle \left\langle f\left(\vec{v}_t\right) \right\rangle \tag{2.37}$$

By writing the equation in this way we assume that the orientation distribution does not change in time and that the ensemble averages at time $t = 0$ and at time t are identical:

$$\langle \cos^2 \theta_0 \rangle \equiv \langle \cos^2 \theta_t \rangle \tag{2.38}$$

With this assumption we can elaborate equation (2.37) in a corresponding way as done in section 2.3.3. The expressions for the parallel and perpendicular polarized component of the fluorescence now become:

$$F_{//} = F_{\perp} = \frac{1}{8} C \left\{ \frac{1}{2} \left(E_x^2 + E_y^2 + E_z^2 \right) + \frac{1}{2} \left(E_x^2 + E_y^2 - 2E_z^2 \right) \langle \cos^2 \theta \rangle \right\} \left\{ 2 - \gamma + \gamma \langle \cos^2 \theta \rangle \right\}$$

The result is obvious: if there is mobility on a timescale much faster than the fluorescence lifetime, polarization of the fluorescence will be completely lost.

2.4. Conclusion

In this chapter the principle of TIRF is explained and the theory for determining the orientation of adsorbed chromophores has been worked out for the special case of porphyrins and cytochrome *c*. For this special case it is possible to study the orientation distribution in one orientation angle (the angle θ). The orientation distribution in θ can be reconstructed from the restricted information using the Maximum Entropy Method. Finally, mobility of the adsorbed molecules which is much faster that the fluorescence lifetime results in the disappearance of the fluorescence polarization.

Chapter 3

Experimental Techniques

In this chapter the experimental methods and materials used in this work will be discussed. The subject of the first section is the Total Internal Reflection Fluorescence (TIRF) measurements; the TIRF set-up, the TIRF flow cell, and data handling will be explained. The second section deals with the optical technique reflectometry with which adsorption kinetics and adsorbed amounts can be measured. In this second section the set-up will be explained and reflectivity calculations made for the silicon/indium tin oxide/solution layer system will be treated in detail. Finally, in the last section the method of applying electrical potentials at the adsorbent interface will be discussed, and some relevant characteristics of the ITO films will be presented.

3.1. TIRF measurements

3.1.1. TIRF set-up

In the literature experimental set-ups for TIRF were first described by Hirschfeld [1965] for measurements at the solid/liquid interface, by Tweet *et al.* [1964] for the liquid/air interface and by Carniglia *et al.* [1972] for high refractive index solid/liquid interfaces. Meanwhile, TIRF has been combined with a variety of conventional fluorescence techniques (like polarization, microscopy, photobleaching recovery and correlation spectroscopy) for a variety of purposes (detection of molecular adsorption, observation of cell/substrate contact regions, kinetics, surface diffusion and adsorbate conformations). As a consequence many different TIRF set-ups have been developed. With regard to this aspect good reviews have been written by Harrick [1967] and Axelrod *et al.* [1984].

In figure 3.1 a schematic diagram is shown of the TIRF apparatus constructed in this study to determine orientation distributions of adsorbed chromophores. A sealed head pulsed nitrogen laser (model VSL-337ND, Laser Science Inc., MA, USA), with an emission wavelenght of 337 nm and a

peak power of 85 kW, was used to pump a dye laser module (model DLM-220, Laser Science Inc.). This dye laser consists of a grating in Littrow configuration, with 2400 lines per mm grating, and is tuneable from 300 to 900 nm. Other specifications, given by the manufacturer of the dye laser, when pumped with the VSL-337ND are: bandwidth 0.3 nm, pulse length 3 ns, pulse energy 50 μJ at 500 nm, peak power 16.7 kW at 500 nm, average power 1 mW at 500 nm. To reduce the beam divergence to 0.5 mrad a beam expander/collimator (NR 337910, Laser Science Inc.) was used. The dye used in the dye laser for the experiments was coumarin 307 ($5.6\ 10^{-3}$ M in methanol) and was obtained from Lambda Physik, Göttingen, Germany. The laser beam from the dye laser module (polarized horizontally) passes through a broad band polarization rotator (model PR-550, Newport, USA) with a transmission of 98%. After passing through a focussing plano convex lens (f = 75 mm, Ø = 40 mm) the light beam enters the 75° Dove prism (40 × 50 × 15 mm) of the TIRF cell (see figure 3.3 number 4). The prism was made of BK7 glass (n = 1.518) obtained from the Department of Physical Chemistry of the University of Amsterdam, The Netherlands. The beam enters and, after being totally reflected near the large face of the prism, leaves the prism normal to the small bevelled faces.

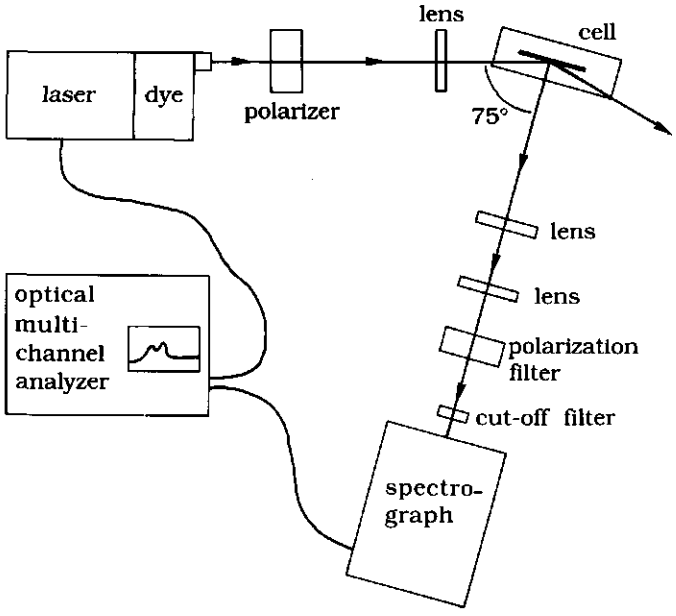

Figure 3.1. *A schematic diagram of the TIRF set-up used for orientation measurements. For explanation see the text.*

A glass microscope slide, with or without a semiconducting indium tin oxide film, is optically coupled to the large face of the prism using immersion oil (Zeiss, n = 1.515 at 20° C) as the refractive matching fluid. The bare glass surface or the ITO-layer serves as one face of the flow chamber for adsorption (see section 3.1.2. figure 3.3). Therefore, the light beam entering the prism, is transmitted through the glass slide and is totally reflected at the glass/solution or the ITO/solution interface. The area of the reflection spot is approximately 1 mm^2. Finally, the reflected laser beam was absorbed by a light trap.

Part of the fluorescence light emitted by chromophores at the solid/liquid interface is transmitted through the prism and is collimated and condensed by two plano convex lenses (f = 75 mm, Ø = 40 mm) into a spectrograph (model 1233, EG&G Princeton Applied Research, Princeton, NJ, USA). A polarization filter (03FPG001, Melles Griot) is used to separately detect the components of the fluorescence polarized perpendicularly and parallelly to the plane of incidence of the laser beam. A cut-off filter (FSR-RG610, Newport) is placed in front of the spectrograph to block scattered excitation light. The fluorescence light, condensed into the spectrograph, is dispersed by a vertical 1200 lines/mm grating onto an intensified photodiode array (model 1420 B-1024-G, EG&G Princeton Applied Research). A consequence of this vertical grating is that light, polarized perpendicularly to the plane of incidence, with a wavelength between 600 and 800 nm, is detected 1.25 times better than light polarized parallelly to the plane of incidence. This ratio of 1.25 is the so-called G-factor and has to be taken into account in the analysis of the fluorescence data. Photons arriving at the photodiode array generate a small current. This current is converted into a voltage signal which in turn is passed through to the Optical Multichannel Analyzer (OMA) (model 1463, EG&G Princeton Applied Research). This OMA was used for data-handling (see section 3.1.4).

Laser pulse intensity

The intensity of the light pulse produced by the nitrogen laser and dye laser depends on the number of pulses the nitrogen laser has already fired. Figure 3.2 shows the average pulse intensity as a function of the number of pulses fired by the laser. The data for this figure have been obtained as follows: ten times 1 shot was fired with the laser and the average intensity was calculated, subsequently ten times two shots were fired with the laser

and again the average intensity was calculated. The same procedure was followed for 3, 4, 6, 8, 10...1000 pulses. From figure 3.2 it can be seen that the average intensity of the first pulses is lower than that of pulses fired later in the sequence. With 100 times 2 shots fired by the laser a standard deviation of 4.5% in intensity was found and in the case of 100 times 100 shots the standard deviation reduced to 0.15%. These values are within the 5% specified by the manufacturer.

This introduction period is due to the warming up of the plasma cartridge of the nitrogen laser. Therefore it is better to ignore the first 50 or 100 pulses before starting the experiment. In practice this can simply be done, but because many high peak power pulses might damage the adsorbed chromophores it was necessary to look for a compromise. In the orientation experiments only 20 pulses were discarded before starting an experiment.

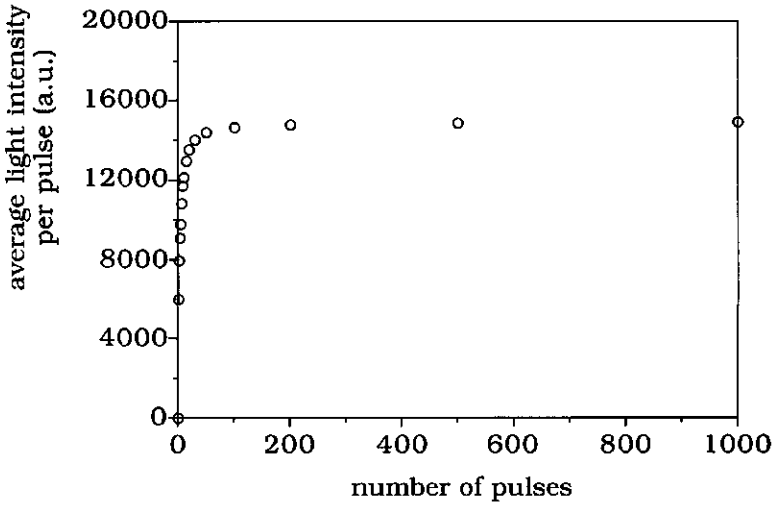

Figure 3.2. *The average pulse intensity as a function of the number of pulses fired by the nitrogen laser.*

3.1.2. The TIRF flow cell

In figure 3.3 the TIRF flow cell is shown. The flow cell consists of a perspex flow chamber (1), a rubber gasket (2), a glass slide (3) and a prism

(4). The 75° Dove prism and the glass slide are kept in place by two perspex blocks (5) each attached to the cell by two screws. The prism was made of BK7 glass with a refractive index of 1.518. Immersion oil is used as the matching fluid between the glass slide and the prism.

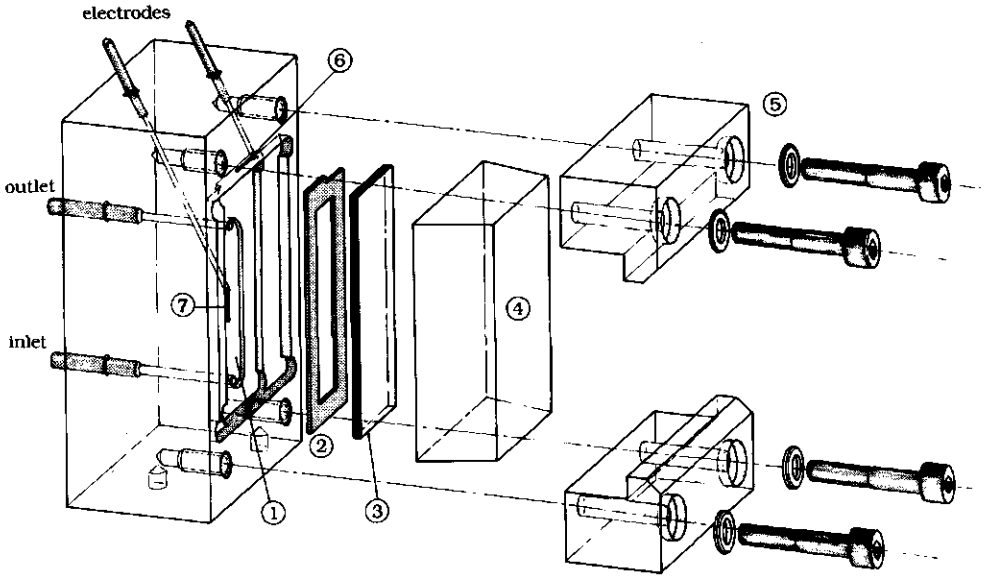

Figure 3.3. *Exploded view of the TIRF flow cell and its components.*

The flow chamber consists of a machined perspex well and the (coated) glass slide. The flow cell is mounted vertically. Solution enters the cell at the bottom of the flow chamber, leaving it at the top. The volume flow rate of the solution, resulting from a hydrodynamic pressure difference, was 2.0×10^{-8} m^3 s^{-1}.

The dimensions of the flow chamber ($1 \times 10 \times 58$ mm) were chosen in such a way that the flow in the cell was laminar at the given rate. A flow chamber of practically the same dimensions has been used by Lok *et al.* [1983a] to investigate the effect of flow rate on the fluorescence signal. They

showed that the flow was laminar and with low concentrations (1-100 mg/ml) of BSA and fibrinogen adsorption of these proteins was found to be diffusion-limited. In the upper right corner of the cell a connection for the working electrode (6) is present. By pressing an ITO coated glass slide to that connection an electrical potential can be imposed on the ITO surface. In the back side of the flow chamber a counter electrode (7) is mounted. A reference electrode is kept outside the flow cell and placed into a small beaker glass which is in contact with the solution inside the flow cell.

3.1.3. Orientation measurements

Data acquisition

For the measurement of fluorescence spectra to be used in the determination of the orientation distributions, a special data acquisition program was written. In figure 3.4 the sequence for the measurement of one spectrum is shown. The Optical Multichannel Analyzer (OMA) has a standard sequence of reading and setting of the detector pixels. This basic sequence consists of a so-called scan and an overhead time and takes 16.7 ms (see figure 3.4). The acquisition program can be split into three parts. At the start of the measurement the OMA gives a so-called pre-read interval or pre-scan in which the detector elements are read and reset. Just after the pre-scan the OMA generates a main trigger. With this trigger the OMA gives a) a command to the laser to fire a shot and b) a command to the 1304 pulse generator which takes care of the gated detection of the fluorescence signal. The program is written so that the first 20 laser pulses are ignored. This is done by ignoring two scans, designated "IGN" in figure 3.4, which is repeated 20 times (20 laser pulses). Due to the fact that the detector elements are grouped in pairs (for signal amplification) one scan now takes 35 ms. After the first 20 pulses of the laser, acquisition of the data starts.

The acquisition of data starts with the OMA triggering the laser and the 1304 pulse generator. The pulse generator builds in a 300 ns delay before the gated detection starts. This delay time is caused by the electronic components in the system, i.e. the pulse laser. Now one scan is added to the memory of the OMA, represented in figure 3.4 with ADD. During this scan

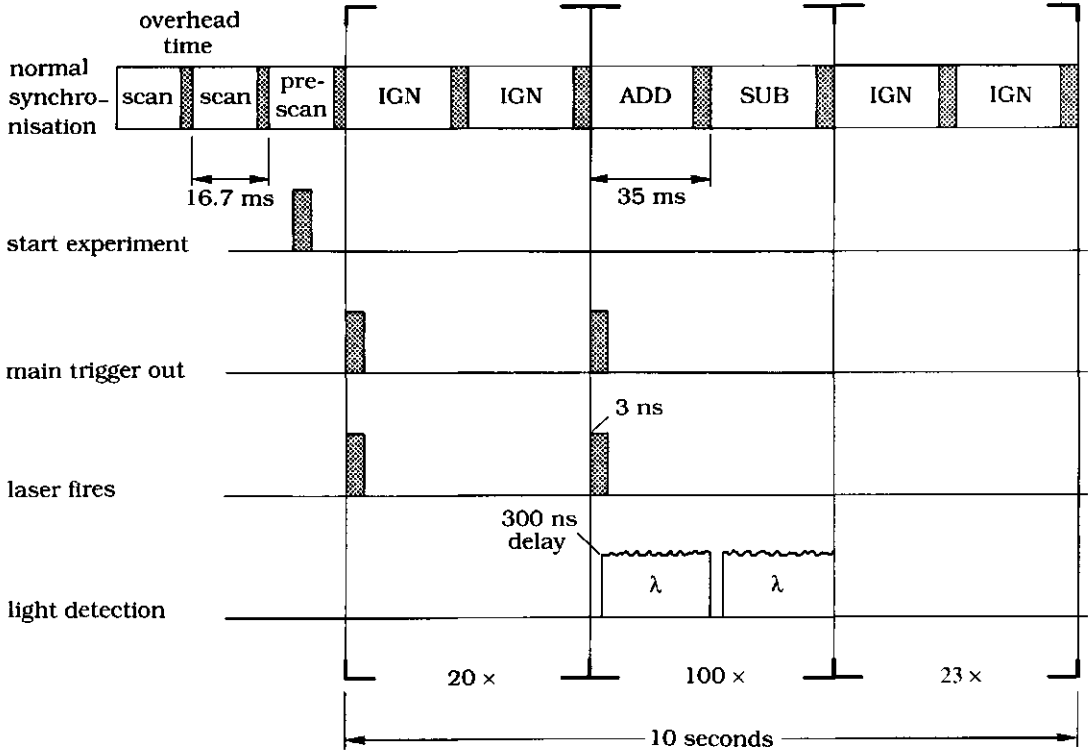

Figure 3.4. *Sequence for measuring a fluorescence spectrum.*

the fluorescence is collected during 35 ms by the photodiode array. Immediately after the ADD scan the background signal is subtracted from the fluorescence signal by the SUB scan. This way of correcting for the background is possible because the fluorescence lifetime is in the order of only 10 ns and therefore the fluorescence is fully detected in the ADD scan. This acquisition cycle is repeated 100 times, and the fluorescence signals are stored in the memory.

Finally, after collecting the data, again two scans are ignored for 23 times. In this way the time between the measurements of two spectra is exactly 10 seconds. This repetition of ignored scans can be extended, in order to collect a spectrum each 1, 5 or 10 minutes, for example.

The time per scan is called the exposure time. The exposure time (35 ms) and the delay time between the 1304 pulse generator and the photodiode array (300 ns) are typical for the experiments with cytochrome *c* and porphyrins performed in the TIRF apparatus described in section 3.1.1. For other chromophores and in other TIRF set-ups different values for the exposure time and the delay time might be a better choice which remains to be found out. There are two ways in which the measuring sensitivity can be increased. First, the number of scans added (100 in the orientation experiments) can be increased resulting in a higher fluorescence signal to noise ratio. Second, the detection system offers the possibility of grouping the detector pixels. This means that, instead of reading 1024 pixels giving 1024 fluorescence intensity values, now 512, 256 or 128 fluorescence intensity values are obtained when the pixels are grouped in sets of 2, 4 or 8. In the orientation measurements performed in this thesis the pixels were grouped as pairs. As a result, the sensitivity increases. However, the spectral resolution decreases by a factor proportional to the grouping number. This might be a problem when a high resolution is needed.

Data analysis

The fluorescence spectra obtained in the way as described above are integrated between 600 and 800 nm by the OMA. In principle it does not matter if the whole spectrum is integrated, only one peak of the spectrum is integrated, or just the peak value is used for analyzing the measurements in terms of orientation distributions (see section 2.3.3). However, integration of whole spectra gives better signal to noise ratios and is therefore preferred.

In chapter 2 it has been made clear that for the determination of the orientation distribution four independent fluorescence signals should be measured, for example $F_{\perp}(0)$, $F_{\perp}(90)$, $F_{//}(0)$ and $F_{//}(90)$. In order to obtain more reliable results each of these four fluorescence values were measured several (n) times in a different order.
It is convenient to rewrite equation (2.25) in a matrix form. For $n = 1$:

$$\begin{pmatrix} F_{//}(0) \\ F_{\perp}(0) \\ F_{//}(90) \\ F_{\perp}(90) \end{pmatrix} = \begin{pmatrix} a(1) & b(1) & c(1) \\ a(2) & b(2) & c(2) \\ a(3) & b(3) & c(3) \\ a(4) & b(4) & c(4) \end{pmatrix} \begin{pmatrix} \frac{1}{8}C \\ \frac{1}{8}C\langle\cos^2\theta\rangle \\ \frac{1}{8}C\langle\cos^4\theta\rangle \end{pmatrix} + \begin{pmatrix} \varepsilon(1) \\ \varepsilon(2) \\ \varepsilon(3) \\ \varepsilon(4) \end{pmatrix} \qquad (3.2)$$

with

$$a(1) = 1/4\,(5 - 2\gamma)\varepsilon_x^2 + (2 - \gamma)\varepsilon_z^2 \qquad b(1) = 1/2\varepsilon_x^2 + 2(\gamma - 1)\varepsilon_z^2$$
$$a(2) = 1/4\,(3 - 2\gamma)\varepsilon_x^2 + (2 - \gamma)\varepsilon_z^2 \qquad b(2) = 3/2\varepsilon_x^2 + 2(\gamma - 1)\varepsilon_z^2$$
$$a(3) = 1/4\,(3 - 2\gamma)\varepsilon_y^2 \qquad b(3) = 3/2\varepsilon_y^2$$
$$a(4) = 1/4\,(3 - 2\gamma)\varepsilon_y^2 \qquad b(4) = 1/2\varepsilon_y^2$$

and

$$c(1) = 1/4(2\gamma + 1)\varepsilon_x^2 - \gamma\,\varepsilon_z^2$$
$$c(2) = 1/4(2\gamma - 1)\varepsilon_x^2 - \gamma\,\varepsilon_z^2$$
$$c(3) = 1/4(2\gamma - 1)\varepsilon_y^2$$
$$c(4) = 1/4(2\gamma + 1)\varepsilon_y^2$$

In equation (3.2) an error vector $\vec{\varepsilon}$ is introduced, in which any experimental errors and inaccuracies in the calculated components of the evanescent field are incorporated. By minimizing this error vector by a least squares (numerical) fit, the best values given the theoretical model and assumptions as described in chapter 2, are obtained for $\langle\cos^2\theta\rangle$, $\langle\cos^4\theta\rangle$ and C. Once $\langle\cos^2\theta\rangle$, $\langle\cos^4\theta\rangle$ and C are fitted, the orientation distribution can be reconstructed (see section 2.3.3).

3.2. Reflectometry measurements

3.2.1. Principle

The principle of reflectometry is illustrated by figure 3.5. In this figure a polarized laser beam is reflected at a silicon/ITO/water interface. The intensities of the parallelly and perpendicularly polarized components of the reflected beam ($I_{//}$ and $I_{\perp}$, respectively) are determined by the Fresnel reflection coefficients at the two-phase boundaries and by interference in the reflected beam. This interference depends on the phase difference between rays reflected at the solvent/ITO surface and at the ITO/silicon surface. The phase difference is determined by the thickness d_f and the refractive index n_f of the indium tin oxide layer, the wavelength of the incident light beam λ_0, and the angle of incidence θ_i. Any material adsorbed at the ITO interface having a refractive index different from that of the solution (water, n_s = 1.333) and the adsorbent material (ITO, n_f = 1.90) will change the polarization of the reflection and from this change the adsorbed amount can be obtained.

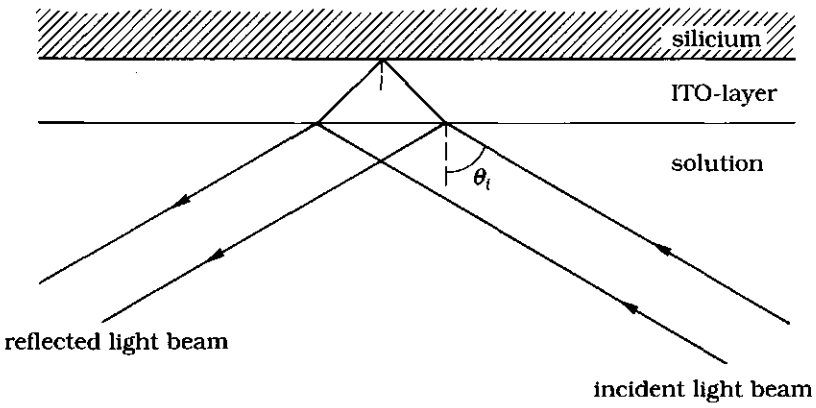

Figure 3.5. *Principle of reflectometry. See text for explanation.*

3.2.2. Theoretical calculations

$I_{//}$ and $I_{\perp}$ can be calculated according to Abeles' method [Hansen, 1968; Born and Wolf, 1975]. The system is modelled as a set of flat parallel

layers of uniform refractive index as shown in figure 3.6. In the presence of an adsorbed (protein) layer it is assumed that the concentration profile $c(z)$ in the adsorption layer and hence the refractive index profile $n(z)$ is uniform. Using the refractive index increment of the adsorbate (dn_p / dc) and the refractive index of the adsorption layer (n_p) one can calculate the corresponding adsorption layer thickness (d_p) for a constant adsorbed amount.

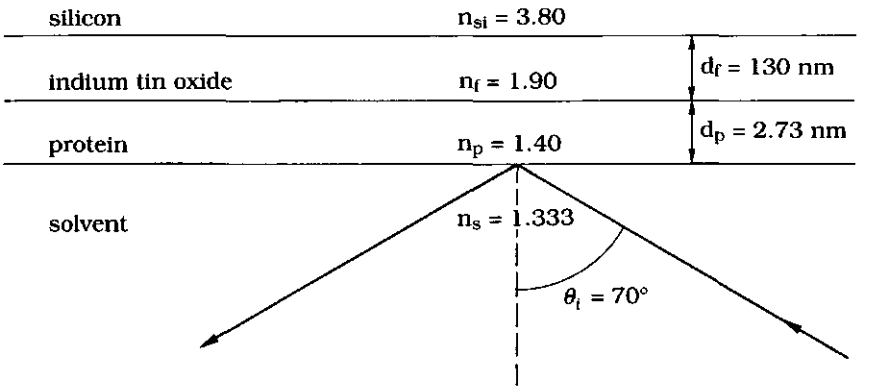

Figure 3.6. *Schematic illustration of the multilayer model for light reflection. The optical constants used in the calculations are indicated.*

The reflected intensities $I_{//}$ and $I_{\perp}$ can be combined to give the output signal S of the reflectometer, defined as [Dijt *et al.*, 1990; Dijt, 1993]:

$$S = \frac{I_{//}}{I_{\perp}} = \frac{f_{//} R_{//} I^0_{//}}{f_{\perp} R_{\perp} I^0_{\perp}} \qquad (3.3)$$

In equation (3.3) the reflected intensities $I_{\perp}$ and $I_{//}$ are expressed in the incident light intensities $I^0_{\perp}$ and $I^0_{//}$, the reflectivities $R_{\perp}$ and $R_{//}$ (for perpendicularly and parallelly polarized light, respectively) of the substrate and the loss factors $f_{\perp}$ and $f_{//}$, respectively. The loss factors account for losses at the reflecting surfaces of the prisms and the beam splitter, and for differences in detection efficiency between the photodiodes.

The relation between the adsorbed amount and the reflectometer signal can be written as [Dijt *et al.*, 1990; Dijt, 1993]:

$$\Gamma = \frac{\Delta S}{S_0}\frac{1}{A_s} \tag{3.4}$$

S_0 is the signal without adsorbate, ΔS the signal increment due to the adsorbate and A_s is the sensitivity factor for adsorption defined by

$$A_s = \frac{1}{\left(R_{//}/R_{\perp}\right)}\frac{d\left(R_{//}/R_{\perp}\right)}{d\Gamma} \tag{3.5}$$

Dijt showed that for the silicon/silica/water and silicon/silica/decaline interface the relation between $R_{//}/R_{\perp}$ and Γ is linear. Furthermore A_s was found to be independent of the concentration profile in the adsorption layer. Therefore, the relation between Γ and ΔS is linear and by calculation of A_s absolute amounts can be obtained. For further details on the determination of A_s the reader is referred to Dijt [1993].

For the system described in figure 3.6 the reflectivities $R_{\perp}$ and $R_{//}$ and the sensitivity factor A_s are given as functions of θ_i and d_f in figure 3.7. The Brewster angle for the silicon/water interface (d_f = 0), where $R_{//}$ = 0, is 70.6°. From figure 3.7b it can be seen that $R_{\perp}$ and $R_{//}$ vary periodically with the thickness d_f of the ITO layer, with a period δ of 223 nm. This figure shows at which values of d_f the signal S is the most sensitive to adsorption, because the slope of the curve is at an extreme value. This is the case at $\delta/4$ (= 55.8 nm) and at $3\delta/4$ (= 167 nm). In figure 3.7c A_s as a function of θ_i is shown, for d_f = 130 nm, the actual thickness of the ITO-layers used in this study. The sensitivity factor shows a broad maximum around the Brewster angle for the silicon/water interface. Therefore the optimum value for θ_i is 70°, but the precise setting is not critical. In figure 3.7d the sensitivity factor is plotted as a function of the ITO layer thickness. The ranges of 30-80 and 130-180 nm are the most suitable for experiments; A_s does not strongly depend on d_f and can therefore be more accurately determined.

Comparing the calculations made with an ITO layer as the substrate with the results Dijt obtained for the silicon/silica/water interface, it appears that the two systems behave similarly.

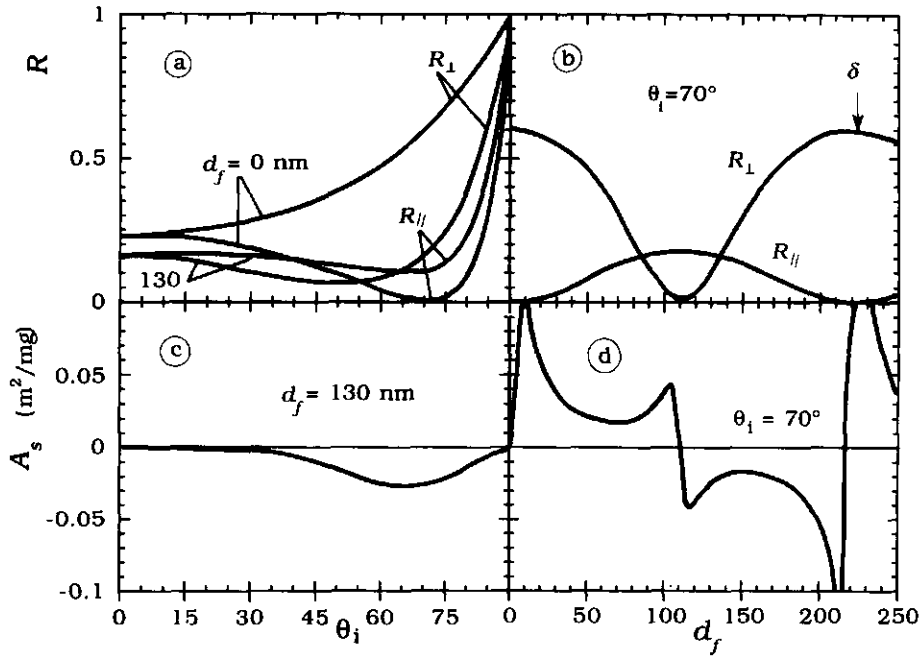

Figure 3.7. *Reflectivities and sensitivity factors for adsorption at the silicon/ITO/water interface. In* **a** *and* **b** *the reflectivities $R_\perp$ and $R_{//}$ are given as functions of the angle of incidence, θ_i and the thickness of the ITO-layers, d_f, respectively. In* **a** *the full curves are for the silicon/water interface ($d_f = 0$) and the dashed curves are for d_f = 130 nm, the thickness of the ITO layers actually used in the experiments. Figure* **b** *is calculated for θ_i = 70°, very near the Brewster angle (70.6°). The thickness δ of a period is indicated by an arrow. In figs.* **c** *and* **d** *the sensitivity factor A_s for adsorption is given as a function of θ_i and d_f, respectively.*
Parameters used: λ_0 = 632.8 nm, n_{si} = 3.80, n_f = 1.90, n_s = 1.333, n_p = 1.40, dn/dc =0.185 $cm^3\,g^{-1}$ [De Feyter, 1978], d_p = 2.73 nm. The value for d_p corresponds to Γ = 1 mg m^{-2}.

3.2.3. Experimental set-up

The experimental set-up is schematically shown in figure 3.8. A polarized He/Ne laser beam (1) enters the cell through a 45° glass prism (2). The laser beam is reflected at the sorbent surface (3) at an angle of incidence of 70.6°. The reflected light beam leaves the cell through a second 45° prism (2) and is split (4) into its parallelly and perpendicularly polarized components (with respect to the plane of incidence). Both components ($I_{//}$ and $I_{\perp}$) are detected by photodiodes (5). The reflection intensities are converted by an analogue signal processor (6) into the signal S ($S = I_{//} / I_{\perp}$).

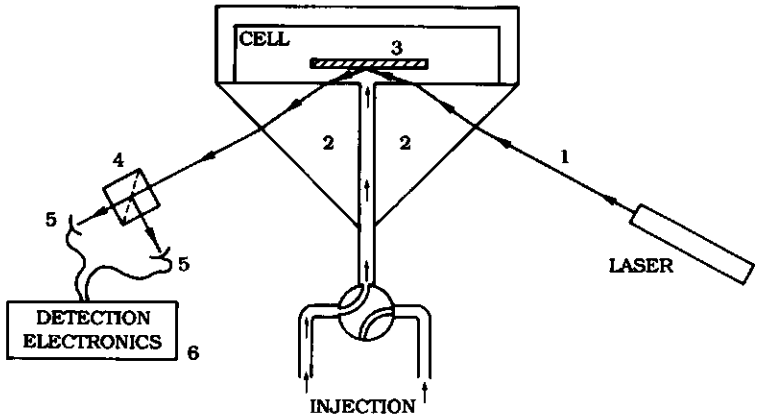

Figure 3.8. *Schematic representation of the reflectometry set-up. The numbers in the figure are explained in the text.*

Solutions are injected into the cell by a so-called "impinging jet" method: the solution flows through a cylindrical channel between the two prisms into the cell (see figure 3.8). The channel is perpendicular to the sorbent surface and the intersection of its symmetry axis and the surface is called the "stagnation point". The reflection point of the laser beam coincides with the stagnation point. The flux J_p of protein molecules to the surface at the stagnation point is given by [Dabros and Van der Ven, 1983; Dijt *et al.*, 1990]:

$$J_p = 0.283 \nu^{-1/3} \Phi^{2/3} R^{-5/3} D^{2/3} c_p \qquad (3.6)$$

where ν is the kinematic viscosity, Φ the volume flux, R the radius of the flow channel, D the diffusion coefficient of the protein in solution and c_p the bulk concentration of the protein. Due to the finite thickness of the laser beam the adsorption is measured not only at the stagnation point itself, but also in a (small) area around it. At a radial distance $R/2$ from the stagnation point the light intensity is half its maximum value and the flux J_p at that distance is found to be 7% lower than at the stagnation point itself. Therefore, using equation (3.6) the flux J_p of protein molecules to the surface is somewhat overestimated. For more specific information about the hydrodynamic properties of the system the reader is referred to Dijt *et al.* [1990] and Dabros and Van der Ven [1983]. In the experimental set-up used in this study $\nu = 10^{-6}$ m^2 s^{-1}, $\Phi = 2.0 \times 10^{-8}$ m^3 s^{-1} and $R = 9.5 \times 10^{-4}$ m.

3.3. Applying a potential at the adsorbent interface

In almost all studies reported in the literature concerning the adsorption process of proteins, the pH of the solution was changed in order to vary the electrostatic interactions between sorbent surface and the protein molecules. By changing the pH of the solution both the surface charge and the charge of the molecules which adsorb are changed. In this work the contribution of electrostatic interactions to the adsorption process was studied by imposing an electrical potential to the sorbent surface. To that end, a conducting sorbent surface has to be used. We have chosen for the semi-conductor ITO as the sorbent material because of its favourable optical and electrical properties: ITO films have a high conductivity and are optically transparent in the visible spectrum. Films of indium tin oxide have a wide range of applications; they are used for example as electrode materials in liquid crystals, solar cells and microelectronics, and for IR-reflecting coatings.

Many methods have been developed for preparing thin ITO films on substrates. Most commonly used are chemical vapour deposition [Maryama and Fukui, 1991a,b], RF magnetron sputtering [Ray *et al.*, 1983; Martinez *et al.*, 1992] and DC magnetron sputtering [Shigorato, 1991]. Specifications with respect to film thickness, conductivity and surface homogeneity are determining for the method of preparation to be chosen.

The ITO films used in this study were obtained from Philips Components Heerlen, The Netherlands, and Philips LCTV Eindhoven, The Netherlands. For the TIRF experiments ITO films were DC sputtered onto a glass slide (n = 1.518) with a thin quartz layer (4 nm, n = 1.47) as the adhesive. These ITO films contain 10 % Sn and the thickness is 120 nm. In the reflectometer experiments silicon wafers with an ITO film thickness of 130 or 140 nm have been used. These wafers were also coated by DC magnetron sputtering and the ITO layers contain 10% Sn. The refractive index specified by the manufacturer was 1.90 for both the ITO films on the glass slides and on the silicon wafers.

3.3.1. Surface characterization

In order to characterize the ITO films deposited onto glass and silicium, Scanning Electron Microscopy (SEM), Atomic Force Microscopy (AFM), streaming potential and sheet resistance measurements were performed and the results will be discussed below. For films used several times the effect of the solutions and the different cleaning procedures have been studied by comparing their properties with new ITO films. Initially, the ITO/silicium plates used for reflectometry were cleaned by heating in a gas flame for 5 seconds (not glowing). In a later stage of this study the wafers were cleaned using UV radiation under ozone. The reasons for switching to another cleaning procedure will become clear in the course of this section. The ITO/glass slides used in the TIRF experiments were cleaned before use by subsequently rinsing 1 minute in 4% chromic acid solution, 1 minute in 1 M HCl, 1 minute in ethanol and extensively with water. The ITO/silicium plates were re-used several times, whereas the ITO/glass plates were disposed of after each experiment.

Scanning Electron Microscopy

Scanning electron micrographs of the ITO-coated silicium wafers have been made to study the homogeneity of the ITO layers. A new plate, a plate used several times in reflectometry experiments and a plate on which an external potential was imposed during reflectometry measurements have been examined. The results are shown in figure 3.9. In figure 3.9a a micrograph of the new plate is shown. The surface is clean and no irregularities are present; the surface appears to be rather smooth.

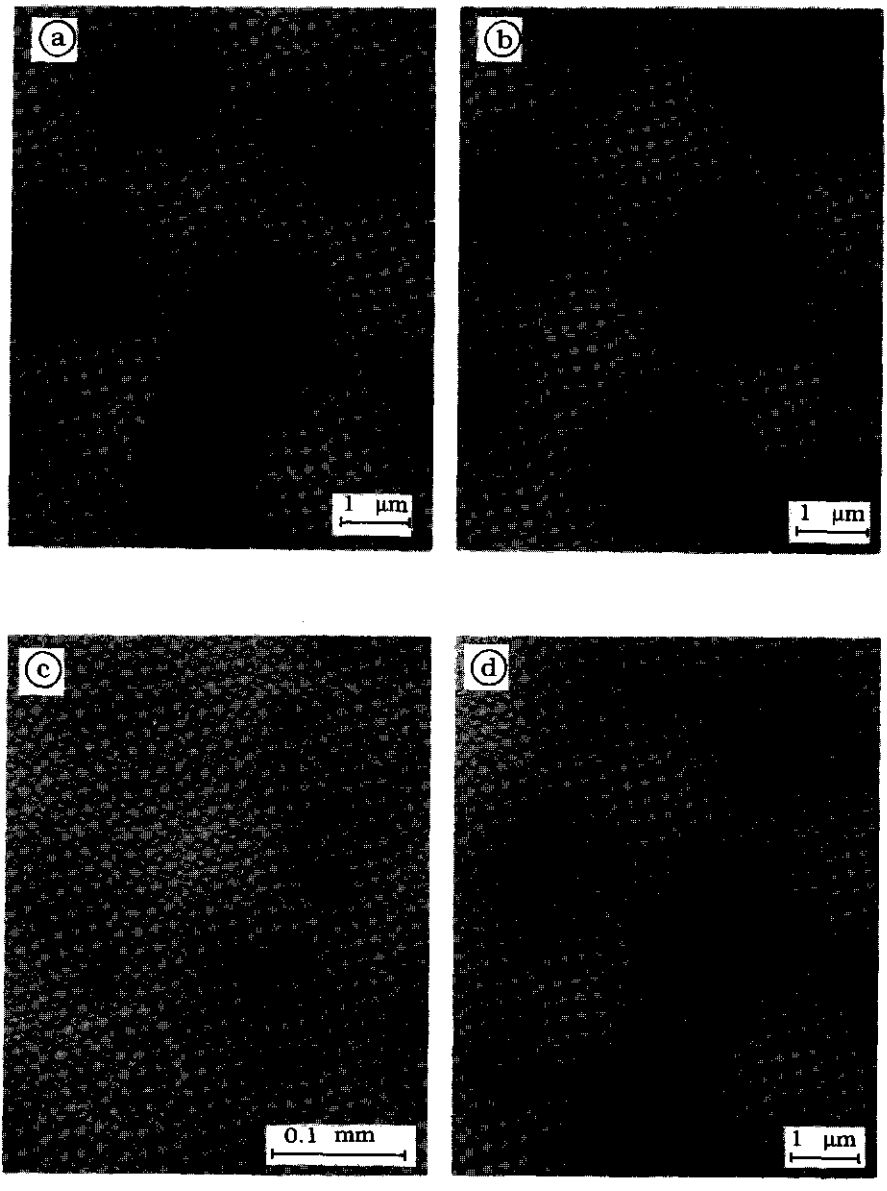

Figure 3.9. *Scanning electron micrographs of three ITO coated silicium wafers and an ITO coated glass slide.* ***a)*** *A new silicium plate.* ***b)*** *A silicium plate used in reflectometry and often cleaned by heating.* ***c)*** *A silicium plate used for reflectometry with and without externally imposed potentials and various times cleaned by heating.* ***d)*** *A new glass slide.*

The used plate (figure 3.9b), several times heated in a gas flame for cleaning, shows no significant differences compared with the new plate. Figure 3.9c shows the plate which was used many times, with and without an externally imposed potential. Now various irregularities are visible and the surface roughness seems to be increased. Such a degeneration of the surface is only observed if external potentials are applied in combination with heating as cleaning procedure. For the UV-ozone method the surface seems to be much more stable. Figure 3.9d shows a micrograph of a new ITO/glass slide. There are no visible differences between the ITO films on silicium or glass.

Atomic Force Microscopy

The homogeneity of the ITO layer was further investigated using AFM. A new ITO/glass slide was cleaned following the standard cleaning procedure adapted in the TIRF experiments (see page 54). After drying the plate, a micrograph was obtained using the Nanoscope III (Digital Instruments) in the constant force mode. Figure 3.10 shows the results. On a scale of 1 µm by 1 µm the ITO/glass surface is very regular with a mean roughness of only 0.323 nm.

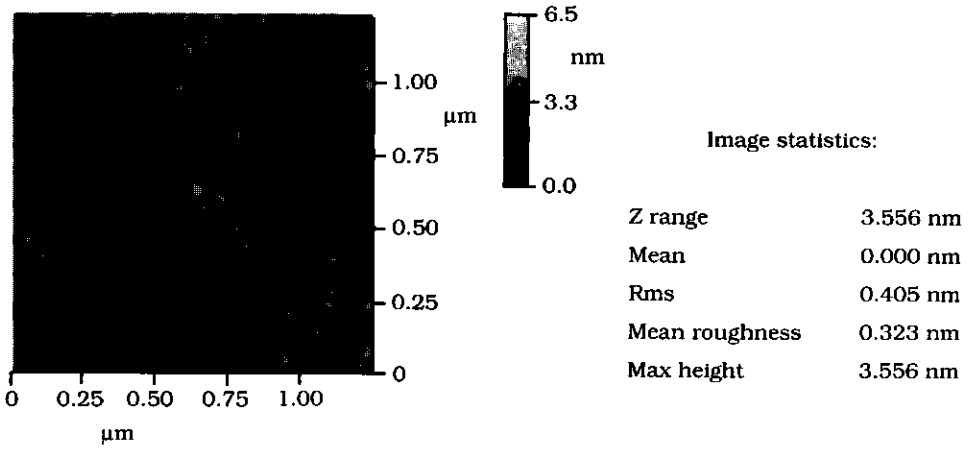

Figure 3.10. *Atomic Force Microscopy image of the ITO/glass surface.*

Streaming potential measurements

In order to determine the isoelectric point (i.e.p.) of both the ITO/silicium and the ITO/glass surface, streaming potential measurements were carried out and the results are shown in figure 3.11. The i.e.p.'s of ITO/silicium and ITO/glass are found at pH 3.4 ± 0.2 and pH 2.9 ± 0.2, respectively. Apparently, the type of substrate has some influence. Streaming potential measurements on bare glass and silicium show i.e.p.'s at pH 2.1 ± 0.2 and below pH 2.1, respectively.

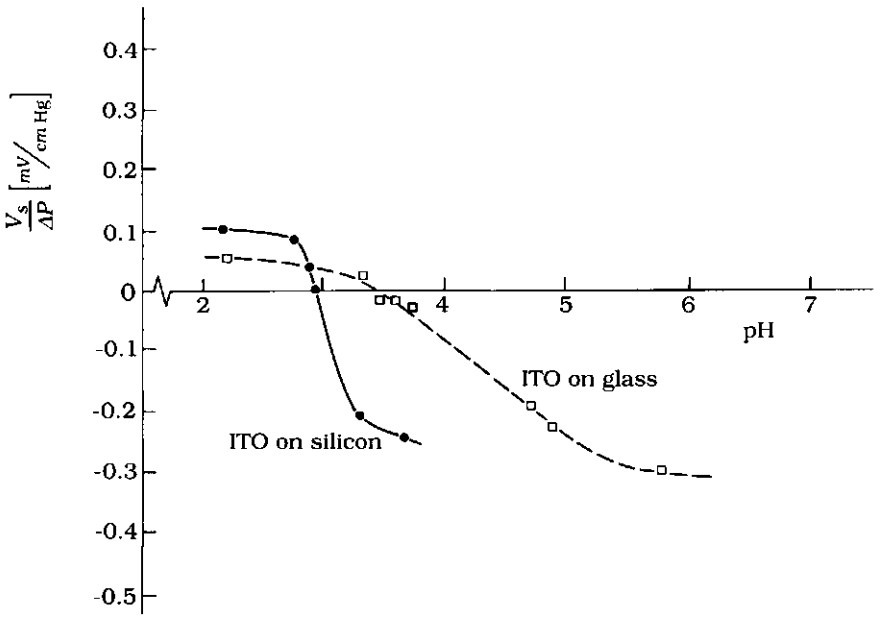

Figure 3.11. *Determination of the isoelectric points of ITO-coated silicium wafers (full curve) and ITO-coated glass slides (dashed curve) by streaming potential measurements.*

Hydrophobicity

The hydrophobicity of the ITO surfaces was determined by water-contact angle measurements. The results are shown in table 3.1. The contact angle on a new ITO/silicium wafer is 83° ± 2°. For plates used in streaming potential measurements an angle of 51° was observed. The longer the ITO/silicium wafer has been in contact with an aqueous solution, the

lower the contact angle and hence the more hydrophilic the surface is. The decrease in contact angle is dependent on the solution in which the ITO/silicium plate was kept. For higher pH values, the contact angle decreases more strongly in time. This can be due to the silica, which might been leached out.

Table 3.1. *Contact angles of water, 10 mM acetate buffer pH 4 and 10 mM phosphate buffer pH 7 on ITO surfaces.*

	ITO on silicon			ITO on glass		
	after str. pot.	after 2 hours	after 3.5 days	new	after cleaning	after 19 hours
water	51°	13°	11°	86°	70°	50°
buffer pH 4	51°	27°	19°	82°	66°	48°
buffer pH 7	51°	11°	2°	90°	69°	38°

Table 3.2. *The effect of the cleaning method on the contact angle of water, 10 mM acetate buffer pH 4 and 10 mM phosphate buffer pH 7 on ITO/silicium surfaces.*

	new	heating in a gas flame	UV-ozone
water	83°	23°	7°
buffer pH 4	82°	32°	17°
buffer pH 7	83°	42°	8°

For the ITO/glass surface the contact angle also decreases with increasing time of contact with the solution and increasing pH. However, the

decrease is not as drastic as in the case of ITO on silicium. Therefore, after being in contact with aqueous solutions the ITO/glass surface is not as hydrophilic as the ITO/silicium surface. The effect of the cleaning procedure used before TIRF measurements is a small decrease in the contact angle of about 15-20°. The effects of the cleaning procedures used for the ITO/silicium plates on the contact angle are shown in table 3.2. The UV-ozone treatment makes the surface more hydrophilic than the heating. Another difference between both methods is the reproducibility of the reflectometer measurements, which is much better for plates cleaned with the UV-ozone method than for plates cleaned by heating in a gas flame.

Table 3.3. *Sheet resistances (Ω/□) of ITO films.*

	ITO on silicon			ITO on glass		
	new	after 2 hours	after 3.5 days	new	after cleaning	after 19 hours
water	87.87	87.80	87.48	24.57	24.72	24.80
buffer pH 4	88.43	95.75	90.47	24.96	25.43	25.98
buffer pH 7	86.30	88.90	86.38	24.41	24.88	25.04a

Sheet resistance

Sheet resistances of the ITO films were measured by the four point method as described by Valdes [1954]. The results are shown in table 3.3. The sheet resistances measured are independent of the types of solution with which the wafers/slides have been in contact. The differences between the sheet resistances of ITO/silicium and the ITO/glass films might be due to the difference in thickness of the ITO film and/or depend on the supporting substrate which might still have an influence on the conductivity, as it influences the i.e.p.'s of both the surfaces. The sheet resistance of ITO/silicium wafers was reduced by a factor of 2 by cleaning with the heating method, whereas cleaning by the UV-ozone method had no effect on the sheet resistance. The cleaning procedure used for the ITO/glass slides did not affect the sheet resistance of these slides.

From the above described characterization experiments it can be concluded that the ITO/silicium and ITO/glass surfaces are rather smooth and hydrophilic. With respect to hydrophilicity, conductivity and i.e.p. there are some rather small differences between the two surfaces. As far as the cleaning procedures in the reflectometry experiments are concerned, it is better to use the UV-ozone method than heating because it is easier and less destructive.

3.3.2. The electrical potential of the ITO/solution interface

Equilibrium potentials

Figure 3.12 shows the equilibrium potential (or open circuit potential or rest potential) of an indium tin oxide layer on a silicium wafer and on glass as a function of the pH. The equilibrium potentials of the ITO/silicium and ITO/glass surfaces were measured versus a saturated calomel electrode (SCE). The isoelectric points for both surfaces are indicated. The corresponding equilibrium potentials amount to +300 mV and +370 mV *vs.* SCE for ITO on silicium and for ITO on glass, respectively.

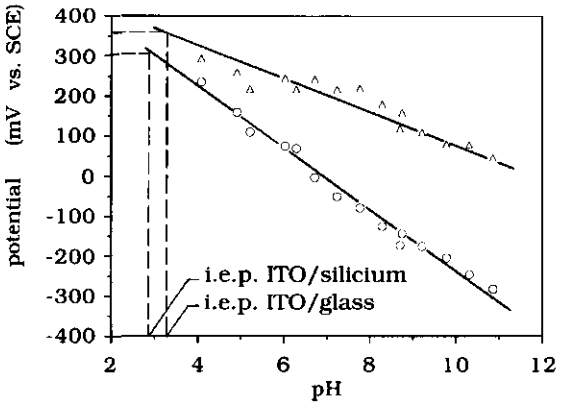

Figure 3.12. *Equilibrium potentials of the ITO/silicium and the ITO/glass surface as a function of pH. The isoelectric points (pH 2.9 and pH 3.4) are indicated.*

Externally imposed potentials

The electrical potential of the ITO layers in the TIRF and reflectometry measurements was varied using a home-built potentiostat. A Pt wire counter electrode and, in the reflectometry measurements, a Ag/AgCl/saturated KCl or, in the TIRF measurements, a Standard Calomel Electrode (SCE) were used as reference electrodes. The presence of an amperometer in the electrical circuit makes it possible to monitor any electrical currents during the measurements.

Voltammetric experiments were performed to check whether the imposed potentials were really established at the ITO/solution interface. These experiments are carried out in a three electrode cell with a Pt-wire as the counter electrode and an Ag/AgCl/3.5 M KCl reference electrode. As a working electrode a Pt-wire, an ITO/silicium wafer or an ITO/glass slide was used. Before each experiment, the solution was stirred and flushed with nitrogen. During the measurements N_2 was passed over the solution. Potentials were applied from a Princeton Research Polarographic Analyzer model 174A and current density-potential (*i-E*) curves were recorded on a Omnigraphic 2000 Recorder. As electroactive species in solution methylviologen (MV^{2+}) and rutheniumtrisbipyridyl $Ru(bipy)_3^{2+}$ were used. The results are shown in figure 3.13.

The oxidation and reduction peaks obtained with the Pt wire are centered around a potential of -641 mV vs. Ag/AgCl/3.5M KCl for methylviologen and +1080 mV vs. Ag/AgCl/3.5M KCl for 5×10^{-3} M $Ru(bipy)_3^{2+}$, in good agreement with the literature values of the standard redox potential E° for the MV^+/MV^{2+} couple (-0.45 V *vs.* NHE) [Harriman and Porter, 1982] and the $Ru(bipy)_3^{2+}/Ru(bipy)_3^{3+}$ couple (+1.26 V *vs.* NHE). The peaks obtained with the ITO/glass are centered around -664 mV *vs.* Ag/AgCl for MV^+/MV^{2+} and around +1094 mV *vs.* Ag/AgCl for $Ru(bipy)_3^{2+}/Ru(bipy)_3^{3+}$. For the ITO/silicium wafer these values are -763 mV *vs.* Ag/AgCl and ca +1120 mV (depending on the scan rate) *vs.* Ag/AgCl, respectively. That is, in the case of methylviologen, ca 20 mV and 100 mV more negative than for a Pt wire and in the case of $Ru(bipy)_3^{2+}/Ru(bipy)_3^{3+}$ 15 mV and 30 mV more positive than for a Pt wire.

The observation that the separation between the reduction and oxidation peaks is larger for the ITO/glass and ITO/silicium electrode than for the Pt wire electrode indicates that the electrode kinetics are slower at the ITO surfaces.

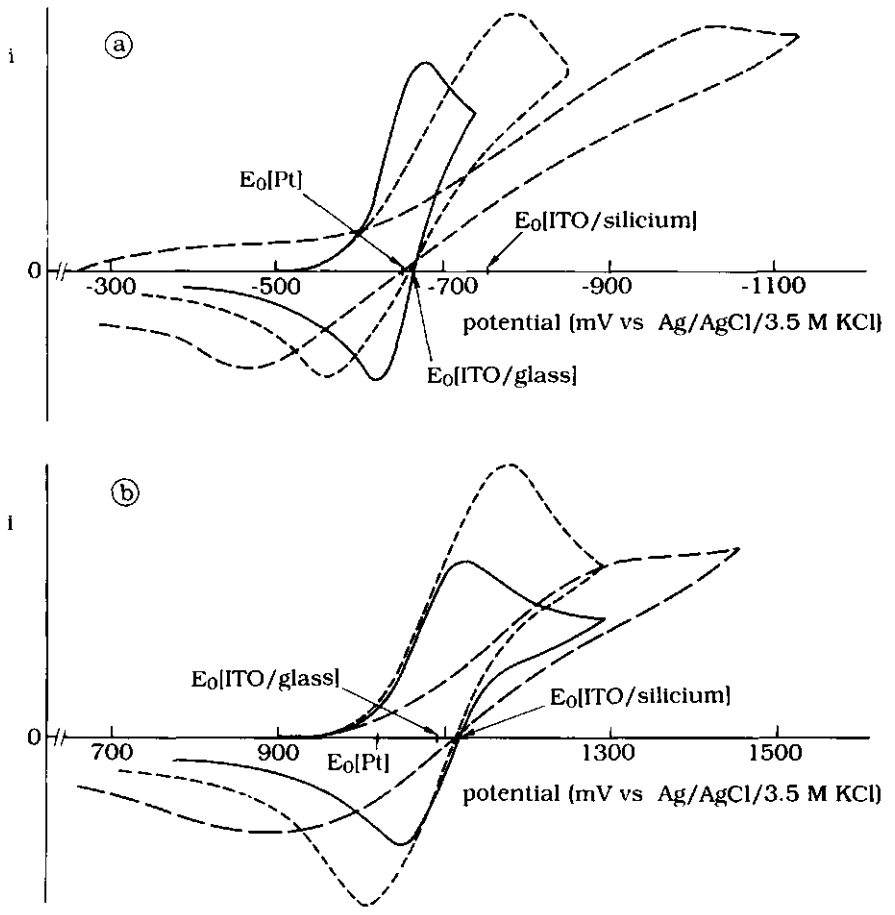

Figure 3.13. *Cyclic voltammograms of a Pt wire electrode (drawn line), an ITO/silicium electrode (dashed line) and an ITO/glass electrode (dotted line) in* **a)** *5×10^{-3} M methylviologen/ 0.1 M KNO_3 solution (scan rate 10 mV/s) and* **b)** *5×10^{-3} M $Ru(bipy)_3^{2+}$/0.2 M Na_2SO_4 solution (scan rates 10 mV/s for ITO/silicium and ITO/glass and 20 mV/s for Pt).*

The voltammetric experiments prove that it is possible to impose an external potential at the ITO/solution interface. From the experiments with both methylviologen and $Ru(bipy)_3^{2+}$ it can be seen that the value of the potential at the ITO/solution interface is in absolute sense somewhat lower than the imposed potential. This difference must be due to the relatively high resistance of the ITO layers, leading to a potential loss between the point where electrical contact is made and the part of the ITO layer in solution.

Chapter 4

Adsorption behaviour of tetramethylpyridinium porphyrin on silica: adsorbed amounts, kinetics, orientation and mobility

4.1. Introduction

Porphyrins, which have the same macrocycle structure as the natural chlorophylls, are widely used as photosensitizers in artificial solar energy systems. They have a very efficient light absorption in the visible part of the of the spectrum, where the solar energy spectrum has a maximum [Boxer, 1983; Fendler, 1985]. For example, porphyrins, adsorbed on a semiconducting surface, are used to generate charge carriers in the semiconductor with photons of lower energy than the band gap energy of the semiconductor [Suto *et al.*, 1988; Yanagi, 1990; Suto *et al.*, 1990]. Recently, Yanagi *et al.* [1990] showed that the orientation of the dye molecules in the sensitization film is important for the observed photoresponse. They found that for an epitaxial film of 5,10,15,20-tetraphenylporphyrin with the molecular planes oriented perpendicular to the surface that the photocurrent is three times greater than for a polycrystalline film, in which the molecules are randomly oriented.

The important role of the porphyrins in the development of an artificial solar energy device was not our direct motive for studying the orientation and mobility of adsorbed porphyrin molecules. Originally, the idea was to study the orientation of adsorbed protein molecules. To that end we used porphyrin cytochrome *c* as the model protein (see chapter 6) of which the porphyrin ring was used as the intrinsic fluorescent group. As this protein is difficult to obtain from the native form and because of the fact that it is sensitive to high light intensities (photodegradation) we were looking for a molecule which is cheap, easy to deal with, fluorescent and which can be used instead of cytochrome *c* for alignment of the equipment and to test the theory described in chapter 2. The choice was simple. Free base tetramethylpyridinium porphyrin (H_2TMPyP) has the same structure as the porphyrin ring system in cytochrome *c* and therefore comparable absorption and emission properties. Although it was not the intention to

study the porphyrin adsorption extensively, over the past years we obtained a great number of data resulting in this chapter. Another consideration to study the adsorption of H_2TMPyP on silica is the fact that very little is known on the adsorption of porphyrins on solid surfaces, as reflected in the scarcity of papers in the literature [Gianellis, 1990; Suto *et al.*, 1988; Yanagi, 1990; Suto *et al.*, 1990].

In this chapter the adsorption behaviour of tetramethylpyridinium porphyrin on silica will be presented. After giving some characteristics of H_2TMPyP in section 4.2, the adsorbed amounts, the adsorption kinetics and the orientation and mobility of adsorbed molecules will be discussed in section 4.3. Finally the results will be summarized in section 4.4.

4.2. Materials and Methods

4.2.1. Materials.

H_2TMPyP

Tetra(4-N-methylpyridyl)porphyrin (TMPyP) is a disc-shaped molecule with four positive charges, a diameter of 1.6 nm and a molecular weight of 678 g/mole. TMPyP used in this study was the free base form (H_2TMPyP), i. e. in the centre of the porphyrin ring instead of a metal atom two hydrogen atoms are present on opposite N-atoms (see figure 2.3). It is one of the few porphyrins which are water-soluble. A three-dimensional impression of H_2TMPyP is given in figure 4.1. The porphyrin ring has a flat structure. The four methylpyridyl side groups make a tilt of 80° to the plane of the porphyrin ring [Hofstra, 1988; Schrijvers *et al.*, 1994].

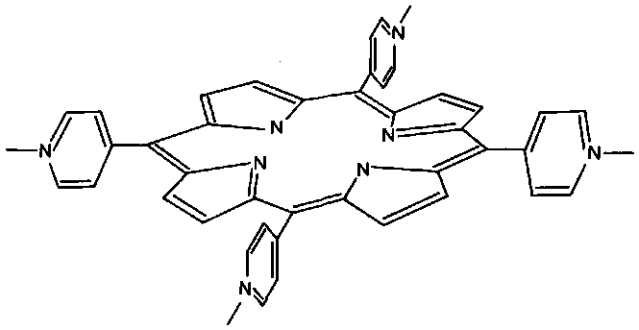

Figure 4.1. *Schematic drawing of tetra-(4-N-methylpyridyl)-porphyrin.*

The four positive charges, stemming from the pyridinium side groups, are delocalized over the whole ring system, resulting in an induced polarity of the molecule upon adsorption on a charged surface. As a result of this induced polarity, dimers and aggregates are formed at concentrations higher than 10^{-6} M [Kano, 1983; 1987].

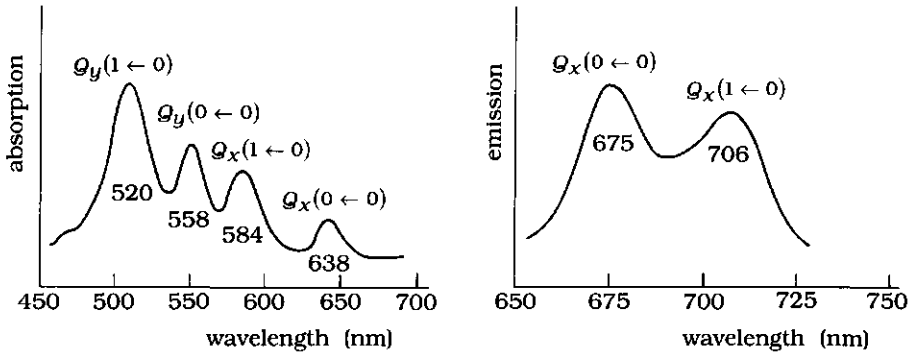

Figure 4.2. *The absorption and emission spectrum of H_2TMPyP.*

Figure 4.2 shows the absorption and emission spectra of H_2TMPyP. In the plane of the porphyrin two absorption and two emission transition dipoles are located along the molecular *X*- and *Y*-axes (see section 2.3.2 and figure 2.3). The absorption and emission bands shown in figure 4.2 have a composed character (see section 2.3). The common names for the absorption bands in the literature are represented in the figure by $Q_x(0,0)$, $Q_x(1,0)$, $Q_y(0,0)$ and $Q_y(1,0)$. The fluorescence spectrum consists of two peaks. The absorption and fluorescence maxima of H_2TMPyP in aqueous solutions at room temperature are given in table 4.1.

Table 4.1. *The absorption and emission maxima of H_2TMPyP in aqueous solution [Kalyanasundaram, 1984].*

Absorption (nm)			Fluorescence (nm)	
soret	Q(1,0)	Q(0,0)	Q(0,0)	Q(1,0)
421	518	554		
	583	638	675	705

TMPyP solutions

H_2TMPyP solutions were prepared from $(H_2TMPyP)I_4$ obtained from Strem Chemicals Inc. $(H_2TMPyP)I_4$ concentrations generally ranged from 0.1 to 100 mg/l in pure water or either 10 mM acetate buffer pH 4 or 10 mM phosphate buffer pH 7. Porphyrin concentrations were determined by measuring the extinction at 424 nm in a Hamamatzu spectrophotometer (molar extinction coefficient = 220×10^3 M^{-1} cm^{-1}. [Kalyanasundaram and Neumann-Spallart, 1982]). The viscosity of the H_2TMPyP solutions was varied by adding sucrose or glycerol (Baker Chemicals). An Ostwald viscosity meter was used to measure the viscosities and the refractive indices of the solutions were determined with an Abbe refractometer.

Sorbent surfaces

For the TIRF measurements a glass surface and for the reflectometry experiments a Si/SiO_2 surface was used for the adsorption of H_2TMPyP. SiO_2 powder (borosilicate), obtained from Solvirel, Levallais, France, with a specific surface area of 0.6 m^2/g, was used in the depletion measurements.

4.2.2. Methods

Depletion measurements.

Adsorption experiments were carried out in 10 cm^3 polycarbonate tubes in which porphyrin solutions of various concentrations were added to a dispersion of SiO_2 in the same buffer. The tubes were gently rotated for about 16 hours. After centrifugation, the porphyrin concentrations in the clear supernatant were determined.

Reflectometry measurements

Adsorbed amounts of H_2TMPyP on a macroscopic Si/SiO_2 surface were determined with reflectometry. A sensitivity factor A_s of 0.022 m^2 mg^{-1} was used (see section 3.2.2.). The porphyrin solution impinges perpendicularly upon a flat surface with a jet flow of 2.0×10^{-8} m^3 s^{-1}. For a more detailed description of the apparatus the reader is referred to section

3.2. More information about the hydrodynamics of the system can be found in Dijt *et al.* [1990].

TIRF measurements

The TIRF instrument used has been described in detail in section 3.1. Adsorption of H_2TMPyP onto a glass plate took place in a laminar flow cell (see figure 3.3) using the earth gravity to obtain a flow rate of 2.0×10^{-8} m^3 s^{-1}. Solutions containing sucrose or glycerol had lower fluxes: solutions of the highest viscosities (concentration sucrose/glycerol higher than 40/60 % (v/v)) were introduced into the cell by hand using a syringe.

4.3. Results and Discussion

4.3.1. Adsorption kinetics and adsorbed amounts

Figure 4.3a shows adsorption isotherms of H_2TMPyP on SiO_2 from pure water obtained with reflectometry and depletion measurements. The results of both types of experiments are in good agreement up to a concentration of 200 mg/l. Above this concentration reflectometry cannot be used due to strong light absorption by the porphyrin solution in the reflectometer cell.

The plateau value of the isotherm in water, ca. 1 mg/m^2, corresponds to a surface area of approximately 2 nm^2 per molecule. This area is large enough for the molecules to adsorb in a compact monolayer with the porphyrin ring parallel to the interface ("side-on" adsorption). Figure 4.3b shows the adsorption of H_2TMPyP from water, 0.1 M KNO_3 and 10 mM phosphate buffer pH 7 obtained with reflectometry. The adsorbed amounts in 0.1 M KNO_3 and 10 mM phosphate buffer pH 7 are remarkably higher than the adsorbed amounts in water. In the case of 0.1 M KNO_3 this must be due to the screening effect of the salt ions, resulting in a lower repulsion between the positively charged porphyrin molecules in the adsorption layer. Although the electrolyte concentration in the phosphate buffer is approximately 10 times lower, the effect on the adsorbed amounts is even higher than the presence of 0.1 M KNO_3. This might be caused by specific adsorption of the phosphate ions, so that the adsorption layer is in fact composed of both positively charged porphyrin molecules and negatively

charged phosphate ions. The adsorbed amounts of 2 to 2.5 mg/m^2 in buffer and 0.1 M KNO_3 correspond to a surface area of 0.8 to 1.0 nm^2 per molecule. As a result the molecules cannot be adsorbed "side-on", but make a tilt with the surface, or are adsorbed in more than one layer. For a compact monolayer in which the molecules are adsorbed "end-on", the area per molecule would be about 0.8 nm^2 [Désormeaux, 1991].

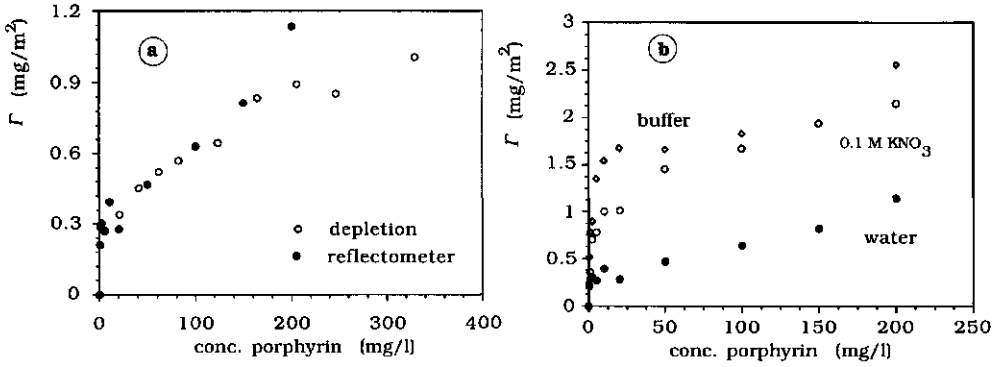

Figure 4.3. a) *Adsorption isotherms of H_2TMPyP in water obtained with reflectometry and depletion measurements.* ***b)*** *Adsorption isotherms of H_2TMPyP in water, 0.1 M KNO_3 and 10 mM phosphate buffer pH 7 obtained with reflectometry.*

The adsorption of H_2TMPyP from water, 0.1 M KNO_3 and 10 mM phosphate buffer pH 7, is given as a function of time in figure 4.4. These results are obtained with reflectometry; the porphyrin concentration was 10 mg/l. It can be seen that the adsorption of porphyrin from buffer continues to rise for a long time. This supports the idea of multilayer formation during adsorption and the co-adsorption of phosphate ions.

The initial adsorption rate $(d\Gamma / dt)_{t\to 0}$ can be compared with the flux J_{por} of the porphyrin molecules to the surface. This flux, shown in figure 4.4b, has been calculated using equation (3.6) with $\nu = 10^{-6}$ m^2 s^{-1}, $\Phi = 2.0 \times 10^{-8}$ m^3 s^{-1}, $R = 9.5 \times 10^{-4}$ m and $D = 4.3 \times 10^{-10}$ m^2 s^{-1}. The diffusion coefficient D used here has been estimated assuming that the diffusibility of the porphyrin molecule is the same as that of a globular molecule with a radius of 0.5 nm.

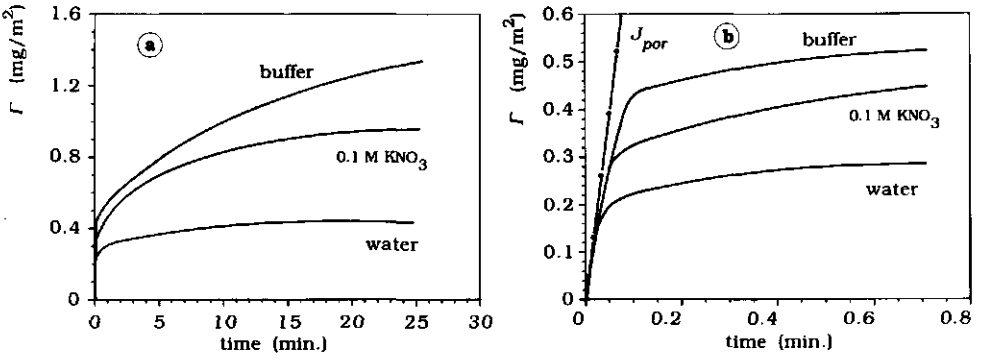

Figure 4.4. a) *Amounts of H_2TMPyP adsorbed from different solvents as a function of time.* ***b)*** *Initial parts of figure 4.5a. The flux J_{por} of porphyrin molecules to the surface is indicated. The porphyrin concentration was 10 mg/l.*

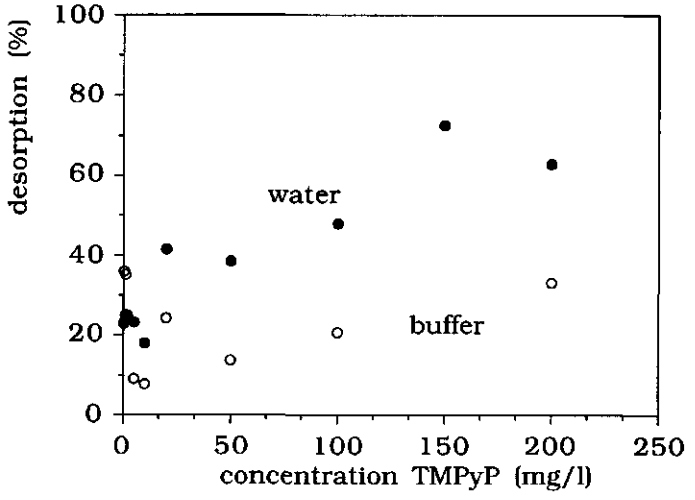

Figure 4.5. *Fraction of the adsorbed amounts that can be desorbed by flushing with the solvent.*

Irrespective of the solvent used, $(d\Gamma / dt)_{t\to 0}$ is equal to J_{por}. Apparently, every molecule that arrives at the surface is attached.

The desorption of the porphyrin in water and phosphate buffer upon flushing with the solvent has been studied as a function of the concentration during adsorption. The results are shown in figure 4.5. The fraction of the adsorbed amount which can be desorbed is higher for water than for the phosphate buffer. This fraction varies between 8 and 30% for buffer and between 20 and 60% for water, depending on the porphyrin concentration in solution during adsorption. The porphyrin molecules are bound more strongly to the surface in the presence of phosphate buffer.

The fluorescence intensity of adsorbed porphyrin molecules has been followed in time with TIRF. Figure 4.6 shows the fluorescence as a function of time for different porphyrin concentrations in phosphate buffer pH 7. For a concentration of 0.1 mg/l a slow increase in the fluorescence was observed resulting in a low maximum value. A faster adsorption was observed in the case of 1 mg/l. A well-established plateau value was reached in time. For 10 and 100 mg/l a very fast initial increase in fluorescence intensity was measured followed by a slower decrease. This overshoot phenomenon is particularly manifest at the porphyrin concentration of 100 mg/l. This decrease in fluorescence cannot be the result of desorption because the reflectometry experiments do not show a decrease in adsorbed amount with time. From orientation measurements (see section 4.3.2) it was concluded that reorientation of the adsorbed molecules could not be the reason for this decay in fluorescence with time. According to the theory, a change from "side-on" to more or less "end-on" adsorption might lead to lower detection efficiencies and therefore to lower fluorescence intensities (see chapter 2). The high amounts adsorbed at this concentration found with reflectometry indicate that probably multilayer adsorption occurs. Therefore enhanced intermolecular interactions can be expected. These intermolecular interactions might cause a shift in the absorption maxima of the adsorbed porphyrin molecules, resulting in less efficient excitation of the molecules and hence a lower fluorescence intensity.

At pH 4.0, comparable fluorescence curves as a function of time were observed as at pH 7. In contrast to what one might expect, the difference between the surface charges at these two pH values had no significant effect on the fluorescence *vs.* time curves, and therefore on the adsorption behaviour.

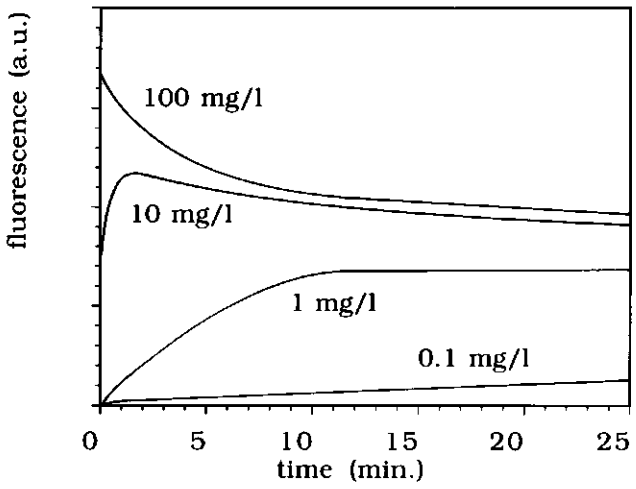

Figure 4.6. *The fluorescence intensity $F(0^0)$ as a function of time for different porphyrin concentrations in 10 mM phosphate buffer pH 7.*

According to Ward and Tordai [1946], at low surface coverages a diffusion controlled adsorption process can be described by

$$M = 2c_0\sqrt{Dt/\pi} \qquad (4.1)$$

in which M is the adsorbed amount (g m^{-2}), c_0 the porphyrin concentration (g m^{-3}), D the diffusion coefficient ($m^2\ s^{-1}$) and t the adsorption time (s). In figure 4.7 the relative fluorescence intensity, F_t / F_{max}, is shown as a function of the square root of time in order to check whether the observed fluorescence is caused by a diffusion-controlled adsorption process. The initial slope is indeed linear up to 4 minutes.

From the way in which the fluorescence signal increases, an important conclusion can be drawn: all fluorescence stems from adsorbed molecules; the contribution of molecules in solution is negligible. If this would not be the case, the fluorescence signal would increase step-wise at t = 0 and the extrapolated curve would not go through the origin. The curve shown in figure 4.7 is representative for all the measurements with a porphyrin

concentration of 1 mg/l, irrespective of the pH of the solution or the viscosity.

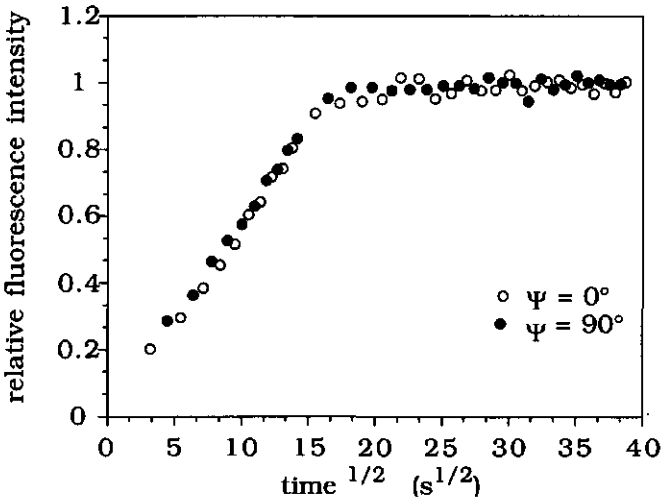

Figure 4.7. *The relative fluorescence intensity F_t / F_{max} as a function of (time)$^{1/2}$ for Ψ is 0° and 90°. Porphyrin concentration 1 mg/l, pH 4.0.*

Another interesting observation made was that the fluorescence intensities in 80% (v/v) glycerol were remarkably higher than in water. It is known that the fluorescence quantum yield can vary with the solvent [Lakowicz, 1963]. Probably the fluorescence quantum yield of the H_2TMPyP molecules in glycerol is higher than that in water (0.047 [Kalyanasundaram, 1984]).

4.3.2. Orientation measurements and mobility of adsorbed molecules

In figure 4.6 the fluorescence intensity as a function of time was shown for different porphyrin concentrations. As stated before, the decrease in fluorescence intensity for a porphyrin concentration of 100 mg/l is not the result of reorientation of the molecules in the adsorption layer. This follows from the data given in figure 4.8. In this figure the four different polarization

combinations $F_{\perp}(0)$, $F_{//}(0)$, $F_{\perp}(90)$ and $F_{//}(90)$ of the fluorescence are shown. All four fluorescence intensities exhibit the same time dependence. This means that the ratios between the fluorescence polarizations are approximately constant. In case of a reorientation process this would not be the case: two of the polarization combinations would decrease, while the other two would increase. Therefore, changes in the orientation distribution of the porphyrin molecules are not the cause of the decrease in fluorescence observed for 100 mg/l. At the lower porphyrin concentrations of 10 and 1 mg/l the ratios of the four polarization combinations are also constant in time. Therefore, at these concentrations reorientation does not occur either.

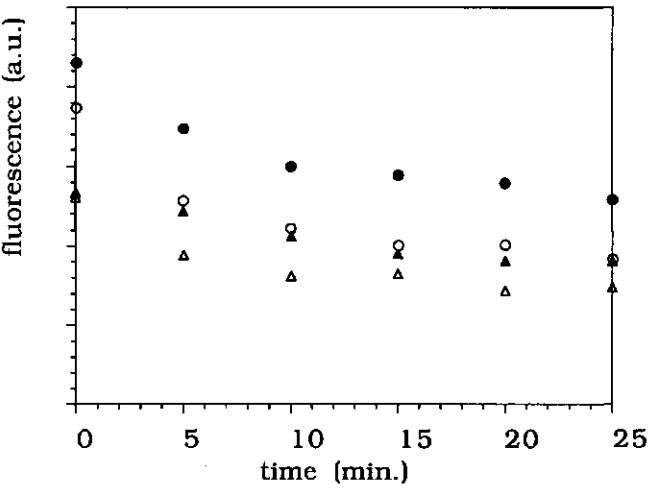

Figure 4.8. *The decrease in fluorescence intensity for the four polarization combinations as a function of time;* ○ $F_{\perp}(0)$, △ $F_{//}(0)$, ● $F_{\perp}(90)$ *and* ▲ $F_{//}(90)$. *Porphyrin concentration 100 mg/l, 10 mM phosphate buffer pH 7.*

For all porphyrin concentrations studied it was found that the fluorescence signal is polarized, i.e. $F_{//}(\Psi) \neq F_{\perp}(\Psi)$ (see for example figure 4.8). From this it can be concluded that mobility of the adsorbed porphyrin molecules on a time scale much faster than the fluorescence life time can be ruled out, since that would lead to a complete loss of polarization (see equation (2.39)).

In chapter 2 it was shown that the fluorescence signal as a function of the polarization of the incident light beam can be written as $F(\Psi) = A + B\cos^2\Psi$. Theoretical curves for $F(\Psi)$ are shown in figure 4.9a for sharp distributions with θ = 0°, 45° and 90°, and for a random orientation. For the components of the evanescent wave ε_x, ε_y and ε_z values of 0.464, 1.082 and 1.009 were used, respectively. These values were obtained using equations (2.3), with n_1 = 1.518 (refractive index of glass), n_2 = 1.333 (refractive index of the solution) and θ_i = 70°. The value for ε_z has been corrected for the adsorption layer according to Thompson [1984]: it is assumed that the point of total reflection is at the interface between the adsorption layer and the solution. For the adsorption layer a refractive index of 1.4 has been used.

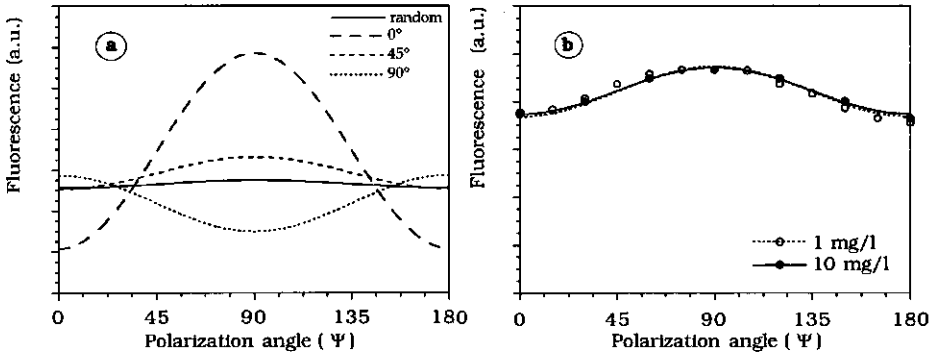

Figure 4.9. *Fluorescence as a function of the polarization angle Ψ of the incident light beam.* ***a)*** *Theoretical curves.* ***b)*** *Experimental points for 1 and 10 mg/l H_2TMPyP in 10 mM phosphate buffer pH 7. The curves through the points are obtained by fitting with $F(\Psi) = A + B\cos^2(\Psi)$.*

Experimental points obtained with TIRF are presented in figure 4.9b. For adsorption from 1 mg/l and 10 mg/l H_2TMPyP solutions practically the same results were found. The good fit of the experimental points with a linear function of $\cos^2\Psi$ proves that the fluorescence stems really from molecules which are excited by the evanescent field and not by stray light of the incident laser beam. Comparing figure 4.9b with the theoretical curves of figure 4.9a, it seems that for both porphyrin concentrations there is an average tilt angle of about 45° between the porphyrin plane and the sorbent

surface. From $F(\Psi)$ alone it is not possible to assess the broadness of the orientation distributions.

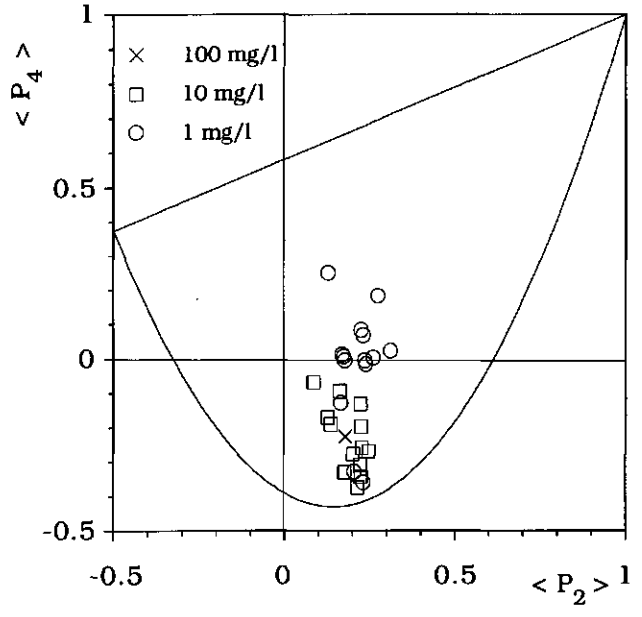

Figure 4.10. *Combinations of $\langle P_2 \rangle$ and $\langle P_4 \rangle$ for different concentrations of H_2TMPyP. The points were obtained at pH values of 4 and 7 and at different viscosities of the solution. The physically realistic combinations of $\langle P_2 \rangle$ and $\langle P_4 \rangle$ are within the area marked by drawn lines.*

At $H_2TMPyPI_4$ concentrations of 1, 10 and 100 mg/l $F_{\perp}(0)$, $F_{//}(0)$, $F_{\perp}(90)$ and $F_{//}(90)$ have been measured. From the values obtained, the order parameters $\langle P_2 \rangle$ and $\langle P_4 \rangle$ have been calculated according to the method explained in sections 2.3.3 and 3.1.3. The results are shown in figure 4.10. All $(\langle P_2 \rangle;\langle P_4 \rangle)$ combinations obtained were found to be in the physically realistic area. The values for $\langle P_2 \rangle$ and $\langle P_4 \rangle$ for a solution concentration of 1 mg/l are around 0.2 and 0.0, respectively. In the case of a concentration of 10 mg/l $\langle P_2 \rangle$ and $\langle P_4 \rangle$ are around 0.2 and -0.2, respectively. The orientation distribution functions corresponding with the points in figure 4.10 are shown in figures 4.11 and 4.12. In these figures $N(\theta)$ is given as a function of θ, therefore the surface area below the curves is not constant. This is because the orientation distribution is normalized with a weight factor $\sin\theta$ (see equation 2.27). The area below curves of

$N(\theta)\sin\theta$ *v s.* θ between $\theta = 0°$ and π is equal to 1. At a porphyrin concentration of 0.1 mg/l orientation distributions could not be obtained, because the fluorescence signal was too weak.

If the rotational mobility of the molecules in the adsorption layer would be of the same time scale as the fluorescence life time, τ_f, we would expect a systematic effect of the viscosity of the solvent on the obtained orientation distribution functions (see section 2.3.4). However, figures 4.11 and 4.12 clearly show that there is no correlation between the viscosity and the shape of the calculated orientation distributions. Mobility on a much shorter time scale than τ_f has been excluded before (section 4.3.2). Therefore, it is tentatively concluded that the rotational mobility of the adsorbed molecules is relatively slow. This conclusion is supported by considering the estimated rotation correlation time of the porphyrin molecules in solution: $\tau_{rot} \approx 0.4$ -18 ns corresponding with a relative viscosity of 1-45. These values have been obtained according to $\tau_{rot} = 8\pi\eta R^3/6kT$ [Axelrod, 1979; Van Holde, 1985] assuming that the porphyrin molecules are spherical. These rotation correlation times are already close to τ_f ($\approx$ 6 ns). For the adsorbed state we expect a much higher value (in the order of 100 times higher) for τ_{rot}.

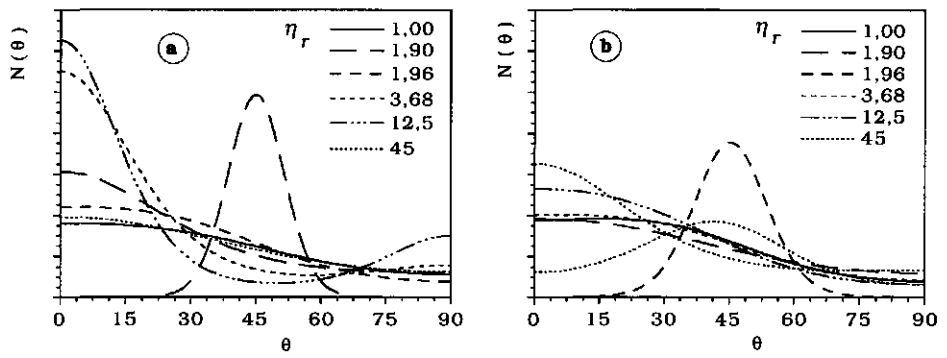

Figure 4.11. ***a)*** *Orientation distributions for 1 mg/l H_2TMPyP in solutions of different viscosities at pH 4.* ***b)*** *Orientation distributions for 1 mg/l H_2TMPyP in solutions of different viscosities at pH 7.*

Furthermore, the obtained orientation distribution functions appear not to depend on the pH of the solution and therefore not on the surface charge density of the sorbent. At pH 4 and pH 7 and an electrolyte

concentration of 10^{-2} M, the surface charge density of SiO_2 is approximately -0.01 C m^{-2} and -0.1 C m^{-2}, respectively [Tadros and Lyklema, 1968].

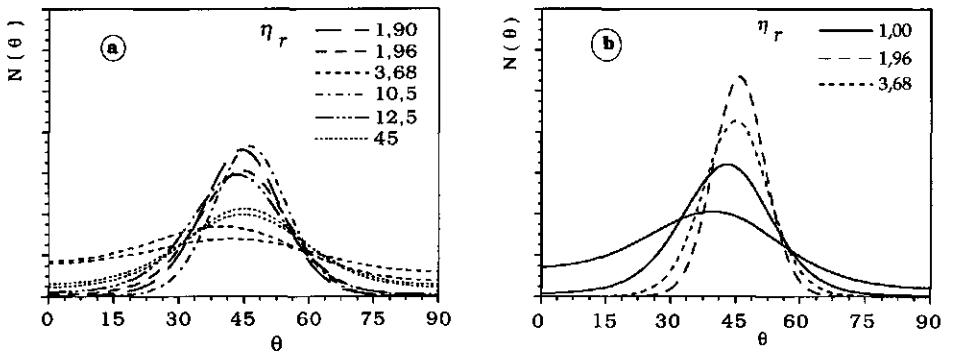

Figure 4.12. a) *Orientation distributions for 10 mg/l H_2TMPyP in solutions of different viscosities in water.* ***b)*** *Orientation distributions for 10 mg/l H_2TMPyP in solutions of different viscosities at pH 7.*

Although the scatter in the obtained order parameters, especially in $\langle P_4 \rangle$, is rather high (see figure 4.10), a certain trend in the orientation distribution with porphyrin concentration in solution can be distinguished. At 1 mg/l the orientation distribution is almost random: on average the combination $(\langle P_2 \rangle; \langle P_4 \rangle)$ is (0.2;0.0) whereas for a random orientation this would be (0.0;0.0). The value of $\langle P_2 \rangle$ and also figures 4.10a and 4.10b indicate that the distribution is not completely random. At concentrations of 10 and 100 mg/l the adsorbed molecules show clearly a preferential orientation angle θ of 45 - 46°. The value of $\langle P_4 \rangle$ (-0.2) indicates a sharper distribution than at 1 mg/l. For a really sharp distribution with θ = 45°, $\langle P_4 \rangle$ would amount to -0.41.

The difference between the orientation distributions at solution concentrations of 1 mg/l and 10-100 mg/l can be related to the degree of surface coverage. At 1 mg/l the adsorbed amount is approximately 0.8 mg m^{-2}, corresponding to an area per molecule of 2.5 nm^2. At 10 mg/l and 100 mg/l these values are about 1.5 mg m^{-2} corresponding to 1.3 nm^2/molecule and 1.8-1.9 mg m^{-2} corresponding to 1.1 nm^2/molecule, respectively. At 1 mg/l (a surface coverage of ca. 30%) there is enough room left at the surface for the molecules to adopt any orientation angle θ without being hindered by neighbouring molecules. This is not the case at the higher degrees of

occupancy. Apparently, the higher degree of ordening at 10 and 100 mg/l is due to intermolecular lateral interactions in the adsorption layer. The observed effect of porphyrin degrees of occupancy on the orientation distribution suggests that adsorption does not occur in clusters, otherwise also at low surface coverages this ordening by intermolecular interactions would occur.

Finally, it is interesting to mention the work of Giannelis [1990]. He studied the adsorption of CuTMPyP from aqueous solutions onto hectorite and fluorohectorite with ESR spectroscopy. ESR spectra were recorded for different sample orientations with respect to the direction of the magnetic field. It was concluded that in the case of hectorite the molecular plane of the porphyrin is oriented parallel to the silicate layers. In the case of fluorohectorite the adsorbed CuTMPyP molecules were found to be oriented with a tilt angle of 45° to the layers. The results we obtained with higher concentrations of H_2TMPyP are comparable with those obtained with fluorohectorite.

4.4 Conclusion

In this chapter the adsorption behaviour of tetramethyl-pyridiniumporphyrin (H_2TMPyP) on silica was presented. Different adsorbed amounts were observed for adsorption from 10 mM phosphate buffer, 0.1 M KNO_3 solution and water. The method for obtaining the orientation distribution functions of adsorbed chromophores, as described in chapter 2 of this thesis, gives statisfying results. However, the reproducibility is still somewhat poor. The obtained orientation distribution function of adsorbed H_2TMPyP molecules on silica depends on the solution concentration. At low concentration, the H_2TMPyP molecules are more or less randomly oriented, while at high concentrations a broad distribution around an angle of 46° between the porphyrin plane and surface was found. The fact that the fluorescence is polarized and the results of measurements with different solution viscosities show that the mobility of the adsorbed porphyrin molecules is on a much larger time scale than the fluorescence life time.

Chapter 5

Influence of the electrical potential of the interface on the adsorption of proteins

Abstract

The adsorption behaviour of various proteins (serum albumin, lysozyme, ribonuclease A, superoxide dismutase, myoglobin and α-lactalbumin) as a function of an externally imposed interfacial potential has been studied by reflectometry. The sorbent surface was a semi-conducting indium tin oxide (ITO) layer deposited on a silicium wafer. At pH 4 and pH 7 the influence of the potential of the interface is surprisingly small and the same for all proteins studied, irrespective of their net charge and structure stability. At pH 9.9 the effect of variation of the potential is somewhat more pronounced for lysozyme and ribonuclease A. The results suggest that electrostatic interactions play a minor role in the process of protein adsorption on hydrophilic surfaces, in contradiction to what has been concluded from earlier studies.

5.1. Introduction

The adsorption of proteins at interfaces is a widespread phenomenon both in natural and synthetic systems. In many medical and technical applications interactions between proteins and interfaces have significant consequences that sometimes are desired and in other cases are undesirable. For example, proteins are often used as stabilizers of colloidal dispersions in pharmaceuticals and food products. In diagnostic tests, biosensors and enzyme-electrodes, immunoglobulins or enzymes are adsorbed on solid surfaces. On the other hand, the highly undesired process of biofouling (e.g. in food processing equipment, artificial kidney devices, units for the desalination of seawater and on ship hulls) generally starts with the adsorption of proteins. Subsequently, biological cells (like bacteria) may adhere on top of the adsorbed pre-cellular layer [Hallström *et al.*, 1981]. Similar phenomena are at the basis of plaque formation on teeth [Ten Cate

et al., 1984] and thrombus development on cardiovascular implant materials [Mulvihill *et al.*, 1985; Sedlácek *et al.*, 1979].

The above-mentioned examples illustrate that it is of crucial importance to find ways to control the process of protein adsorption. This process is complex and still not fully understood. Over the past years in our department the adsorption behaviour of various kinds of proteins on adsorbents of different hydrophobicities and surface charges has been investigated [Norde, 1986; Norde *et al.*, 1986; Shirahama *et al.*, 1990; Norde *et al.*, 1991; Norde and Lyklema, 1991]. From this it has been concluded that the adsorption behaviour of proteins with a high internal stability, the so-called *"hard"* proteins, is governed by electrostatic and hydrophobic interactions between protein and sorbent surface. These proteins do not adsorb on hydrophilic surfaces unless there is electrostatic attraction. On hydrophobic surfaces these proteins do adsorb and might undergo structural changes upon adsorption. Protein molecules with a low internal stability, the *"soft"* proteins, tend to adsorb on all surfaces irrespective of electrostatic interactions, due to a gain in conformational entropy resulting from adsorption.

In these studies the surface charges were either fixed or determined by pH and electrolyte concentration of the solution. In the latter case variation of the surface charge by changing the pH of the solution also affected the charge of the protein molecules and hence their structure stability. Therefore, electrostatic interactions between surface and protein molecules was not the only variable in those studies. Morrissey *et al.* [1976] investigated the effect of the surface potential of the adsorbent on the adsorbed amounts and the compactness of the adsorbed layer of the blood proteins fibrinogen, γ-globulin and serum albumin. These authors varied the potential of a Pt electrode in positive direction *after* adsorption of protein had taken place at the open circuit potential (in literature often called the relaxed or equilibrium potential). The adsorbed amounts and the extension of the adsorption layers were monitored simultaneously with ellipsometry. For the proteins studied, all negatively charged at the pH value used (pH 7.4), the influence of the imposed potential on the adsorbed amounts was negligible until a certain "onset potential" was reached. Above this potential (+0.4 - +0.8 V *vs.* SCE, depending on the protein) additional adsorption took place. The conformation of all three proteins was changed by altering the potential of the surface. Desorption never occurred after applying a potential.

In this chapter we present the adsorption behaviour of various proteins (both "hard" and "soft" proteins, of different sizes and isoelectric points) as a function of the electrical potential of the interface. The technique used to study the properties of adsorbed proteins is reflectometry, which has proven to be suitable to monitor protein adsorption [Dijt *et al.*, 1990; Shirahama *et al.*, 1991]. The silicium wafers used in the experiments are coated with a semiconducting layer of indium tin oxide (ITO), which makes it possible to vary the potential of the interface systematically, keeping the solution composition constant. Following this approach it might be well possible to determine the relative importance of electrostatic interactions in the process of protein adsorption.

5.2. Materials and Methods

5.2.1. Materials

Bovine serum albumin (BSA), lysozyme (LSZ) from hen's egg, ribonuclease A (RNase) from bovine pancreas, bovine liver superoxide dismutase (SOD), myoglobin (MGB) from horse heart and α-lactalbumin (αLA) from bovine milk were obtained from Sigma Chemical Company. All proteins were used without further purification. Some characteristics of the proteins relevant to their adsorption behaviour are listed in table 5.1.

All other chemicals used were of analytical grade. Water was purified using a Millipore purification system, involving reverse osmosis and subsequent percolation through charcoal and a mixed-bed of ion resins.

Buffer solutions used are phosphate for pH 7, acetate for pH 4 and borax for pH 10; the concentration of the buffers was 0.01 M.

In the reflectometer experiments the sorbent surface was indium tin oxide (ITO), containing 10% Sn. This material is deposited in a thin layer (130 nm or 140 nm) onto silicium wafers by LCTV-Philips, Eindhoven, The Netherlands. ITO is a semi-conducting material; the sheet resistance of the ITO layers is 75±4 Ω/□. The mean roughness is 0.32 nm, measured with Atomic Force Microscopy. From streaming potential measurements it was found that the isoelectric point (i.e.p.) of the ITO layer deposited on Si, is at pH 2.9 ± 0.2. Contact angle measurements were performed with purified water, 10 mM acetate buffer pH 4 and 10 mM phosphate buffer pH 7.0 and

are 11° ± 2°, 21° ± 2° and 7° ± 2° respectively, revealing that the ITO surface is rather hydrophilic.

Table 5.1. *Some physical-chemical properties of the proteins used.*

	BSA	LSZ	RNase	MGB	αLA	SOD
Molar mass (g/mole)	67,000	14,600	13,680	17,800	14,200	15,500
Dimensions (nm)	11.6× 2.7×2.7	4.5×3.0 ×3.0	3.8×2.8 ×2.2	4.5×3.5 ×2.5	3.7×3.2 ×2.5	3.3×3.6 ×6.7
Diff. coeff. (m^2/s)	7.4× 10^{-11}	1.04× 10^{-10}	1.26× 10^{-10}	1.10× 10^{-10}	1.06× 10^{-10}	
Gibbs energy of denaturation(J/g)	?[a]					?[a]
heat[b]		-4.1	-3.2	-2.8	-1.5	
denaturant[b]		-4.0	-3.9	-3.1	-1.9	
I.e.p. (pH units)						
literature values[c]	4.7	11.1	9.4	7.0	4.3	4.6
measured[d]	4.8	>10	9.3	7.2		

[a] BSA has a low structure stability; F. Peters, 1985; SOD has a relatively high structure stability [Wei, 1991].

[b] Privalov, 1979.

[c] Norde *et al.*, 1991; Norde and Favier, 1992; Wei, 1991.

[d] Measured by 2D-Isoelectric Focussing (2D-IEF) in the buffers used in this study (± 0.2 pH unit).

5.2.2. Reflectometer experiments

The experimental set-up is schematically shown in figure 5.1. A polarized He/Ne laser beam (1) enters the cell through a 45° glass prism (2). The laser beam is reflected at the sorbent surface (3) at an angle of incidence of 70.6°. The reflected light beam leaves the cell through a second 45° prism (2) and is split (4) into its parallel and perpendicular polarized components (with respect to the plane of incidence). Both components ($I_{//}$ and $I_{\perp}$) are detected by photodiodes (5). The reflection intensities are converted by an analogue signal processor (6) into a signal S ($S = I_{//} / I_{\perp}$). Any material adsorbed at the interface that has a refractive index different

from that of the solution and the sorbent material will change the polarization of the reflection and thus the signal S. It has been shown that there is a linear relationship between a change in the adsorbed amount Γ

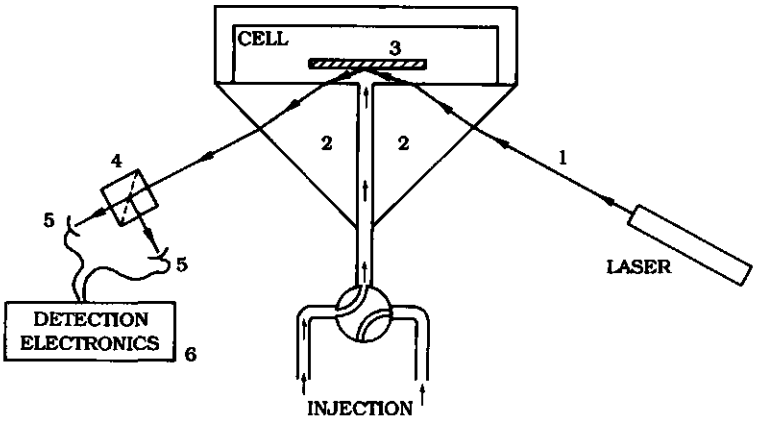

Figure 5.1. *Schematic diagram of the reflectometer set-up. For explanation of the numbers see text.*

and a change in S [Dijt *et al.*, 1990]. From computer simulations using the theory for reflection in multilayer systems [Hansen, 1968; Born and Wolf, 1975] it was found that an adsorbed amount of 1 mg/m^2 of protein corresponds to a change in S of $-0.0255 \times S_0$ for a deposited ITO layer of 130 nm and a change in S of $-0.0193 \times S_0$ for an ITO layer of 140 nm, with S_0 the reflectometer signal in the absence of a protein adsorption layer.

The electrical potential of the ITO layer was varied using a home-built potentiostat. A Pt wire counter electrode and a small Ag/AgCl/saturated KCl reference electrode (MI-402, Microelectronics, Inc. USA; potential 193 mV *vs.* NHE) were placed in the cell. The presence of an amperometer in the electrical circuit makes it possible to monitor any electrical currents during measurements.

Protein solutions are injected into the cell (originally filled with pure buffer solution) by a so-called "impinging jet" method: the solution flows through a cylindrical channel (radius 0.95 mm) between the two prisms into the cell (see figure 1). The channel is perpendicular to the sorbent surface and the intersection of its symmetry axis and the surface is called the

"stagnation point". The distance between the end of the channel and the surface is 1.6 mm. The reflection point of the laser beam coincides with the stagnation point. The volume flux in the experiments was 2.0×10^{-8} m^3/s.

The flux J_p of protein molecules to the surface in the stagnation point is given by [Dabros and Van der Ven, 1983; Dijt *et al.*, 1990]:

$$J_p = 0.283 \nu^{-1/3} \Phi^{2/3} R^{-5/3} D^{2/3} c_p \qquad (5.1)$$

were ν is the kinematic viscosity, Φ the volume flux, R the radius of the flow channel, D the diffusion coefficient of the protein in solution and c_p the bulk concentration of the protein. For more details concerning the geometry and hydrodynamics of the system the reader is referred to Dijt *et al.* [1990].

5.2.3. Voltammetric experiments

Experiments were carried out in a three-electrode cell with a Pt wire as counter electrode and an Ag/AgCl/3.5 M KCl reference electrode (potential 193 mV *vs.* NHE). As a working electrode either a Pt wire or an ITO/silicium wafer was used. Cyclic voltammetric curves were measured at a scan rate of 10 mV/s in 0.1 M KNO_3 solution. As an electroactive species methylviologen (MV) was used in a concentration of 5×10^{-3} M. Before each experiment, the solution was stirred and flushed with nitrogen. During the measurements N_2 was passed over the solution. Potentials were applied from a Princeton Research Polarographic Analyzer model 174A and *i-E* curves were recorded on a Omnigraphic 2000 Recorder.

Open circuit potentials of the ITO/silicium wafers were measured *vs.* a saturated calomel electrode (SCE, potential 242 mV *vs.* NHE) using a pH/mV meter.

All experiments were conducted at room temperature (20 °C).

5.3. Results

5.3.1. Electrical potential of the ITO/solution interface

Figure 5.2 shows the open circuit potential (or equilibrium potential) of the indium tin oxide layer on a silicium wafer as a function of the pH. The isoelectric point of the ITO/solution interface is at pH 2.9.

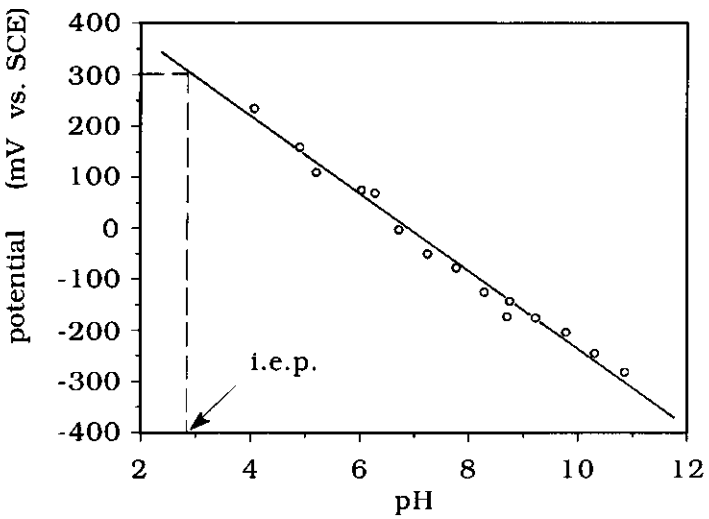

Figure 5.2. *Equilibrium potential of the ITO/silicium wafer as a function of pH. The isoelectric point (pH 2.9) is indicated.*

In order to test whether an externally imposed potential is really established at the ITO/solution interface, we conducted some voltammetric experiments. Figure 5.3 shows the current density-potential (*i-E*) curves for a Pt wire electrode and an ITO/silicium wafer in a 5×10^{-3} M methylviologen/0.1 M KNO_3 solution. The oxidation and reduction peaks obtained with the Pt wire electrode are centred around a potential of -641 mV *vs.* Ag/AgCl/3.5 M KCl, in good agreement with the literature value of the standard redox potential E^0 for the MV^+/MV^{2+} couple (-0.45 V *vs.* NHE; Harriman and Porter, 1982). The peaks obtained with the ITO/silicium wafer are centred around -743 mV *vs.* Ag/AgCl, i.e. ca 100 mV more negative than for the Pt electrode. This difference must be due to the relatively high resistance of the ITO layer, leading to a potential loss between the point where electrical contact is made and the part of the ITO-layer in solution. The observation that the separation between the reduction and oxidation peaks is larger for the ITO/silicium electrode than for the Pt electrode indicates that the electrode kinetics are slower at the ITO surface. Anyway, these measurements show that it is possible to apply an external potential at the ITO/solution interface, although, in cases of electrical

current through the system, the absolute value of the potential at the ITO/solution interface is somewhat lower than the chosen potential.

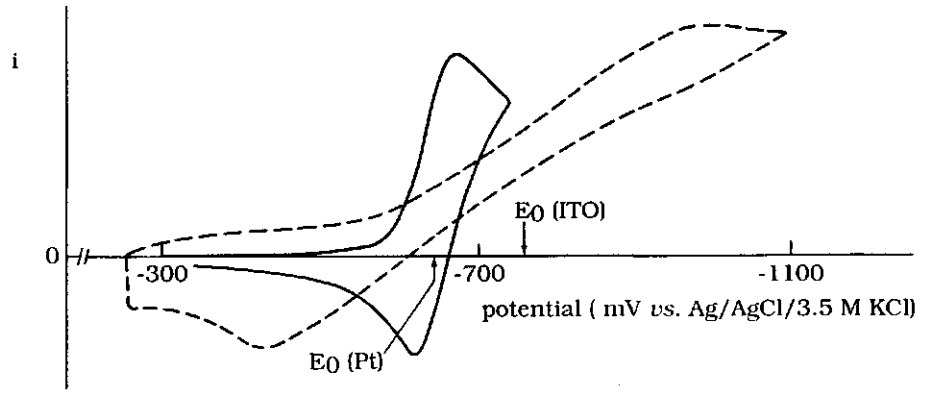

Figure 5.3. *Cyclic voltammograms of a Pt wire electrode (drawn lines) and a ITO/silicium electrode (broken lines) in a 5 x 10^{-3} M methylviologen/0.1 M KNO_3 solution. Scan rate 10 mV/s.*

An interesting observation we made in the reflectometer experiments is the following. Every time an external potential was applied to the ITO layer a change of the signal S, ΔS, was observed. The relation between the applied potential and ΔS is practically linear, as shown in figure 5.4. The change in S was found to be completely reversible, and independent of the presence of (adsorbed) protein and the type and concentration of electrolyte. Therefore, the change in signal on applying a potential to the surface must be attributed to a change in the optical properties of the ITO layer due to a change in the concentration of charge carriers in the solid. Variations in the ionic composition at the solution side of the electric double layer do not significantly affect S. The change in S is practically instantaneous for the buffer concentrations used in this study, *i.e.* much faster than the change in S due to protein adsorption. The mentioned change in the optical properties of the ITO layer may be a change in the refractive index of the ITO layer. From computer simulations, using the theory for reflection in multilayers [Hansen, 1968; Born and Wolf, 1975], we inferred that the measured change in the reflectometer signal, ΔS, corresponds to a change in the refractive

index of the ITO layer of 0.001. Such a small change has hardly any effect (< 1%) on the calibration factor for determination of the adsorbed amounts.

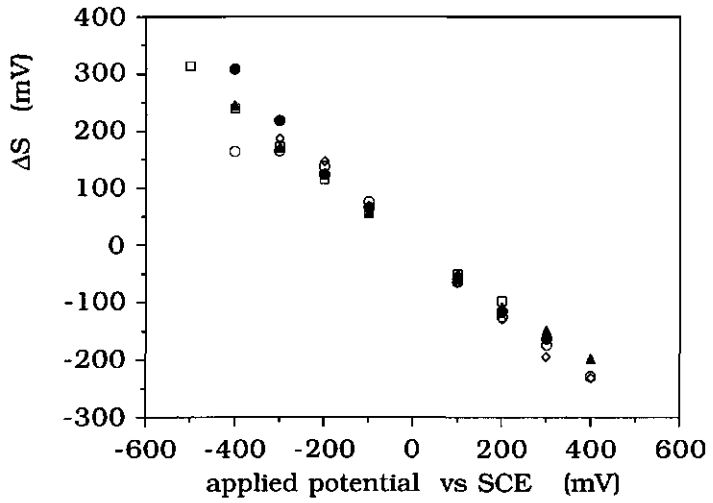

Figure 5.4. *Change of the reflectometer signal S as a result of imposing an external potential to the ITO/silicium wafers. Electrolytes used (0.1 M):* ● *KCl;* ▲ *KNO_3;* □ *NH_4OH ;* ◇ *$Mg(SO_4)_2$ and* ○ *KCl (0.001M).*

5.3.2. Protein adsorption at pH 7

The amounts of the proteins adsorbed after 15 minutes on the ITO layer at pH 7.0 are shown in figure 5.5. At this pH value the ITO surface is negatively charged. The plateau values for adsorption, Γ_{max}, are qualitatively in agreement with the electrostatic interactions between proteins and surface except for BSA: LSZ is the most positively charged protein at pH 7 and its plateau value amounts to 2.0 mg/m^2; RNase, which is less positively charged, has a lower plateau value of about 1.4 mg/m^2 and MGB, at pH 7.0 in its isoelectric point, has a Γ_{max} of 1.3 mg/m^2. For the negatively charged αLA we hardly found any adsorption. SOD, also negatively charged, does not adsorb at all on ITO at pH 7.0, and therefore is not shown in figure 5.5. In contrast to αLA and SOD, the negatively charged BSA molecules do adsorb in substantial amounts on the negatively charged hydrophilic ITO surface. Besides the hydrophobic effect, the driving force for BSA adsorption at pH 7 on ITO might be caused by structural rearrange-

ments leading to a higher conformational entropy in the protein molecule. The same order in adsorbed amounts for these proteins for adsorption on silica and glass at pH 7 has been reported by Norde and co-workers [Shirahama *et al.*, 1990; Norde *et al.*, 1991; Norde and Anusiem, 1992].

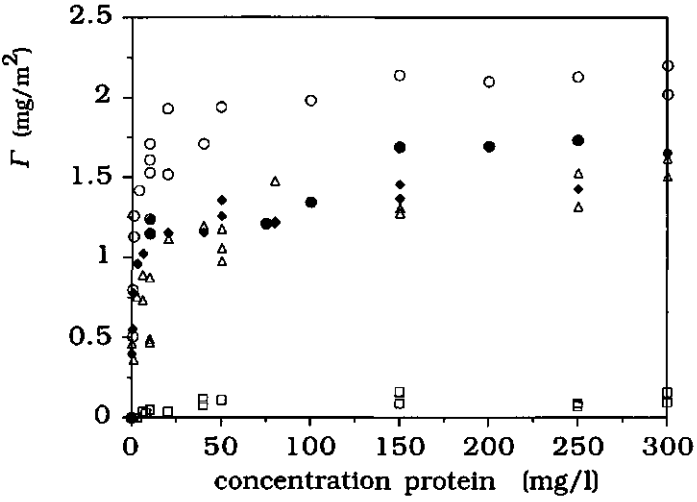

Figure 5.5. *Amounts of the various proteins adsorbed after 15 minutes at the equilibrium potential of the ITO/solution interface at pH 7 (0.01 M phosphate buffer).* ● *BSA;* ○ *LSZ;* ◆ *RNase;* △ *MGB;* □ *αLA. At this pH SOD does not adsorb.*

In figure 5.6 the adsorption of the proteins at pH 7 is given as a function of time. The protein concentration was 10 mg/l. The initial adsorption rate $(d\Gamma / dt)_{t\to 0}$ can be compared with the flux J_p of protein molecules to the surface (see equation 5.1). With $\nu = 10^{-6}$ m^2 s^{-1}, $\Phi = 2.0 \times 10^{-8}$ m^3 s^{-1}, $R = 9.5 \times 10^{-4}$ m and D from table 5.1 the flux has been calculated and the result is also included in figure 5.6. The electrical charges of the protein molecules are roughly indicated by plus and minus signs. For all proteins $(d\Gamma / dt)_{t\to 0}$ is smaller than J_p. Apparently, not every protein molecule that arrives at the surface is attached. We can define a "sticking probability" p_{ads} as the fraction of protein molecules arriving at the surface which do adsorb. In table 5.2 the p_{ads} values are given for the proteins arriving at the ITO surface, and also for protein adsorption at negatively charged silica and polystyrene-coated silica surfaces [Norde *et al.*,

1991; Norde and Anusiem, 1992]. For adsorption on ITO the same trend and qualitatively comparable results are found as for silica, *i.e.* the greater the electrostatic attraction, the higher the probability factor, even for BSA.

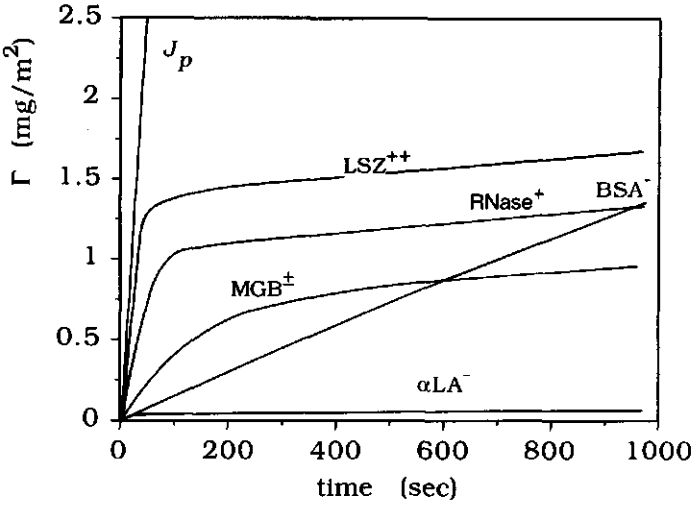

Figure 5.6. *Amounts of the proteins adsorbed as a function of time at pH 7. The flux J_p of the protein molecules to the sorbent surface is indicated. (Protein concentrations 10 mg/l; 0.01 M phosphate buffer.)*

For αLA p_{ads} is very low at both ITO and silica, but at the hydrophobic polystyrene-coated silica surface, despite the unfavourable electrostatic interaction, p_{ads} for this protein is higher than for LSZ and RNase. This can be related to the relatively low structural stability of αLA (see table 5.1), so that structural rearrangements in the molecule contribute to the Gibbs energy of adsorption [Norde, 1986; Norde *et al.*, 1986, 1991]. The low p_{ads} for adsorption of αLA at the negatively charged ITO and silica surfaces shows that for this small protein (its molecular weight is five times smaller than that of BSA!) the contribution from structural changes to the adsorption affinity does not compensate for the electrostatic repulsion and hydrophilic dehydration. This and the fact that SOD, a negatively charged structure-stable protein, does not adsorb on ITO at pH 7.0 is in line with our observations that the nature of the ITO surface is, like that of silica, hydrophilic.

Table 5.2. *Fractions p_{ads} of the protein molecules arriving at various sorbent surfaces that adsorb at pH 7.0. (All sorbent surfaces are negatively charged; the charge of the protein molecules is roughly indicated.)*

	ITO[a]	silica	PS/silica[b]
BSA$^-$	0.04	0.03[c]	-
RNase$^+$	0.29	0.34[b]	0.55
MGB$^\pm$	0.11	-	-
SOD$^-$	0	-	-
αLA$^-$	< 0.01	0.02[b]; 0.02[c]	0.82
LSZ^{++}	0.66	0.47[b]; 0.60[c]	0.65

[a] This study; 0.01 M phosphate buffer pH 7, T = 293 K

[b] Norde *et al.*, 1991; 0.05 M phosphate buffer pH 7, T = 298 K

[c] Norde and Anusiem, 1992; 0.01 M phosphate buffer pH 7.0, T = 293 K

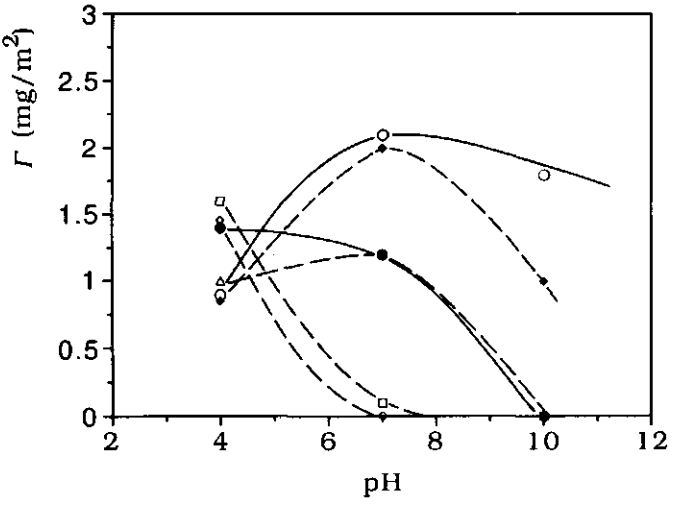

Figure 5.7. *Amounts of the various proteins adsorbed on ITO after 15 minutes as a function of pH. Protein concentrations 10 mg/l.* ● *BSA;* ○ *LSZ;* ◆ *RNase;* △ *MGB;* □ *αLA and* ◇ *SOD.*

In figure 5.7 the amounts adsorbed of various proteins after 15 minutes of adsorption on ITO, are shown as a function of the pH (for i.e.p.'s of the proteins see table 5.1). The protein concentration was 10 mg/l. The data strongly suggest that electrostatic interactions between protein and the surface are a prominent factor in the adsorption behaviour. Even for the "soft" protein BSA at pH 9.9, structural rearrangements and the hydrophobic effect do apparently no longer outweigh the electrostatic repulsion. The same pH dependence was found in the adsorbed amounts of a number of these proteins on silica [Shirahama *et al.*, 1990, Norde *et al.*, 1991; Norde and Anusiem, 1992].

5.3.3. Protein adsorption as a function of applied potential

We studied the adsorption of the various proteins upon application of an external potential at different pH values. The adsorbed amounts after 15 minutes are shown in figures 5.8, 5.9 and 5.10.

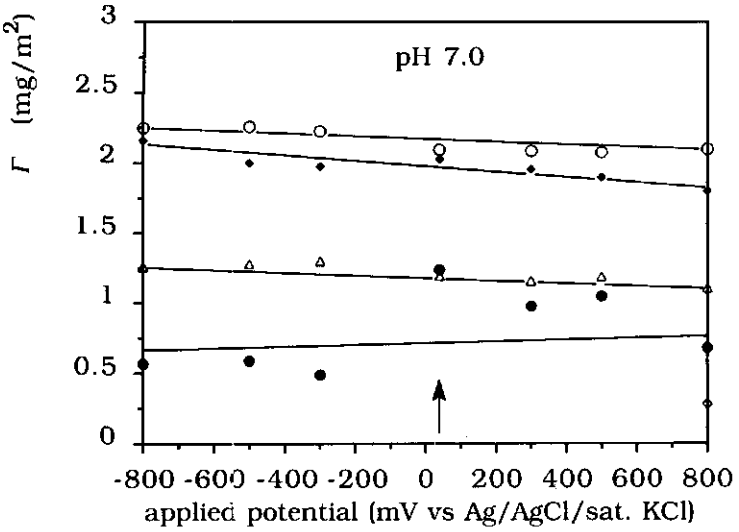

Figure 5.8. *Adsorbed amounts after 15 minutes as a function of an externally applied potential at pH 7.0 (0.01 M phosphate buffer). Symbols as in figure 5.7. Points obtained at the equilibrium potential at this pH (+40 mV) are indicated.*

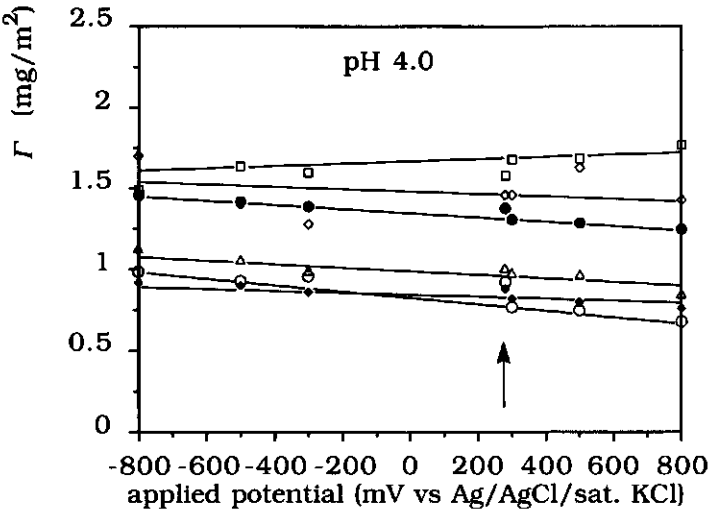

Figure 5.9. *Adsorbed amounts after 15 minutes as a function of an externally applied potential at pH 4.0 (0.01 M acetate buffer). Symbols as in figure 5.7. Points obtained at the equilibrium potential at this pH (+280 mV) are indicated.*

At pH 7.0 αLA does not or hardly adsorb, irrespective of the applied potential, and is therefore not shown in figure 5.8. SOD, negatively charged at this pH value, adsorbs only at an applied potential of +800 mV, but the adsorbed amount is rather small (0.28 mg/m²). In general, the influence of the applied potential on the adsorption process is surprisingly small at this pH, which is also reflected in the initial adsorption rates $(d\Gamma / dt)_{t\to 0}$ of the various proteins. Also at pH 4 for all proteins the influence of the applied potential is small (see figure 5.9). At pH 9.9 the adsorbed amounts of LSZ (i.e.p at pH 11.1) and RNase (i.e.p at pH 9.4) show a much stronger dependence on the applied potential (see figure 5.10). Hardly any dependence on the applied potential was found for potentials below +300 mV. Above +300 mV enhanced adsorption for both LSZ and RNase was observed. The other proteins, MGB, BSA, SOD and αLA, do not adsorb at all at this pH, irrespective of the applied potential.

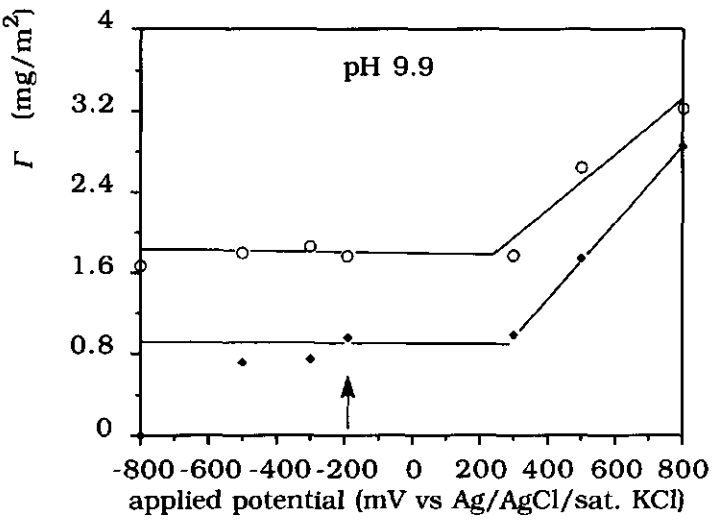

Figure 5.10. *Amounts adsorbed after 15 minutes as a function of the externally applied potential at pH 9.9 (0.01 M borax buffer). Symbols as in figure 5.7. Points obtained at the equilibrium potential at this pH (-190 mV) are indicated.*

5.4. Discussion

Before we discuss the above results in some detail it should be noted that the imposed potentials are referred to an Ag/AgCl/saturated KCl electrode. However, the potential difference between the ITO/solution interface and the bulk solution determines whether the protein molecules are electrostatically attracted or repelled when approaching the interface. From figure 5.2 it can be seen that at the i.e.p. of ITO (pH 2.9) the open circuit potential amounts to ca. +300 mV *vs.* SCE. This corresponds to a potential of ca. +350 mV *vs.* Ag/AgCl/saturated KCl. In the i.e.p. the potential difference between the sorbent surface and the bulk solution is zero. (Strictly speaking, at the i.e.p. the potential at the plane of shear, the zeta-potential, is zero with respect to the bulk solution. We assume that the point of zero charge and the i.e.p. are practically the same.) Therefore, imposed potentials below +350 mV *vs.* Ag/AgCl/saturated KCl correspond with negative surface charges and negative potentials with respect to the

bulk solution. Above +350 mV *vs.* Ag/AgCl/saturated KCl the surface charge and potential with respect to the bulk solution are positive.

From the observation that the adsorption of proteins hardly depends on the applied potential, one could wonder if the applied potentials are really established at the ITO/solution interface. However, the voltammetric results presented in figure 5.3 clearly show that this is indeed the case. This has been confirmed by experiments with the low molecular weight ionic surfactants sodium dodecylsulphate (SDS) and cetyl trimethyl ammonium bromide (CTAB). In contrast to the proteins, the adsorption behaviour of these surfactants do show a clear dependence on the applied potential.

BSA molecules have a large tendency to rearrange their structure upon adsorption. Therefore, for this particular protein it is not surprising that the adsorption behaviour is not very strongly affected by the electrical potential of the interface. At pH 4 BSA is slightly positively charged (i.e.p. at pH 4.7), so the trend that the adsorbed amount is lower when the applied potential is more positive (see figure 5.9) might be due to electrostatic interactions changing gradually from attractive to repulsive. At pH 7 the BSA molecules are negatively charged, and accordingly, the opposite trend is found. On the other hand, it is not clear why BSA does not adsorb at pH 9.9 when a positive potential is applied.

RNase and LSZ are both structure-stable proteins with i.e.p.'s at high pH values (see table 1); at pH 4 and at pH 7 both are positively charged. The ITO surface is rather hydrophilic and generally the hydrophilicity of a surface increases when an electrical potential is imposed on it. Therefore, it is expected on the basis of earlier studies that under these circumstances electrostatic interactions are dominating in the adsorption process. As the applied potentials are more positive, the adsorbed amounts are indeed somewhat lower. However, this is only a very small effect, not different from that observed for the adsorption of BSA at pH 4. Even if the surface charge (or potential with respect to the bulk solution) is positive (> +350 mV *vs.* Ag/AgCl/saturated KCl) RNase and LSZ still adsorb in considerable amounts, in contradiction with the earlier observations that structure-stable proteins do not adsorb on hydrophilic surfaces unless there is electrostatic attraction (see Introduction). At pH 9.9, both RNase and LSZ are close to their respective isoelectric points, so they possess almost equal numbers of positively and negatively charged groups. These proteins show the similar behaviour as a function of applied potential: a fairly constant adsorbed amount (0.8 and 1.5 mg/m^2 respectively) as long as the surface is negatively

charged (applied potential ≤ 300 mV) and a strong increase in adsorbed amounts with increasing positive charge of the surface.

SOD is a structure-stable protein, but also for this protein the influence of the applied potential on its adsorption behaviour is small. At pH 4 it is slightly positively charged (i.e.p. at pH 4.6) and no effect of the applied potential was observed. At pH 7 it is negatively charged and does not adsorb at any potential applied, except for + 800 mV, at which a small adsorbed amount of 0.28 mg/m^2 was found. At pH 9.9 this protein does not adsorb at all.

αLA, is a "soft" protein, with i.e.p. at pH 4.3. Although at pH 4 the protein molecule bears a small positive charge, the adsorbed amounts tend to be higher when the applied potentials are more positive, but again the effect is small. At pH 7 the protein hardly adsorbs (≤ 0.1 mg/m^2) and at pH 9.9 it does not adsorb at all. Comparing these results with those obtained with SOD, a "hard" protein of approximately the same size and i.e.p., no significant differences in adsorption behaviour are found (see figure 5.7).

MGB takes an intermediate position between the "soft" and "hard" proteins. At pH 4 it is positively charged, so this might explain the small decline in adsorbed amounts with increasing potential. However, at pH 7, i.e. at the i.e.p. of MGB, the same effect is observed. No adsorption was observed at pH 9.9, irrespective of the applied potential.

From the above discussion it is clear that most of the trends in the adsorbed amounts as a function of the applied potential can be explained in terms of electrostatic interactions, but the effects are much smaller than expected. For example, the earlier conclusion that structure-stable proteins do not adsorb on a hydrophilic surface in case of electrostatic repulsion seems to be refuted: e.g. LSZ also adsorbs at pH 7 when positive potentials are applied. Also, no pronounced differences in the adsorption as a function of interfacial potential are found between "soft" and "hard" proteins.

A cause for the relatively unimportant role of the applied potential and therefore of electrostatic interactions in the process of protein adsorption might be that protein molecules can adjust their charge when approaching a sorbent surface. If the surface is positively charged, the concentration of H^+ (OH^-) in the double layer is lower (higher) than in the bulk solution. This locally increased pH leads to a shift in the protein charge towards less positive/more negative values. The opposite holds for negatively charged surfaces. In other words, any electrical repulsion is compensated for by

adjustment of the charge of the protein molecules in the electrical double layer. This might explain for example why LSZ shows an enhanced adsorption at high positive potentials at pH 9.9: in the bulk solution the protein has a small positive charge, but this changes into a (small) negative charge near the surface.

Apparently in contradiction with the small influence of the applied potential, the adsorption behaviour of the various proteins as a function of the pH seems to show a strong correlation with the electrostatic interactions between protein molecules and the surface (figures 5.5, 5.6 and 5.7). This apparent contradiction must be due to indirect effects, related to the complex nature of the process of protein adsorption. Firstly, there is also a correlation between the charge of a protein molecule and its structure-stability. In its i.e.p. the structure stability is the highest. Far from the i.e.p. structural rearrangements will become a more important factor in the adsorption, even for the "hard" proteins. Such structural arrangements might not only lead to an entropy gain in the adsorbing protein (this effect being stronger for larger protein molecules), but they can also diminish the effect of hydrophilic dehydration (the protein molecule can adsorb with hydrophobic parts from its interior), or lead to more favourable local interactions between charged groups on the protein and the surface. Secondly, and in connection with this latter point, not only the overall ("smeared out") potential of the interface is of importance, but also local interactions between charged groups of the protein and the surface. A point to consider when comparing the results obtained at open circuit potentials and those obtained with externally imposed potentials, is the fact that the surface charge is established in quite different ways. In the first case the surface charge is the result of H^+-association and -dissociation of hydroxyl-groups of the oxide surface: at low pH the surface is positively charged and contains many OH_2^+-sites. On the other hand, in case of imposed potentials, the overall charge results from a change in the concentration of charge carriers in the oxide phase. A positive charge results in the dissociation of H^+ from the surface, so that now the surface concentration of negatively charged groups is relatively high. Finally, we point to the effect that the hydrophilicity of the surface increases further from its i.e.p. or when an external potential is applied, but no doubt there are more variables in the system than mentioned here that vary together with the states of charge of the protein molecules and of the surface.

5.5. Conclusions

The results obtained at the equilibrium potential, including results from earlier studies on silica and glass [Shirahama *et al.*, 1990; Norde *et al.*, 1991; Norde and Anusiem, 1992], suggest that electrostatic interactions play a decisive role in the adsorption of structure-stable proteins on hydrophilic surfaces. On the other hand, protein adsorption is found to be hardly affected by externally imposed interfacial potentials, irrespective of the structure-stability of the protein. The cause for the apparent contradiction in these results, must be that in both experimental approaches, but in different ways, together with the electrostatic interactions other properties of the system are varied. (For example on changing the pH, the net charge of the protein molecules changes, but also their structure-stability; together with increasing surface potentials, the surface becomes more hydrophilic; and, in case a constant potential is externally applied to the surface, the adsorbing protein molecules may largely adapt their properties.) Therefore it is difficult to assess the importance of the contribution of electrostatic interactions in the process of protein adsorption. Presumably, in the past protein adsorption as a function of the pH has been interpreted in a too simplified manner, overestimating the role of electrostatic interactions.

Chapter 6

Adsorption behaviour of native and porphyrin cytochrome *c*: adsorbed amounts, kinetics, influence of the applied potential and orientation

6.1. Introduction

General introduction

Cytochrome *c* is an electron-carrying protein found in mitochondria of all aerobic organisms. It is part of the terminal oxidation chain, which completes the breakdown of foods to CO_2 and H_2O, storing the absorbed energy in molecules of ATP. Cytochrome *c* is an iron-porphyrin protein made up of one haem group and one polypeptide chain. The iron atom, present in the native form, alternates between the ferro (+2) and the ferri (+3) oxidation state as the molecule interacts with cytochrome reductase and cytochrome oxidase, both large multimolecular complexes [Margoliash and Schejter, 1966].

The structure of cytochrome *c* has been extensively studied over the past decades. There are two main reasons for this. First, to understand the mechanism of electron transfer to and from cytochrome *c* requires a detailed knowledge of its molecular structure (conformations) in both the ferric and ferrous state. Second, the three-dimensional structure of cytochrome *c* is a tool for studying the process of molecular evolution, because cytochrome *c* is found across the entire spectrum of animals, plants and aerobic micro-organisms. Until now, the primary structure of cytochrome *c* from about 80 species is known, among which that of horse heart cytochrome *c*. X-ray crystallography was the technique with which these structures were determined [Dickerson *et al.*, 1971; Takano *et al.*, 1973; Takano and Dickerson, 1981]. This technique was also used to compare the ferri and ferrous structures of cytochrome *c* [Takano and Dickerson, 1981].

Not until 1977 the redox behaviour of cytochrome *c* was studied by electrochemical techniques. Before that time it was recognized that electron transfer between redox proteins and (metal) electrodes hardly occurs.

Eddowes and Hill [1977] showed that by making use of bipyridyl as the mediating compound, electron transfer between cytochrome *c* and a gold electrode was feasible. Promoted by the development of biosensors and biocatalytic devices, the adsorption of redox proteins on electrode surfaces at monolayer coverage became of interest from a practical point of view.

Nowadays a number of techniques have been applied to obtain fundamental knowledge concerning the structure, the biological function, the electron-transfer behaviour and the adsorption of cytochrome *c*. Among these techniques are Resonance Raman Spectroscopy [Taniguchi *et al.*, 1984; Hildebrandt, 1991], cyclic voltammetry [Willit and Bowden, 1989], Visible Absorption Spectroscopy [Collison and Bowden, 1992], AC impedance measurements [Sagara *et al.*, 1990; Matsumura and Kleijn, 1993], and Total Internal Reflection Fluorescence [Fraaije *et al.*, 1990].

The importance of the orientation in the adsorbed state of proteins used in (bio)sensors like immunoassays and other diagnostic tests has been explained in chapter 1. In chapter 2 the method for determining orientation distributions of adsorbed molecules using TIRF has been discussed. In this work cytochrome *c* has been chosen as a model protein to test and illustrate this method, because of its well-documented crystallographic structure, its availability and ease of purification, and its well-characterized physical-chemical properties. Furthermore, cytochrome *c* has a chromophoric group (the haem) which can be made fluorescent by removing the Fe-atom. The protein without the Fe-atom is called porphyrin cytochrome *c*. Another interesting feature of cytochrome *c* is its relatively strong electric dipole moment (325 Debye at pH 7 [Koppenol and Margoliash, 1982]). This might offer a possibility to influence the orientation of cytochrome *c* molecules at the sorbent surface by variation of the interfacial potential.

This chapter presents data concerning the adsorption behaviour, the orientation distribution of adsorbed molecules and the effect of an imposed interfacial potential on the adsorption of native and porphyrin horse heart cytochrome *c*. Because strong structural changes of the protein molecule upon adsorption would make it impossible to draw conclusions on the orientation of the adsorbed molecule from the orientation distribution of the porphyrin group, ample attention will be paid to the structure-stability of both forms of cytochrome *c*.

Horse heart cytochrome c

Horse heart cytochrome *c* is a redox protein with an almost spherical molecule, having dimensions of 2.8 × 3.0 × 3.4 nm and a weight of 12200 g/mole. The polypeptide chain consists of 104 amino acids. There are no disulphide bridges. This chain is folded around the haem group which is covalently bonded to the protein chain by thioester links to cysteinyl residues 14 and 17 (see figure 6.1). Four of the octahedral ligands to the iron atom come from the porphyrin ring itself, the fifth is an imidazole nitrogen of histidine 18 and the last one is the methionyl residue 80. The haem group is surrounded by many densily packed hydrophobic side chains. As a result, the redox potential of cytochrome *c* is more positive (corresponding to having a higher electron affinity) than that of the same haem complex in aqueous solution without the polypeptide chain.

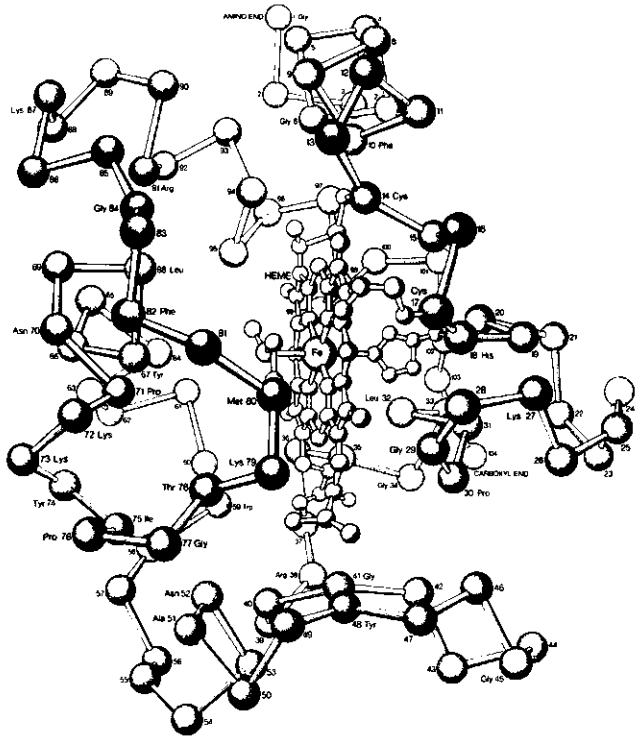

Figure 6.1. *Alpha-carbon structure of horse heart cytochrome c. Only α-carbon atoms and those side chains which are bonded to the haem group are shown [Dickerson and Timkovich, 1975].*

Cytochrome *c* has a remarkably high lysine content (18%). Together with 2 arginines and only 12 acidic residues it is a basic protein, with its isoelectric point (i.e.p.) at pH 10. The inhomogeneous distribution of the charged amino acids over the exterior of the protein is responsible for the high electrical dipole moment of 1.08×10^{-27} Cm (325 Debye) at pH 7, and plays almost certainly a role in the binding to cytochrome *c* reductase and cytochrome *c* oxidase [Dickerson and Timkovich, 1975; Koppenol and Margoliash, 1982]. Comparison of the amino acid sequences of more than eighty cytochrome *c*'s from different species resulted in the striking finding that 26 of the 104 residues have been invariant during evolution. Many hydrophobic residues in contact with the haem, the two haem ligands His 18 and Met 80, a sequence of 11 residues from residue 70-80 and most of the glycine residues have been preserved [Dickerson and Timkovich, 1975].

Interaction of cytochrome c with its oxidase and reductase

Cytochrome *c* carries electrons from the cytochrome *c* reductase complex to the cytochrome *c* oxidase complex. It has been shown that the distribution of charged residues on the surface of the protein plays an important role in the recognition and binding of the reductase and oxidase [Dickerson and Timkovich, 1975; Koppenol and Margoliash, 1982]. Modification of the lysine side chains around the haem crevice on one face of the protein leads to a reduction in the oxidase activity. Furthermore, polylysine competes with cytochrome *c* in the binding with reductase and oxidase.

Two kinds of mechanisms have been proposed for the transfer of an electron by cytochrome *c*. Firstly, an electron could be transferred between the haem groups in different proteins by a relay of aromatic side chains. Secondly, an electron could be transferred directly from one haem group to another. The last mechanism is the most likely because an electron is partially delocalized over the whole π-system of the haem, the haem group of cytochrome *c* is accessible for direct electron transfer and the free energy required to form a free-radical anion of an aromatic side chain is high.

Spectroscopic properties of cytochrome c

In figure 6.2 the absorption spectra of the native and the porphyrin form of cytochrome *c* are given. The *Q*-bands represent absorption along the

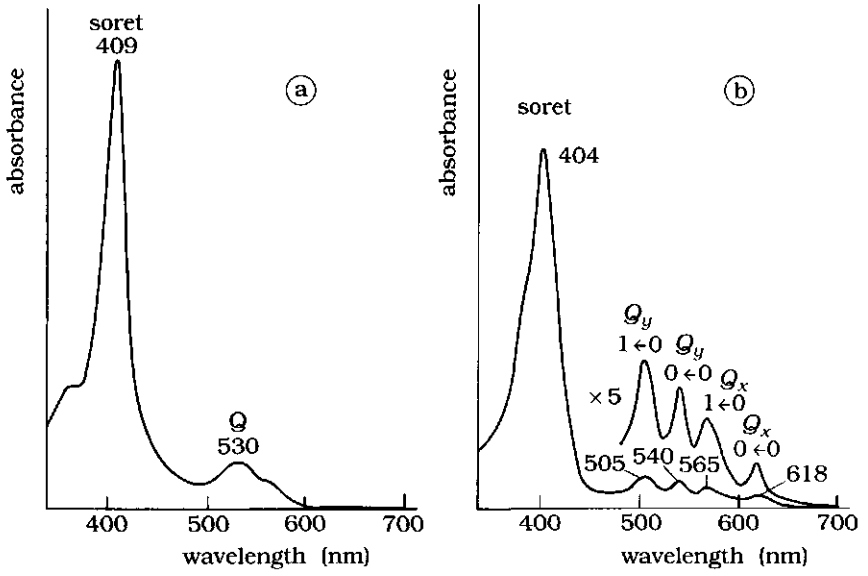

Figure 6.2. a) *Absorption spectrum of native cytochrome c.* ***b)*** *Absorption spectrum of porphyrin cytochrome c. These spectra were recorded in 10 mM phosphate buffer pH 7 and 0.1 M NaCl.*

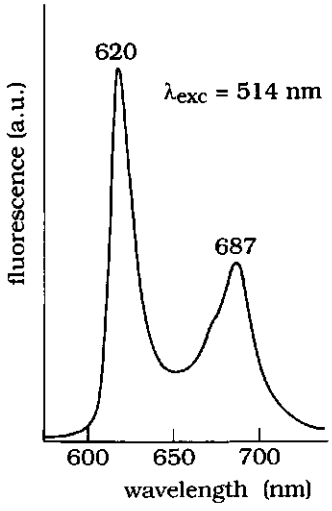

Figure 6.3. *Emission spectrum of porphyrin cytochrome c in 10 mM phosphate buffer pH 7 and 0.1 M NaCl. The excitation wavelength was 514 nm.*

two transition dipole moments of the porphyrin ring system. In the free base (= porphyrin) derivative the two transition dipole moments have a different absorption energy due to the presence of two protons on opposite pyrrole rings. The 0←0 bands are the result of pure electronic transitions, whereas the 1←0 bands also represent vibrational transitions. The result is a characteristic four-banded visible spectrum.

The porphyrin form is fluorescent, in contrast to the native form, of which the emission spectrum is quenched by the central Fe-atom. The emission spectrum of the porphyrin form is shown in figure 6.3. For more details on the spectroscopic properties of this molecule the reader is referred to section 2.3.2.

Structural stability of native and porphyrin cytochrome c

The structural stability of native cytochrome *c* molecules in solution is high. No structural changes of importance take place between pH 3 and pH 12 [Timkovich, 1975; Dickerson and Timkovich, 1975]. The haem group is covalently attached to the peptide chain and has a constant orientation in the molecule. It has been shown from tryptophan fluorescence and CD measurements that there are no significant structural differences between the native and the porphyrin form of cytochrome *c* molecules [Fisher *et al.*, 1973; Vanderkooi and Erecinska, 1975; Vos *et al.*, 1987] (see figure 6.4). This is confirmed by the observation that in FPLC chromatograms the peaks of native and porphyrin cytochrome *c* are at exactly the same position [Fraaije *et al.*, 1990]. However, porphyrin cytochrome *c* has a somewhat lower structural stability towards guadinin-HCl and heat-denaturation treatments. Moreover, it has been observed that it undergoes deterioration in the presence of light [Fisher *et al.*, 1973; Vanderkooi and Erecinska, 1975].

There are, as far as we know, only few literature data available concerning the structural stability of cytochrome *c* upon adsorption [Wei, 1991] . Norde [1986] has made an analysis of the structure-determining factors for the proteins HPA (human plasma albumin) and RNase (ribonuclease). It leads to the conclusion that RNase is much less able than HPA to adopt its structure at sorbent surfaces. Cytochrome *c* resembles RNase with respect to a number of structure-determining properties, e.g. molecular weight, size and shape, hydrophobicity and Gibb's energy for transition to the unfolded state [Timkovich, 1979; Norde, 1986; Creighton,

1983; Privalov, 1976]. Therefore, it is likely that the cytochrome *c* molecule retains its structure upon adsorption on hydrophilic surfaces. This is further corroborated by the finding that in the adsorbed state cytochrome *c* has, within experimental error, still its crystallographically determined dimensions [Reynaud *et al.*, 1986].

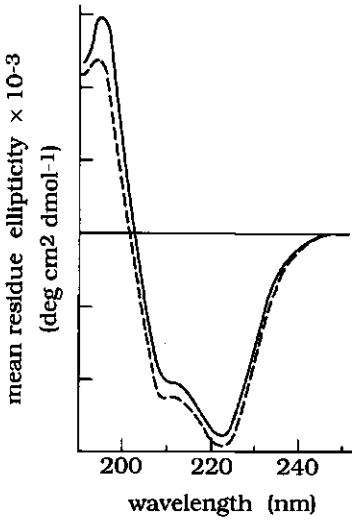

Figure 6.4. *CD spectra of ferri- (——) and porphyrin cytochrome c (---). [Vos et al., 1987].*

6.2. Materials and Methods

6.2.1. Materials

Cytochrome c solutions

Cytochrome *c* solutions were prepared from horse heart cytochrome *c* (obtained from Sigma, type III) or from porphyrin cytochrome *c* (obtained as described in section 6.2.2). Cytochrome *c* concentrations generally ranged from 0.1 to 100 mg/l in pure water or either 10 mM acetate buffer pH 4 or 10 mM phosphate buffer pH 7. Cytochrome *c* concentrations were determined measuring the extinction at 404 nm in a Hamamatzu spectrophotometer (molar extinction coefficient = 81 × 1 0^3 M^{-1} cm^{-1} [Vanderkooi *et al.*, 1976]).

Sorbent surfaces

For the TIRF measurements a glass surface and an indium tin oxide (ITO) film deposited on glass (see sections 3.3.1 and 3.3.2) were used. For the reflectometry experiments a macroscopic Si/SiO_2 or Si/ITO surface were used for the adsorption of both forms of cytochrome *c*. Sorbent materials used for depletion measurements are SiO_2 powder (borosilicate obtained from Solvirel, Levallais, France, with a specific surface area of 0.6 m^2/g), ruthenium dioxide (RuO_2 prepared by thermal decomposition of $RuCl_3$ under O_2 at 400° C, point of zero charge at pH 5.7 [Kleijn and Lyklema, 1987], specific surface area 25 m^2/g) and polystyreen latex (specific surface area 8.9 m^2/g, diameter 630 nm, σ_0 = -0.05 Cm^{-2}).

6.2.2. Methods

Preparation of porphyrin cytochrome c

Porphyrin cytochrome *c* was prepared following a method first described by Flatmark and Robinson [1968]. 100 mg of horse heart cytochrome *c* (Sigma, type III) was added to 2-3 ml anhydrous hydrogen fluoride (HF), which was distilled in a Teflon beaker placed in a Dewar flask filled with liquid nitrogen. After 2-3 minutes of stirring the reaction vessel was taken out of the liquid nitrogen and the HF was removed by applying a vigorous stream of nitrogen. When all the HF was removed, the purple coloured paste was dissolved in 3 to 4 ml 0.1 M ammonium acetate pH 5. The solution was dialysed against the same buffer for 24 hours and finally the protein was lyophilised and stored at -18° C.

Depletion measurements

Adsorption experiments were carried out in 10 cm^3 polycarbonate tubes in which the solutions of cytochrome *c* in various concentrations were added to a dispersion of sorbent material in the same buffer. The tubes were gently rotated for about 16 hours. After centrifugation the cytochrome *c* concentrations in the supernatants were determined by measuring the extinction at 404 nm in a Hamamatzu spectrophotometer.

Reflectometry measurements

The amounts of cytochrome *c* adsorbed on a macroscopic Si/SiO_2 or Si/ITO surface were determined with reflectometry. The cytochrome *c* solution impinges perpendicular upon the flat surface with a flow rate of 2.0×10^{-8} m^3 s^{-1}. For a more detailed description of the apparatus the reader is referred to section 3.2. More information about the hydrodynamics of the system the reader can find in Dijt *et al.* [1990]. The electrical potential of the ITO layer was varied using a home-built potentiostat. A Pt wire counter electrode and a small Ag/AgCl/saturated KCl reference electrode (MI-402, Microelectronics, Inc. USA; potential 193 mV *vs.* NHE) were placed in the cell. The presence of an amperometer in the electrical circuit makes it possible to monitor any electrical currents during measurements (see sections 3.2.2 and 3.2.3).

TIRF measurements

Cytochrome *c* solutions with different concentrations in water, 10 mM acetate buffer, 10 mM phosphate buffer or 10 mM borax buffer were used in the TIRF measurements. The TIRF instrument used has been described in detail in section 3.1. Adsorption of cytochrome *c* took place in a laminar flow cell (see figure 3.3) using the earth gravity to obtain a flux of 2.0×10^{-8} m^3 s^{-1}.

All experiments were performed at room temperature.

6.3. Results and Discussion

6.3.1. Adsorbed amounts and adsorption kinetics of native and porphyrin cytochrome c

In figure 6.5 the adsorption isotherms at pH 4, 7 and 9 for native cytochrome *c* on glass powder are shown. With increasing pH the adsorbed amounts increase, possibly because the sorbent surface becomes more negative and the protein molecules become less positive, so that more molecules can adsorb before the electrical potential in the adsorption layer is no longer favourable.

Assuming the cytochrome *c* molecule to be spherical with a diameter of 3.4 nm, the adsorbed amount for a fully covered surface would be 2.3 mg/m^2. The plateau values found at pH 4, 7 and 9 indicate that not more than a complete monolayer of molecules is adsorbed at the surface. The initial slopes of the adsorption isotherms are a measure for the affinity of the protein for the surface (Gibbs adsorption energy). Figure 6.5 clearly shows that the affinity of cytochrome *c* for the glass surface is high.

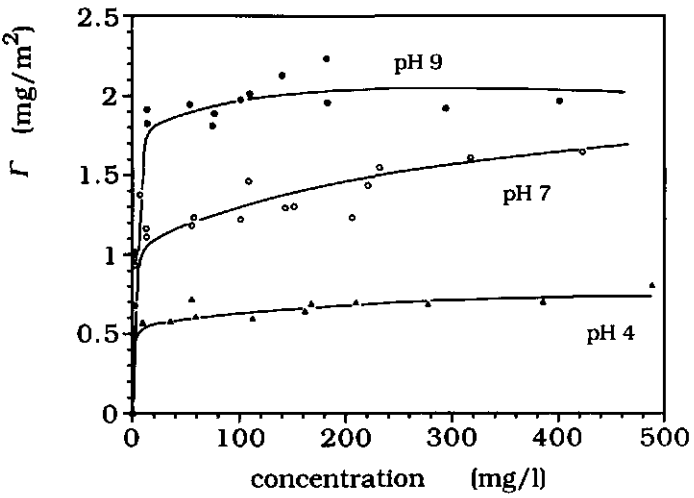

Figure 6.5. *Amounts of native cytochrome c adsorbed on glass (borosilicate) powder from 10 mM acetate buffer pH 4, 10 mM phosphate buffer pH 7 and 10 mM borax buffer pH 9.*

In figure 6.6 the amounts of cytochrome *c* adsorbed on different types of surfaces from 10 mM buffer solutions containing 100 mg/l protein are shown. The amounts adsorbed on ITO were obtained by reflectometry, those on silica, RuO_2 and latex from depletion experiments. ITO and silica, having low i.e.p's (pH 2-3), are negatively charged over the pH range studied. RuO_2 is positively charged below pH 5.7 (its point of zero charge) and negatively charged above this pH. The (PS) polystyrene latex particles bear a negative charge, independent of pH. The oxide surfaces (silica, RuO_2, ITO) are hydrophilic, the PS surface is hydrophobic.

For all sorbent surfaces the amounts adsorbed increase with increasing pH. This might be due to changes in the electrostatic

interactions: for the oxide surfaces the charge is more negative at higher pH values, whereas the positive charge on the cytochrome *c* molecule is lower, resulting in less repulsion between the molecules in the adsorption layer. For RuO_2 the amount adsorbed is almost negligible at pH 4, where the surface is positively charged. This adsorption behaviour is in line with that of structure-stable proteins like RNase and lysozyme on hydrophilic surfaces [Norde, 1986, 1992; Norde *et al.*, 1991;]. See also section 1.3 of this thesis.

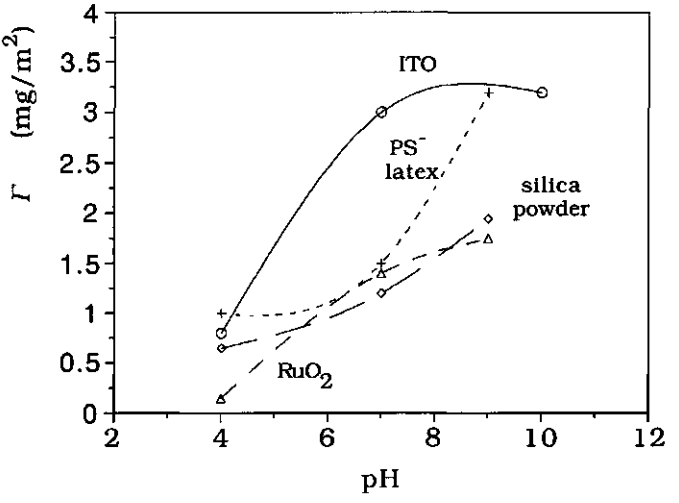

Figure 6.6. *Amounts of native cytochrome c adsorbed on various surfaces as a function of pH. The protein concentration was 100 mg/l in 10 mM acetate buffer pH 4, 10 mM phosphate buffer pH 7 or 10 mM borax buffer pH 9.*

On the PS latex the adsorbed amounts are relatively high at all pH values, at pH 9 even somewhat higher than monolayer coverage. We suspect that at this pH phase separation occurs, induced by the hydrophobic surface; cytochrome *c* is almost uncharged so electrostatic repulsion between the molecules is low. On ITO higher adsorbed amounts are found than on the other oxide surfaces. This might be partly due to the difference in technique. From depletion experiments performed with silica and RuO_2 as the sorbent material it was found that both the plateau of the adsorption

isotherm and the initial slopes decrease with increasing electrolyte (KNO_3) concentration. This indicates that the adsorption of cytochrome *c* is accompanied by exclusion of small ions from the adsorption layer [Fraaije *et al.*, 1991a,b,c].

In figure 6.7 the amounts of bovine serum albumin (BSA), ribonuclease (RNase), lysozyme (LSZ), α-lactalbumin (αLA) and native cytochrome *c* (Cyt. *c*) adsorbed on ITO after 15 minutes are shown as a function of the pH. The protein concentration in solution was 10 mg/l. The data strongly suggest that electrostatic interactions between protein and the surface are a prominent factor in the adsorption behaviour (see section 5.3.2). Native cytochrome *c* shows qualitatively the same pH dependence as the structure-stable proteins LSZ and RNase. The same pH dependence was found in the adsorbed amounts of a number of these proteins on silica [Shirahama *et al.*, 1990; Norde *et al.*, 1991; Norde and Anusiem, 1992].

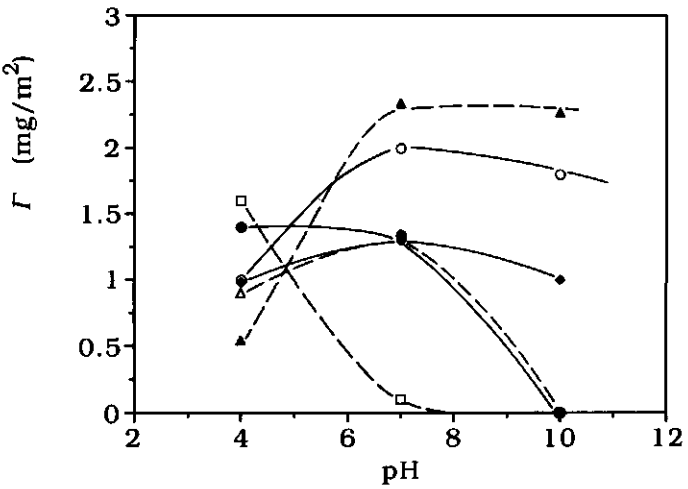

Figure 6.7. *Amounts of the various proteins adsorbed on ITO after 15 minutes as a function of pH obtained with reflectometry. Protein concentration 10 mg/l.* ● *BSA;* ○ *LSZ;* ◆ *RNase;* △ *MGB;* □ *αLA and* ▲ *Cyt. c.*

In the above the behaviour of native cytochrome *c* as a function of pH and sorbent surface was treated and compared with that of other proteins. From this it is concluded that native cytochrome *c* behaves like a "hard" protein, i.e. it does not significantly change its conformation upon adsorption on a hydrophilic surface. In the orientation measurements the porphyrin form of cytochrome *c* has been used. In order to check whether the adsorption behaviour of the porphyrin form resembles that of native cytochrome *c* additional adsorption experiments were performed.

The amounts of native and porphyrin cytochrome *c* absorbed on ITO after 15 minutes of adsorption at pH 4, 7 and 10 are shown in figure 6.8 and 6.9. At these pH values the ITO surface is negatively charged. The trend in the adsorbed amounts are comparable to that found for adsorption of cytochrome *c* on silica presented in figure 6.5. Both forms of cytochrome *c* have a high affinity for ITO. Generally, the amounts adsorbed on ITO are higher than on silica: for native cytochrome *c* on ITO at pH 4 a plateau value of 0.9 mg/m^2 was found, for pH 7 and pH 10 these values are 2.8 and 3.2 mg/m^2, respectively. For porphyrin cytochrome *c* these values are 0.7, 6 and 13 mg/m^2 , respectively.

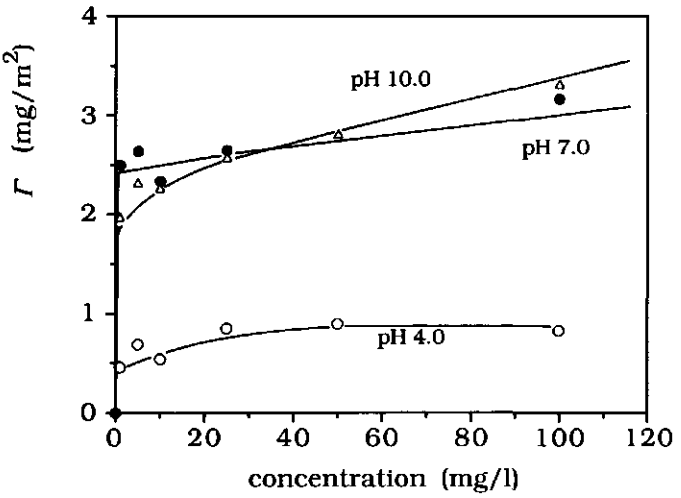

Figure 6.8. *Amounts of native cytochrome c adsorbed on ITO after 15 minutes of adsorption from 10 mM acetate buffer pH 4 (○), 10 mM phosphate buffer pH 7 (●) and 10 mM borax buffer pH 10 (Δ).*

The amounts adsorbed on ITO at pH 4 are more or less the same for both forms of the protein. However, at pH 7 and 10 they are remarkably higher for the porphyrin form. In fact, the adsorbed amounts are so high that monolayer adsortion is no more feasible. Especially, at pH 10 aggregation or a phase separation must occur at the surface. The lack of electrostatic repulsion between the protein molecules at this pH might explain such an adsorption behaviour.

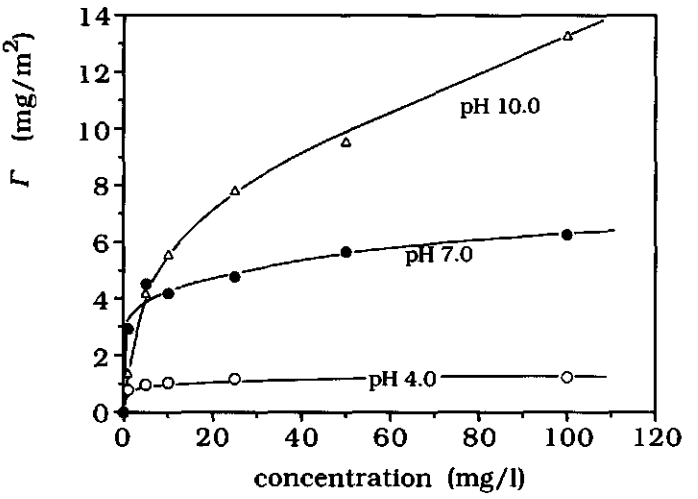

Figure 6.9. *Amounts of porphyrin cytochrome c adsorbed on ITO after 15 minutes of adsorption from 10 mM acetate buffer pH 4, 10 mM phosphate buffer pH 7 and 10 mM borax buffer pH 10.*

In figure 6.10 the adsorption of native and porphyrin cytochrome *c* at different pH values is given as a function of time. The protein concentration was 10 mg/l. The initial adsorption rate $(d\Gamma / dt)_{t\to 0}$ can be compared with the flux J_p of the protein molecules to the surface. With $\nu = 10^{-6}$ m^2 s^{-1}, $\Phi = 2.0 \times 10^{-8}$ m^3 s^{-1}, $R = 9.5 \times 10^{-4}$ m and $D = 1.14 \times 10^{-10}$ m^2 s^{-1} [Sober, 1968] the flux has been calculated and the result is indicated in figure 6.10. For both the native and porphyrin form of cytochrome *c* $(d\Gamma / dt)_{t\to 0}$ is smaller than J_p. Apparently, not every protein molecule that arrives at the surface is attached. The fraction of protein molecules arriving at the surface which do adsorb, p_{ads}, is given in table 6.1.

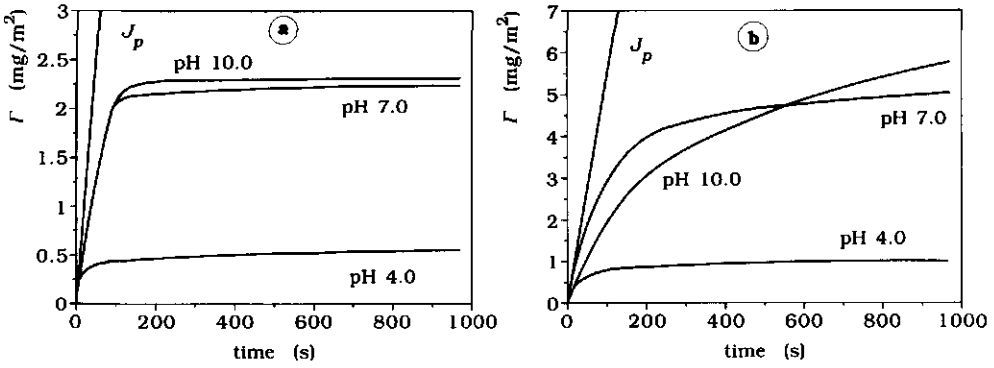

Figure 6.10. *Amounts of cytochrome c adsorbed on ITO as a function of time at pH 4, 7 and 10.* ***a)*** *The native form.* ***b)*** *The porphyrin form. The flux J_p of the protein molecules to the sorbent surface is indicated. The protein concentration was 10 mg/l. Buffers as in figure 6.8.*

At every pH studied comparable values of p_{ads} for the two forms of cytochrome *c* have been found. In contrast to the total amounts adsorbed, the probability factor is lower for higher pH values. This might be explained from the fact that p_{ads} is calculated from the initial adsorption rate, where lateral repulsion between molecules in the adsorption layer does not yet play a role.

In conclusion, the adsorption behaviour of porphyrin cytochrome *c* resembles that of the native protein at pH 4; at pH 7 and 10 the initial adsorption rates of the two forms of cytochrome *c* are also comparable, but the total amounts adsorbed are much higher for the porphyrin form. It seems that porphyrin cytochrome *c* has a stronger tendency than the native protein to aggregate or precipitate at the solid/liquid interface.

Table 6.1. *The probability factor p_{ads} for native and porphyrin cytochrome c as a function of pH.*

protein	pH 4.0	pH 7.0	pH 10.0
native cyt. c	0.69	0.47	0.45
porphyrin cyt. c	0.67	0.61	0.34

6.3.2. Competition and displacement measurements

In figure 6.11 the competitive adsorption behaviour of native and porphyrin cytochrome *c* on glass is given. The total protein concentration was 10 mg/l. Single adsorption of porphyrin cytochrome *c* is represented by the curve with 100%. The curves represented by 75, 50 and 25% are measurements where the ratios of porphyrin/native cytochrome *c* in solution were 3:1, 1:1 and 1:3, respectively. In the case of single adsorption of native cytochrome *c* hardly any fluorescence was observed. Figure 6.10 shows that there is no clear preferential adsorption of one of the forms of cytochrome *c*. Apparently, the two forms of the protein have the same affinity for the sorbent surface. For a total protein concentration of 70 mg/l simular results were obtained.

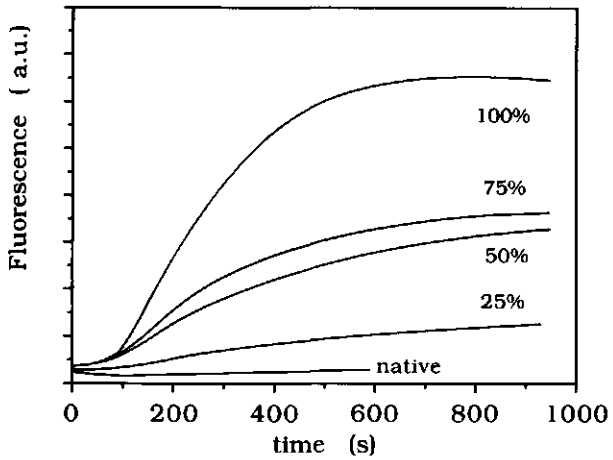

Figure 6.11. *TIRF competition measurements between native and porphyrin cytochrome c on glass from 10 mM phosphate buffer pH 7 containing 10 mg/l of protein.*

In figure 6.12 the results of displacement experiments are given. Figure 6.12a shows the displacement of porphyrin cytochrome *c* by native cytochrome *c*. Firstly, porphyrin cytochrome *c* was allowed to adsorb for 10 minutes from a 100 mg/l solution. After that time solutions of native cytochrome *c* with concentrations of 5, 10, 25 and 100 mg/l were

introduced into the cell to displace the porphyrin cytochrome *c* molecules. From the decrease in the fluorescence signal it can be seen that native cytochrome *c* can displace the porphyrin cytochrome *c* molecules for 25% at the most. Most of this effect is already obtained at low displacer concentration (10 mg/l). Higher displacer concentrations had hardly any further effect on the displaced amount nor on the time necessary for displacement.

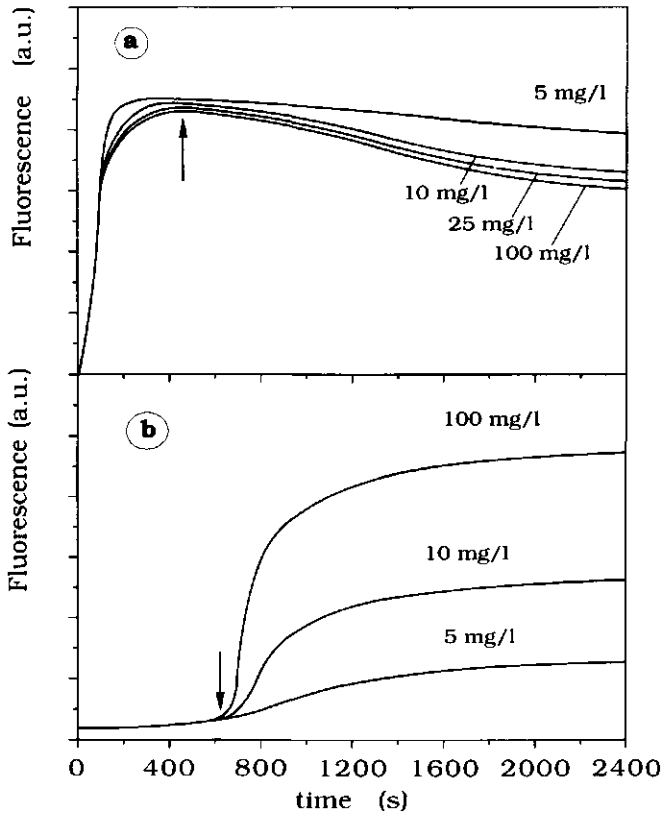

Figure 6.12. a) *Displacement of porphyrin cytochrome c adsorbed from a 100 mg/l solution by native cytochrome c for different displacer concentrations. The arrow indicates the time at which the displacer was introduced into the cell.* ***b)*** *Displacement of the native form of cytochrome c adsorbed from a 100 mg/l solution by the porphyrin form. As solvent a 10 mM phosphate buffer pH 7 was used.*

In figure 6.12b the results of the displacement of native cytochrome *c* by the porphyrin form are shown. For 10 minutes the native form was allowed to adsorb from a 100 mg/l solution, followed by the porphyrin form. Now the displacer concentrations were 5, 10 and 100 mg/l. Immediately after introducing the porphyrin form into the cell the fluorescence starts to increase. This effect is stronger for higher displacer concentrations. Therefore, one might conclude that the displaced amounts are higher for higher displacer concentrations, and also that porphyrin cytochrome *c* displaces the native protein from the surface more effectively than the other way around. However, from reflectometer experiments (not shown here) we found that the total adsorbed amounts, in the case of displacement of native cytochrome *c* by the porphyrin form, increase strongly after introduction of the displacer into the cell. Therefore the increase in the fluorescence observed cannot be explained in terms of displacement alone, but has to be partly attributed to additional adsorption. Such an additional adsorption was not observed in the case porphyrin cytochrome *c* was displaced by the native form of cytochrome *c*. These phenomena can be understood considering that the adsorption plateau of porphyrin cytochrome *c* under the conditions employed here (10 mM phosphate buffer pH 7) is much higher than that of the native protein.

6.3.3. *Adsorption of native and porphyrin cytochrome c as a function of the applied potential*

By reflectometry the adsorption of native and porphyrin cytochrome *c* on ITO at different pH values was studied as a function of the electrical potential of the interface. The amounts adsorbed after 15 minutes of adsorption are shown in figures 6.13 and 6.14. The potential of the ITO/solution interface in these and in other figures in this section is referred to the Ag/AgCl/saturated KCl reference electrode used in the experimental set-up. The i.e.p. of the ITO surface (pH 2.9) was obtained with streaming potential measurements. At this pH the open circuit potential amounts to ± + 300 mV *vs* SCE or + 350 *vs* Ag/AgCl/sat. KCl (see figure 5.2). Therefore, imposed potentials below + 350 mV *vs* Ag/AgCl/sat. KCl correspond with a negative surface whereas above + 350 mV *vs* Ag/AgCl/sat. KCl the surface charge is positive.

At pH 4 the adsorbed amounts of native cytochrome *c* do not depend on the interfacial potential during adsorption; the adsorbed amount is ± 1.1 mg/m^2. Porphyrin cytochrome *c* shows higher adsorbed amounts as the interfacial potential is more positive: these amounts range from 0.8 mg/m^2 at -800 mV to 1.8 mg/m^2 at +800 mV *vs* Ag/AgCl/sat. KCl. This trend is the opposite of what is expected on the basis of electrostatic interactions, since the protein is positively charged at this pH.

At pH 7 hardly any effect of the applied potential on the adsorbed amounts of both native and porphyrin cytochrome *c* was found. Over the whole potential range studied there is a small decline of 0.3 mg/m^2 in the adsorbed amounts of native cytochrome *c* and a small increase of 0.4 mg/m^2 for porphyrin cytochrome *c*. Both forms of the protein are positively charged at this pH.

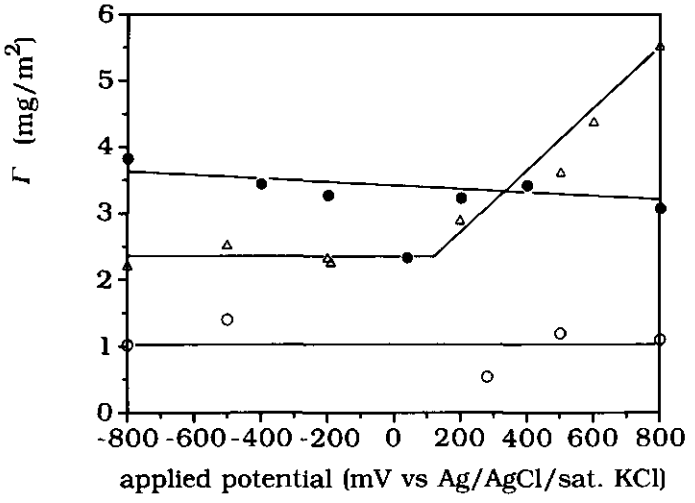

Figure 6.13. *Amounts of native cytochrome c adsorbed on ITO after 15 minutes of adsorption as a function of the externally applied potential at different pH values.* ○ *pH 4;* ● *pH 7;* △ *pH 10. The buffer concentrations were 10 mM.*

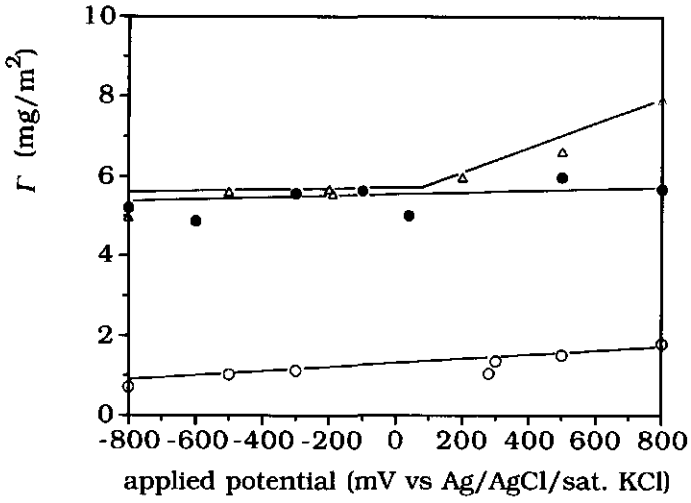

Figure 6.14. *Amounts of porphyrin cytochrome c adsorbed on ITO after 15 minutes of adsorption as a function of the externally applied potential at different pH values. ○ pH 4; ● pH 7; △ pH 10. The buffer concentrations were 10 mM.*

At pH 10, the i.e.p. of cytochrome *c*, the adsorbed amounts of native and porphyrin cytochrome *c* show a slightly stronger dependence on the applied potential. Below + 200 mV the adsorbed amounts are fairly constant; above + 200 mV enhanced adsorption of both forms of cytochrome *c* was observed.

The initial rates of adsorption for both forms of cytochrome *c* as a function of the applied potential are given in figure 6.15 (shown is the change in the reflectometer signal S; $d\Gamma/dt$ is linear with dS/dt; see section 3.2.2). There is no dependence of $(dS/dt)_{t\to 0}$ on the applied potential at pH 4 and 7. Even at pH 10, where the total adsorbed amounts increase above + 200 mV, no effect on the initial adsorption rates was observed. At every pH studied the initial adsorption rates of native and porphyrin cytochrome *c* are practically the same.

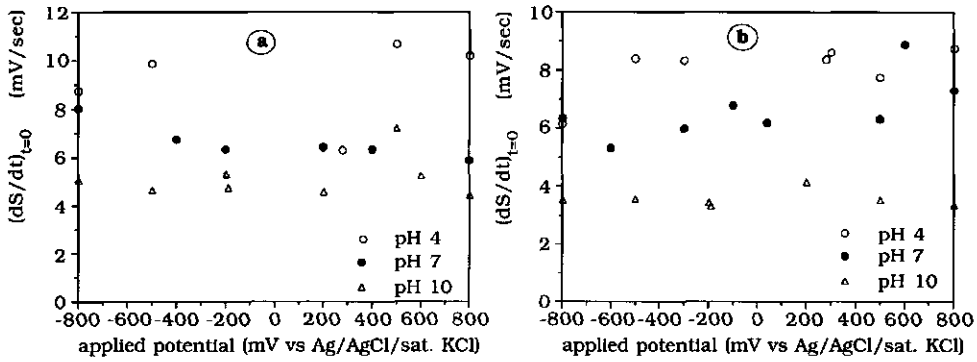

Figure 6.15. *Initial rates of adsorption of cytochrome c on ITO as a function of the applied potential.* ***a)*** *Native cytochrome c.* ***b)*** *Porphyrin cytochrome c. (Protein concentration 10 mg/l, 10 mM buffer solutions).*

Although the adsorbed amounts for the porphyrin form are relatively high, the two forms of cytochrome *c* show almost the same dependence on the applied potential. At pH 4 and 7 the influence of the applied potential is small. Even when the surface is positively charged (above + 350 mV *vs* Ag/AgCl/sat. KCl) native and porphyrin cytochrome *c* adsorb in considerable amounts. At pH 10, the cytochrome *c*'s are close to their i.e.p. At this pH the adsorbed amounts are constant in the potential range corresponding to negative surface charges, whereas at higher positive potentials they show an upward trend. Comparing these results with those obtained for other proteins (see chapter 5), it is concluded that native and porphyrin cytochrome *c* show the same adsorption behaviour as a function of the applied interfacial potential as the structure-stable proteins LSZ and RNase.

For a more detailed discussion on the effect of the applied potential on protein adsorption in general, the reader is referred to section 5.4 of this thesis.

6.3.4. Orientation measurements on adsorbed porphyrin cytochrome *c* molecules

In chapter 4 of this thesis it was shown that TIRF is suitable to obtain the orientation distribution of adsorbed chromophores, such as H_2TMPyP. Here, the same method has been applied to adsorbed porphyrin cytochrome *c* molecules. As sorbent surfaces glass and indium tin oxide were used; in some cases an electrical potential was externally imposed on the ITO/solution interface.

Figure 6.16 shows the theoretical and measured fluorescence signals as a function of the polarization angle Ψ of the incident light beam. In chapter 2 it was shown that the theoretical curves for the fluorescence signal can be written as $F(\Psi) = A + B\cos^2\Psi$. The values for the components of the evanescent field, ε_x, ε_y and ε_z, were obtained using Abeles' method for reflectivities [Hansen, 1968], with the assumption that the point of total reflection is at the interface between the adsorbed protein layer and the solution [Thompson *et al.*, 1984]. Refractive indices used are 1.518 for glass, 1.90 for ITO, 1.333 for the solution phase and 1.40 for the adsorbed protein layer. This results in the following: ε_x = 0.464, ε_y = 1.082, ε_z = 1.009 for glass as the sorbent surface and ε_x = 0.426, ε_y = 0.600 and ε_z = 0.927 for an ITO-film (120 nm thickness) on glass as the sorbent surface. In figures 6.16c and 6.16d the calculated curves are shown for sharp distributions of 0° and 90°, and a random distribution of the angle θ between the plane of the porphyrin ring and the sorbent surface. Figures 6.16a and 6.16b show the measured fluorescence as a function of the polarization of the incident light beam for porphyrin cytochrome *c* adsorbed on glass and ITO. The protein concentration was 10 mg/l in 10 mM phosphate buffer pH 7. The solid lines represent the best fit (least squares) of $A + B\cos^2\Psi$ through the data. This dependence on $\cos^2\Psi$ proves that the detected fluorescence originates from molecules excited by the evanescent field and not by stray light. From a comparison of the experimental results with the theoretical curves it appears that for adsorption on glass an average angle of 20° to 50° between the porphyrin ring plane and the sorbent surface is the most likely, and for adsorption on ITO this seems to be approximately 50°. From $F(\Psi)$ alone it is not possible to assess the broadness of the distributions.

The fluorescence curves obtained after adsorption from solutions with other protein concentrations (i.e. for different surface coverages) show approximately the same depence on Ψ. In addition imposing an external potential at the interface during or after adsorption of the protein does not significantly change the shape of $F(\Psi)$. Apparently, in all cases the orientation distribution of the porphyrin rings is roughly the same.

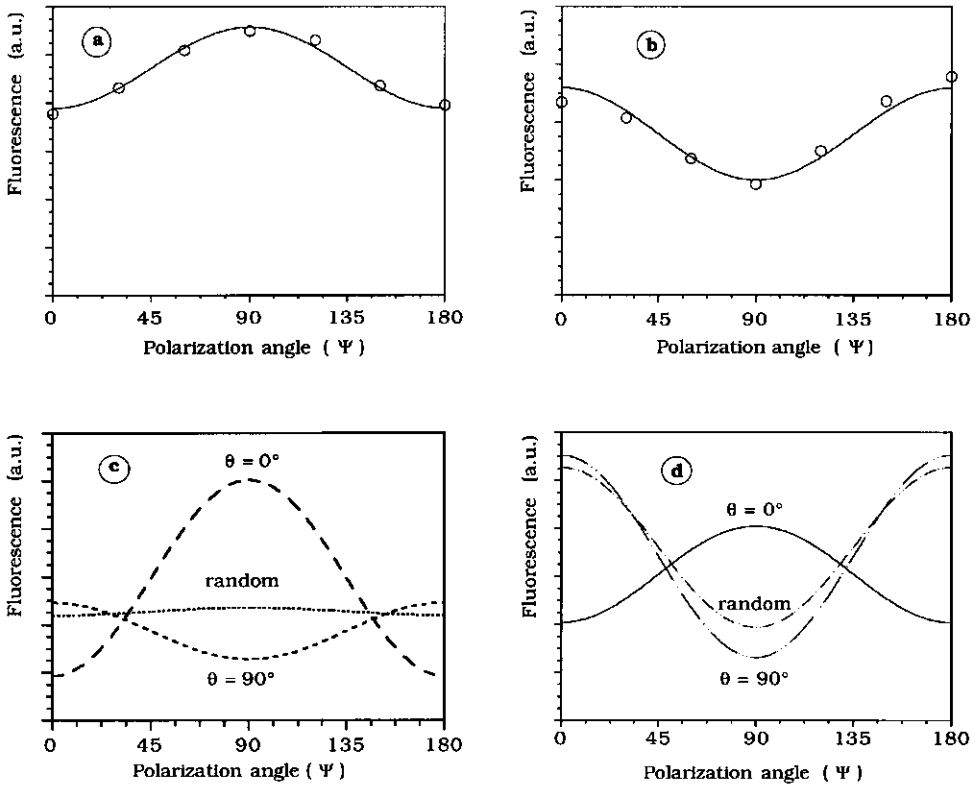

Figure 6.16. *Fluorescence signal as a function of the polarization of the incident light beam.* ***a)*** *and* ***b)*** *Experimental points and fitted curves* ($F(\Psi) = A + B\cos^2\Psi$) *for porphyrin cytochrome c on glass and ITO, respectively. The concentration protein in solution was 10 mg/l; 10 mM phosphate buffer pH 7.* ***c)*** *and* ***d)*** *Calculated curves for the adsorption on glass and ITO, respectively, for a random distribution and sharp distributions with orientation angle* $\theta = 0°$ *and* $\theta = 90°$.

To obtain more specific information on the orientation distribution, i.e. the order parameters $\langle P_2 \rangle$ and $\langle P_4 \rangle$, the fluorescence signals $F_{//}(0°)$, $F_{//}(90°)$, $F_{\perp}(0°)$ and $F_{\perp}(90°)$ have been measured under various experimental conditions (see sections 2.3.2 and 2.3.3). Most of the obtained values for $\langle P_2 \rangle$ and $\langle P_4 \rangle$ are shown in figure 6.17; some of these values are lying outside the axes of figure 6.17. From this figure it can be seen that for the same experimental conditions different combinations of $\langle P_2 \rangle$ and $\langle P_4 \rangle$ have been found. Furthermore, there is neither a clear correlation with the protein concentration of the solution from which adsorption took place (i.e. the surface coverage) on glass nor with the interfacial potential imposed during or after adsorption on ITO. The $\langle P_2 \rangle$ values in the physically realistic area are all between -0.05 and +0.5, whereas $\langle P_4 \rangle$ is found to be rather undefined.

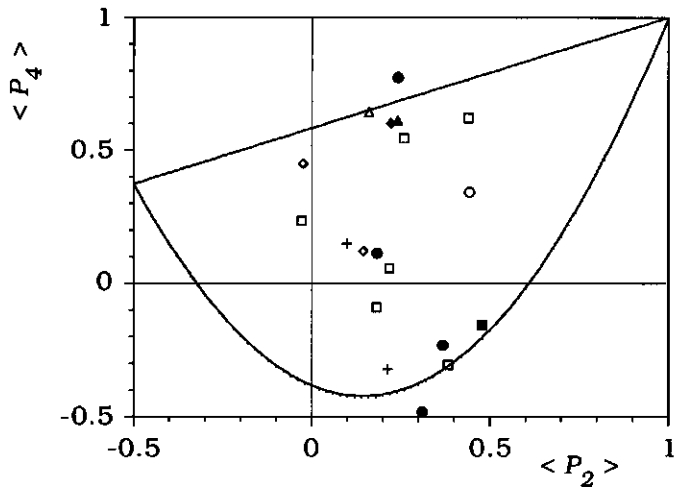

Figure 6.17. *Combinations of the order parameters $\langle P_2 \rangle$ and $\langle P_4 \rangle$ calculated from experimental results. The physically realistic combinations of $\langle P_2 \rangle$ and $\langle P_4 \rangle$ are within the area marked by drawn lines. Open symbols: adsorption on glass from ○ 1 mg/l, □ 10 mg/l, △ 25 mg/l, ◇ 70 mg/l and + 100 mg/l protein solutions. Closed symbols: adsorption on ITO: ● equilibrium potential, ■ -400 mV applied after adsorption at the equilibrium potential, ▲ +500 mV applied during adsorption and ◆ +800 mV applied during adsorption; protein concentration 10 mg/l.*

Measurements with H_2TMPyP clearly showed that TIRF is a suitable technique to obtain the orientation distributions of adsorbed molecules (see chapter 4). The results presented here for porphyrin cytochrome *c* gave no clear orientation distribution of the adsorbed protein molecules because of the scatter in the $\langle P_2 \rangle$ and $\langle P_4 \rangle$ data. The main reason for this scatter is the low signal to noise ratio (S/N) in the fluorescence signal from the adsorbed porphyrin cytochrome *c* molecules. This is particularly the case for the $F_{//}(0°)$ value of which the fluorescence intensity is twice as low as for the other three polarization combinations. Of course, any errors in the assumptions made in the theoretical model used, e.g. concerning the rotational mobility of the adsorbed molecules (see below) and that no interactions occur between the chromophoric groups of different protein molecules, might cause errors in the determination of the orientation distribution of the porphyrin group. Also uncertainties in the evanescent field components caused by the not exactly known refractive indices of the ITO layer and protein layer and thickness of the ITO layer could introduce errors in the reconstruction of the orientation distribution. However, errors in the assumptions and in the physical parameters used would lead to systematic deviations and cannot be the cause for the observed scatter in $\langle P_2 \rangle$ and $\langle P_4 \rangle$.

A way to improve the sinal to noise ratio of the fluorescence intensity is to measure over a longer time period (giving more light pulses). Unfortunately, exposure of adsorbed porphyrin cytochrome *c* molecules to high light intensities or long time periods of light exposure results in changes in the fluorescence spectrum. Fraaije *et al.* [1990] observed changes in the fluorescence spectrum after adsorption on quartz (see figure 6.18). They found an ingrowth of a new peak at a wavelength of 650 nm. In the normal fluorescence spectrum (see figure 6.3) this peak is not present. Such an increase of the fluorescence at 650 nm was also observed in some of our experiments, although it was not expressed that strongly. It points to a change in the structure after adsorption resulting in exposure of the porphyring ring to the solvent [Lakowicz, 1983]. This spectral change was also observed in mixtures of native and porphyrin cytochrome *c* indicating that it is not a energy transfer effect [Fraaije *et al.*, 1990].

The mobility of adsorbed porphyrin cytochrome *c* molecules is assumed to be much slower than the fluorescence lifetime. Vanderkooi and Erecinska [1975] found a rotational correlation time of 200 ns for cytochrome *c* molecules bound to phospholipids, estimated from

polarization data. In the presence of a solid surface we expect that this rotational correlation time is even higher. Also the irreversibility of protein adsorption (see chapter 1) and the fact that the fluorescence is polarized (see section 2.3.4) are indications that mobility of the adsorbed protein molecules does not play a role in the orientation measurements.

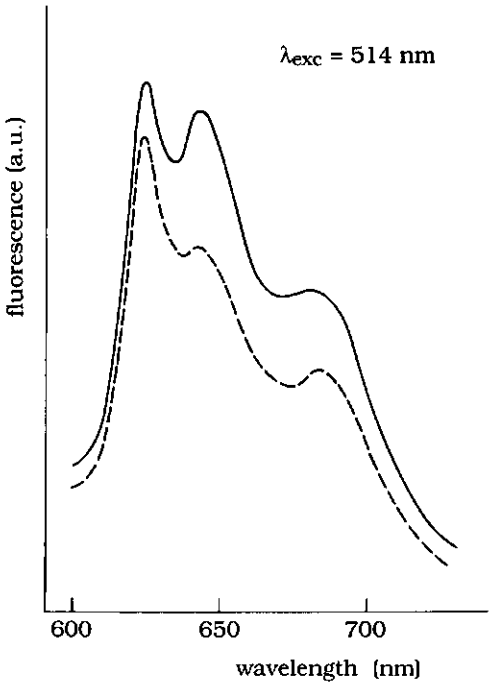

Figure 6.18. *Fluorescence spectrum of porphyrin cytochrome c molecules adsorbed at the quartz/solution interface after 1.5 hours. The full curve is for TM polarized incident light and the dashed curve is for TE polarization. The protein concentration was 9 μM (≈ 100 mg/l) in 10 mM phosphate buffer pH 7 + 0.1 NaCl. [Fraaije et al., 1990].*

The direction of the electrical dipole moment of horse heart cytochrome *c* at pH 7 is known [Koppenol and Margoliash, 1982]. The angle between this dipole moment and the plane of the haem group is 33° at this pH. If this also applies to the adsorbed porphyrin cytochrome *c* molecule, a perfect alignment of the electrical dipole along the electric field of the sorbent surface would yield values for $\langle P_2 \rangle$ and $\langle P_4 \rangle$ of -0.055 and -0.352.

None of the experimental obtained combinations of $\langle P_2 \rangle$ and $\langle P_4 \rangle$ are close to these values.

Changing the interfacial potential *after* adsorption took place did not result in a change in the measured fluorescence signals. This is in line with the observations made by Fraaije *et al.* [1990] that applying a potential at the SnO_2/glass slide after adsorption had no effect on the orientation of adsorbed porphyrin cytochrome *c* molecules and with Matsumura and Kleijn [1993] who found that the orientation of adsorbed native cytochrome *c* molecules could not be modulated by the electrical field of a Pt electrode.

Fraaije *et al.* [1990] concluded that the orientation of cytochrome *c* molecules can be affected by the interfacial potential *during* the process of adsorption. Here, we did not find a correlation between the $\langle P_2 \rangle$ and $\langle P_4 \rangle$ values and the imposed interfacial potential, but again this could be caused by the scatter in the results. However, for the various interfacial potentials applied the same total fluorescence $F(\Psi)$ curves were obtained. The $F(\Psi)$ curves have a much better S/N ratio then the $F_{//}(0°)$, $F_{//}(90°)$, $F_{\perp}(0°)$ and $F_{\perp}(90°)$ curves. Therefore, in contradiction to the conclusion of Fraaije *et al.*, it is concluded here that it is not possible to influence the orientation of the porphyrin cytochrome *c* molecules by the interfacial potential *during* adsorption.

A dipole $\vec{p}$ in an electric field $\vec{E}$ has an energy of $\vec{p} \cdot \vec{E}$. At the equilibrium potential at pH 7, and an electrolyte concentration of 10 mM, the electric field strength near the ITO surface is in the order of 10^8 V m^{-1}. The energy difference per molecule cytochrome *c* between the parallel and antiparallel orientation of its dipole in the field of the interface is in the order of 30 kT. Therefore, if electrostatic interactions would be determining for the orientation in the adsorbed state, alignment of the molecules according to their dipole would be expected under these conditions. At an imposed potential of +350 mV *vs.* Ag/AgCl/sat. KCl (where the surface charge is zero) no alignment would occur. Since no difference was found between the $F(\Psi)$ curves for different imposed potentials, we conclude that the orientation of the adsorbed molecules is not determined by electrostatic interactions. The minor role of electrostatics is supported by our protein adsorption experiments as a function of imposed interfacial potentials described in chapter 5. Furthermore, in the case of porphyrin cytochrome *c* adsorption on glass and ITO at pH 7 and pH 10 leads to the formation of multilayers or aggregation at the surface; this diminishes the influence of the interfacial potential on the orientation distribution even further.

Another important point is of course the structural stability of the porphyrin cytochrome *c* molecule upon adsorption. It is still not quite sure that the free base derivative of cytochrome *c* does not change its conformation during the adsorption process. On the one hand, its adsorption behaviour resembles in many aspects that of the native protein and of other structure-stable proteins. On the other hand, it is more sensitive to heat and guanidine-HCl treatments than native cytochrome *c* and under influence of light conformational changes at the interface might occur, as explained before (see figure 6.18). Therefore, it is still an open question whether or not we can draw conclusions concerning the orientation of the protein from the orientation of the porphyrin group, which is in fact what is determined by the TIRF orientation measurements. Anyway, the $F(\Psi)$ curves in figures 6.16a and 6.16b point to a certain ordening of the adsorbed molecules; the orientation of the porphyrin groups is not (completely) random. This orientation distribution does not depend on the interfacial potential nor on the degree of surface coverage by the protein molecules.

6.4. Conclusions

In this chapter the adsorbed amounts, the kinetics, the influence of an imposed potential and the orientation of adsorbed cytochrome *c* molecules have been presented. We have shown that the adsorption behaviour of native cytochrome *c* resembles that of structure-stable proteins such as lysozyme and ribonuclease. Porphyrin cytochrome *c* behaves in many aspects the same as the native form, however the adsorbed amounts at pH 7 and 10 are much higher. The adsorbed amounts and adsorption kinetics of both forms of cytochrome *c* are found to be hardly affected by externally imposed interfacial potentials. With regard to the orientation measurements it was impossible to interpret the data in terms of orientation distribution functions because of the scatter in the results. This scatter is mainly caused by the low signal to noise ratio. Improvement of this scatter is difficult because of the photo-deterioration of the adsorbed protein molecules. However, the total fluorescence as a function of the polarization angle Ψ of the incident light beam points to orientation distributions which do not depend on the surface coverage and cannot be influenced by imposing an electrical potential on the sorbent surface.

Chapter 7

Summary, conclusions and perspectives

The aim of the study in this thesis was to develop a method for determining the orientation of adsorbed protein molecules and to study the influence of the electrical potential of the interface on the interfacial properties of proteins, including their orientation.

In the adsorption of proteins on solid surfaces many factors play a role. The most important are electrostatic and hydrophobic interactions between the protein molecules and the sorbent surface, and structural rearrangements in the protein molecules. From earlier studies it was concluded that proteins with regard to their adsorption behaviour can be roughly divided into "hard" and "soft" proteins. For the "hard" proteins structural changes upon adsorption are negligible and these proteins do not adsorb on hydrophilic surfaces unless there is electrostatic attraction. "Soft" proteins have a tendency to unfold partially upon adsorption and they adsorb on all kind of surfaces, irrespective of any electrostatic repulsion, partly caused by a gain of conformational entropy during adsorption.

The orientation of adsorbed protein molecules plays an important role in the effectivity and the development of immunoassays and diagnostic tests. One can imagine that if the orientation of an antibody (or enzyme) is not the right one, no recognition of the antigen (or substrate) occurs. Therefore, either much research is done to develop methods to adsorb antibodies and enzymes in the proper orientation or in ways to steer the adsorption process. In the development of biosensors knowledge of and insight into the adsorption process and the orientation of the adsorbed proteins molecules (used as the selector molecules) on inorganic materials also play essential roles.

In this study two optical techniques have been used: Total Internal Reflection Fluorescence (TIRF) and reflectometry. With both techniques it is possible to monitor quantitatively and qualitatively the adsorption process of proteins *in situ*.

TIRF has been used over the past 20 years for the measurement of protein adsorption kinetics and adsorbed amounts, and to study the exchange of proteins between sorbent surface and solution. A relatively new

research topic for which TIRF is used is to obtain information on the orientation of adsorbed (protein) molecules. The principle of TIRF is as follows: A light beam is totally reflected at an interface between two media 1 and 2 with the refractive index of medium 1 higher than that of medium 2, and the angle of incidence exceeding its critical angle value. Due to interference between the incident and the reflected light beam an evanescent wave penetrates into medium 2. The amplitude of this electromagnetic wave decays exponentially with distance normal to the interface. The penetration depth of this wave depends on the wavelength of the light used, and the refractive indices of the media. For visible light striking a quartz/water interface it is in the order of 100 nm. If medium 2 consists of a solution with fluorescent molecules, the evanescent wave will excite the molecules that are close enough to the interface; the emitted fluorescence is detected. In the case of adsorption and not too high bulk concentrations, the fluorescence signal is almost completely stemming from molecules in the adsorption layer.

With the optical technique reflectometry the adsorption of molecules on an (optically flat) solid surface can be monitored. A linearly polarized light beam is reflected from the adsorbing surface, and the reflected beam is split into its parallelly and perpendicularly polarized components. The intensity ratio between these two components is measured continuously. This ratio changes upon adsorption, and after calibration the adsorbed amount (mass/area) is obtained.

In this work TIRF has been used for the determination of the orientation distribution of adsorbed molecules. Therefore, the existing theory had to be extended (chapter 2). Cytochrome *c* has been chosen as a model protein to test and illustrate the method, because of its well-documented crystallographic structure and its well-characterized physical-chemical properties. Furthermore, cytochrome *c* has a chromophoric group which can be made fluorescent by removing the Fe-atom. The protein without the Fe-atom is called porphyrin cytochrome *c*. From various literature data it is inferred that the native cytochrome *c* molecule is rather structure-stable. Another interesting feature of the protein is its relatively large electric dipole moment (325 Debye at pH 7), which might offer a possibility to influence the orientation in the adsorbed state by variation of the surface charge.

The method for determination of the orientation of adsorbed molecules is based on the principle that by changing the polarization of the incident

light beam the direction of the electric field component of the evanescent wave is modified. As a result the interaction between the transition dipole moment of the adsorbed molecules and the evanescent wave alters, which in turn, gives rise to a change in the fluorescence intensity. To obtain order parameters from which the orientation distribution can be reconstructed, one has to measure not only the intensity but also the polarization of the fluorescence as a function of the polarization of the incident light beam. The theory has been elaborated especially for orientation measurements on porphyrins and cytochrome *c*. In the porphyrin ring two transition dipole moments are lying perpendicularly to one another. For this system it is possible to study the orientation distribution in one orientation angle from the restricted information: the angle θ between the plane of the porphyrin ring and the interface. The orientation distribution in θ can be reconstructed using the Maximum Entropy Method. With regard to the mobility of the adsorbed molecules, which might interfere with the orientation measurements, it is shown that rotational mobility much faster than the fluorescence lifetime would result in the disappearance of the fluorescence polarization.

Firstly, some experiments with a simple porphyrin (tetramethyl-pyridinium porphyrin, H_2TMPyP) have been performed (chapter 4). Prior to the orientation measurements, its adsorption behaviour was studied by reflectometry. For adsorption on silica from pure water, from 0.01 M phosphate buffer pH 7 and from 0.1 M KNO_3 solution different adsorbed amounts have been found. From the TIRF orientation measurements satisfying results were obtained, although the reproducibility leaves still something to desire. The orientation distribution of adsorbed H_2TMPyP molecules on silica depends on the concentration of porphyrin in the solution from which adsorption takes place. At low concentration, the H_2TMPyP molecules are more or less randomly oriented, while at high concentrations a broad distribution around an angle of 46° between the porphyrin plane and surface was observed. The fact that the fluorescence is polarized and the results of measurements with different solution viscosities show that the mobility of the adsorbed porphyrin molecules is on a much larger time scale than the fluorescence life time (5 ns).

To study the influence of the electrical potential (charge) of the sorbent surface on the adsorption behaviour of proteins, a semi-conducting indium tin oxide (ITO) surface was used. This material was deposited in a thin layer (120-140 nm) on glass or silicium plates. The ITO surfaces have

been characterized by streaming potential measurements, scanning electron microscopy, atomic force microscopy and resistance measurements. The results have been described in chapter 3.

The adsorption behaviour of various proteins (serum albumin, lysozyme, ribonuclease A, superoxide dismutase, myoglobin and α-lactalbumin) as a function of an externally imposed interfacial potential has been studied using reflectometry (chapter 5). The sorbent surface was again a semi-conducting ITO layer deposited on a silicium wafer. The results obtained at the equilibrium potential as a function of pH suggest that electrostatic interactions play a decisive role in the adsorption of structure-stable proteins on hydrophilic surfaces. On the other hand, protein adsorption is found to be hardly affected by externally imposed interfacial potentials, irrespective of the structure-stability of the protein. The cause for the apparent contradiction in these results must be that in both experimental approaches, but in different ways, together with the electrostatic interactions other properties of the system are also varied. (For example, on changing the pH, the net charge of the protein molecules changes, but also their structure-stability; together with increasing surface potentials, the surface becomes more hydrophilic; and, in the case a constant potential is externally applied, the adsorbing protein molecules may largely adapt their properties.) Therefore it is difficult to assess the importance of the contribution of electrostatic interactions in the process of protein adsorption. Presumably, in the past protein adsorption as a function of the pH has been interpreted in a too simplified manner, overestimating the role of electrostatic interactions.

In chapter 6 the adsorption behaviour of native and porphyrin cytochrome *c* was the subject of study. Special attention is given to the adsorbed amounts, the adsorption kinetics and the influence of externally applied potentials for both forms of cytochrome *c* and the orientation of adsorbed porphyrin cytochrome *c* molecules. It was shown that the adsorption behaviour of native cytochrome *c* resembles that of structure-stable proteins such as lysozyme and ribonuclease. In many aspects porphyrin cytochrome *c* behaves the same as the native form. However the adsorbed amounts at pH 7 and 10 are much higher. The adsorbed amounts and adsorption kinetics of both forms of cytochrome *c* are found to be hardly affected by externally imposed potentials. With regard to the orientation measurements it was not possible to interpret the data in terms of orientation distribution functions because of the scatter in the results.

This spread is mainly caused by the low signal to noise ratio. Improvement of this ratio is difficult because of photo-deterioration of the adsorbed protein molecules. However, the total fluorescence as a function of the polarization angle of the incident light beam points to orientation distributions which do not depend on the surface coverage and cannot be influenced by imposing an electrical potential on the sorbent surface.

In summary, in this work it is shown that TIRF is a suitable technique to determine orientation distributions of adsorbed fluorescent molecules. Furthermore, it was found that it is not (or hardly) possible to influence the adsorption behaviour of proteins, irrespective of their structural stability, by externally imposing an electrical potential to the sorbent surface.

Perspectives

In this work we have developed a method to obtain the orientation distributions of adsorbed chromophores by making use of the optical technique TIRF. The results obtained with a simple porphyrin show that the method works. So far, application of this method to adsorbed proteins is limited, since the protein should be structure-stable upon adsorption and carry a fluorescent group. It was not possible to reconstruct the orientation distribution of cytochrome *c* molecules because of the scatter in the order parameters obtained. In order to obtain the orientation distribution it is necessary to improve the signal to noise ratio of the fluorescence measurements. This could be done by measuring the fluorescence over a longer time. In the case of cytochrome *c* this fails because the adsorbed molecule appears to undergo structural rearrangements in the presence of light.

For other structure-stable proteins, it might be possible to determine the orientation distribution in the adsorbed state. If the molecules do not have a fluorescent group, one might consider to label them; prerequisite is that the fluorescent label is fixed in the molecule with a known orientation to the rest of the molecule. However, a caveat is that introducing a fluorescent label might lead to structural changes within the molecule and hence influence the adsorption behaviour of the protein. Another possibility to obtain orientation distributions of adsorbed proteins with TIRF is to make use of the fluorescence of the aromatic amino acids tryptophan and tyrosine. These amino acids have a fixed place in the structure and their excitation wavelength is in the UV. This sets higher demands to the optical

parts in the experimental set-up. Furthermore, the presence of more than one of these amino acids can cause energy transfer from one amino acid to the other. As a result it is not known where the fluorescence is stemming from and the information about the orientation is lost. Another disadvantage is that protein molecules might be damaged by the UV light.

Meanwhile, the TIRF method for determining the orientation of adsorbed chromophores is already used in a study concerning the development of "organic" solar energy cells, conducted in the Department of Molecular Physics of the Wageningen Agricultural University. In this study porphyrin molecules are used as sensitizers to generate charge carriers in a semiconducting surface. The adsorption of porphyrins on this surface, especially their orientation, is a prominent factor determining the efficiency of the system. The more parallel the molecules lie on the surface, the higher the energy transfer is. The results obtained here with H_2TMPyP and presented in chapter 4 were promising enough to use the method for studying the orientation of several derivatives of H_2TMPyP.

In our own department the method is now also used to investigate the order in Langmuir-Blodgett (LB) layers of phospholipids, which stand model for biological membranes. In the near future the structure and permeability of such phospholipid layers will be studied as a function of the electrical potential of the substrate. To that end, the LB layers will be deposited onto optically transparent conducting ITO films on quartz slides. With different fluorescent probes it is hoped that information on the rotational mobility and/or reorientation is obtained.

Integration of TIRF with time-resolved fluorescence measurements can provide more detailed information on the structure and orientation of adsorbed molecules and on dynamic processes taking place on the time scale of fluorescence, e.g. rotation of the whole molecule or parts of it.

In conclusion, the potentials of TIRF to study orientations are not exhausted.

References

Allain, C., Auserré, D., and Rondelez, F., **1982**, *Phys. Rev. Lett.*, 49, 1694-1697

Anderson, A.B., Darst, S.A., and Robertson, C.R., **1987**, in *"Proteins at interfaces: Physicochemical and biochemical studies"*, J.L. Brash and Th.A. Horbett, Editors, ACS Symposium series no. 343. ch. 20, 306-323

Andrade, J.D., **1985**, in *"Surface and interfacial aspects of biomedical polymers"*, J.D. Andrade, Editor, Vol. 2 *"Protein adsorption"*, Plenum Press, New York, Ch. 1, 1-80

Arai, T., and Norde, W., **1990a**, *Colloids and Surfaces*, 51, 1-16

Arai, T., and Norde, W., **1990b**, *Colloids and Surfaces*, 51, 17-28

Auserré, D., Hervet, H., and Rondelez, F., **1985**, *J. Physique Lett.*, 46, L929-L934

Axelrod, D., **1979**, *Biophys. J.*, 26, 557-573

Axelrod. D., Burghardt, T.P., and Thompson, N.L., **1984**, *Ann. Rev. Biophys. Bioeng.*, 13, 247-268

Beissinger, R.L., and Leonard, E.F., **1980**, *Amer. Soc. Artif. Organs*, 3, 160

Bevensee, R.M., **1983**, *"Maximum entropy solutions to scientific problems"*, Prentice-Hall Inc., New Jersey

Brash, J.L., and Lyman, D.J., **1969**, *J. Biomed. Mater. Res.*, 3, 175

Born, M., and Wolf, E., **1975**, *"Principles of optics"*, Pergamon, Oxford

Boxer, S.G., **1983**, *Biochim. Biophys. Acta*, 726, 265

Burghardt, T.P., and Axelrod, D., **1981**, *Biophys. J.*, 33, 455-468

Burghardt, T.P., and Axelrod, D., **1983**, *Biochemistry*, 22, 979-985

Burghardt, T.P., and Thompson, N.L., **1984**, *Biophys. J.*, 46, 729-737

Cantor, C.R., and Schimmel, P.R., **1980**, *"Biophysical chemistry"*, Part II, *"Techniques for the study of biological structure and function"*, W.H. Freeman and Co., San Francisco.

Carniglia, C.K., Mandel, C., and Drexgage, K.H., **1972**, *J. Opt. Soc. Am.*, 62, 479

Cate ten, J.M., Leach, S.A., and Arends, J., **1984**, in *"Proceedings of a workshop on bacterial adhesion to biosurfaces, with special emphasis on dental problems"*, Paterswolde, The Netherlands, IRL Press, Oxford

Caucheteux, I., Hervel, H., Jerome, R., and Rondelez, F., **1990**, *J. Chem. Soc., Faraday Trans.*, 86, 1369-1375

Cheng, Y.L., Lok, B.K., and Robertson C.R., **1985**, in *"Surface and interfacial aspects of biomedical polymers"*, J.D. Andrade, Editor, Vol. 2 "*Protein adsorption*", Plenum Press, New York, Ch. 3, 121-160

Cheng, Y.L., Darst, S.A., and Robertson, C.R., **1986**, *J. Colloid Interface Sci.*, 118, 212-223

Collison, M., and Bowden, E.F., **1992**, *Anal. Chem.*, 64, 1470-1476

Creighton, T.E., **1983**, *"Proteins. Structures and molecular properties"*, W.H. Freeman and Co., New York, 515 pp

Dabros, T., and Van de Ven, T.G.M., **1983**, *Colloid Polym. Sci.*, 26, 694-707

De Feyter, J.A., Benjamins, J., and Veer, F.A., **1978**, *Biopolymers*, 17, 1759-1772

Désormeaux, A., Rinquet, M., and Leblanc, R.M., **1991**, *J. Colloid Interface Sci.*, 147, 57-66

Dickerson, R.E., Takano, T., Eisenberg, D., Kallai, O.B., Samson, L., Cooper, A., and Margoliash, E., **1971**, *J. Biol. Chem.*, 246, 1511-1535

Dickerson, R.E., and Timkovich, R., **1975**, in *"The Enzymes"*, Vol XI, "Oxidation-reduction", part A., P.D. Boyer, Editor, Academic Press, New York, 397-547

Dijt, J.D., Cohen Stuart, M.A., Hofman, J.E., and Fleer, G.J., **1990**, *Colloids Surfaces*, 51, 141-158

Dijt, J.C., **1993**, Ph.D.-thesis *"Kinetics of polymer adsorption. Desorption and exchange."*, Wageningen Agricultural University, Wageningen, The Netherlands

Eddowes, M.J., and Hill, H.A.O., **1977**, *J. Chem. Soc. Chem. Comm.*, 771-772

Eddowes, M.J., Hill, H.A.O., and Uosaki, K., **1979**, *J. Am. Chem. Soc.*, 101, 7113-7114

Eddowes, M.J., Hill, H.A.O., and Uosaki, K., **1980**, *J. Electroanal. Chem.* 116, 527-537

Eisenberg, D., Weiss, R.M., Terwilliger, T.C., and Wilkox, W., **1982**, *Faraday Symp. Chem. Soc.*, 17, 109-120

Elgersma, A.V., **1990**, Ph.D.-thesis "*Competitive adsorption of albumin and monoclonal immuno γ-globulin molecules on polystyrene latices*", Wageningen Agricultural University, Wageningen, The Netherlands

Elgersma, A.V., Zsom, R.L.J., Lyklema, J., and Norde, W., **1991**, *Colloids Surfaces*, 65, 17-28

Elwing, H., Welin, S., Askendal, A., Nilsson, U., and Lundström, I., **1987a**, *J. Colloid Interface Sci.*, 119, 203-210

Elwing, H., Askendal, A., and Lundström, I., **1987b**, *J. Biomed. Mat. Res.*, 21, 1023-1028

Fendler, J.H., **1985**, *J. Phys. Chem.*, 89, 2730

Feynman, R.P., Leighton, R.B., and Sands, M., *"The Feynman Lectures on Physics"*, **1965**, Vol. 1, Addison-Wesley Publ. Co., Reading, Massachusetts

Fina, L.J., and Tung, Y., **1991**, *Appl. Spectrosc.*, 45, 986

Fisher, W.R., Taniuchi, H., and Anfinsen, C.B., **1973**, *J. Biol. Chem.*, 248, 3188-3195

Flatmark, T., and Robinson, A.B., **1968**, in *"Structure and function of cytochromes"*, Okumuki, K., Kamen, M.D., and Sekuru, I., Editors, University Park Press, Baltimore, 383-547

Fraaije, J.G.E.M., Kleijn, J.M., Van der Graaf, M., and Dijt, J.C., **1990**, *Biophys. J.*, 57, 965-975

Fraaije, J.G.E.M., Murris, R.M., Norde, W., and Lyklema, J., **1991a**, *Biophys. Chem.*, 40, 303-315

Fraaije, J.G.E.M., Norde, W., and Lyklema, J., **1991b**, *Biophys. Chem.*, 40, 317-327

Fraaije, J.G.E.M., Norde, W., and Lyklema, J., **1991c**, *Biophys. Chem.*, 41, 263-276

Giannelis, E.P., **1990**, *Chem. Mater.*, 2, 6, 627-629

Gingell, D., Heavens, O.S., and Mellor, J.S., **1987**, *J. Cell. Sci.*, 87, 677-693

Gölander, C.G., Lin, Y.S., Hlady, V., and Andrade, J.D., **1990**, *Colloids Surfaces*, 49, 289-302

Gouterman, M., and Stryer, L., **1962**, *J. Chem. Phys.*, 37, 2260-2260

Hallström, B., Lund, D.B., and Trägård, C., **1981**, in *"Proceedings international workshop on the fundamentals and applications of surface phenomena associated with fouling and cleaning in food processing"*, Tylösand, Sweden

Hansen, W.N., **1968**, *J. Opt. Soc. Amer.*, 58, 380-390

Harrick, N.J., **1965**, *J. Opt. Soc. Amer.*, 55, 851

Harrick, N.J., **1967**, *"Internal Reflection Spectroscopy"*, Inter Science Publishers, John Whiley and Sons, New York, 327 pp.

Harriman, A., and Porter, G., **1982**, *J. Chem. Soc. Faraday Trans.* 2, 78, 1937-1943

Hasegawa, M., and Kitano, H., **1992**, *Langmuir*, 8, 1582-1586

Hildebrandt, P., **1991**, *J. Mol. Struct.*, 242, 379-395

Hirschfeld, T., **1968**, *Can. J. Spectrosc.*, 10, 128

Hlady, V., Van Wagenen, R.A., and Andrade, J.D., **1985**, in *"Surface and interfacial aspects of biomedical polymers"*, J.D. Andrade, Editor, Vol. 2 *"Protein adsorption"*, Plenum Press, New York, Ch. 2, 81-120

Hlady, V., and Andrade, J.D., **1989**, *Colloids Surfaces*, 42, 85-96

Hofstra, U., **1988**, Ph.D. thesis *"Photoinduced electron transfer in model systems of photosynthesis"*, Wageningen Agricultural University, Wageningen, The Netherlands

Holde van, K.E., **1985**, *"Physical Biochemistry"*, 2nd edition, Prentice-Hall Inc., New Yersey

Janson, M., and Katz, J.J., **1979**, in *"The Porphyrins"*, D. Dolphin, Editor, *"Physical Chemistry"* Part B, Vol. IV, Academic Press, New York.

Kano, K., and Miyake, T., **1983**, *J. Chem. Soc. Japan*, 37, 1867

Kano, K., and Nakajima, T., **1987**, *J. Chem. Soc. Japan*, 60, 1281

Kayanasundaram, K., and Neumann-Spallart, M., **1982**, *J. Phys. Chem.*, 86, 5163-5169

Kayanasundaram, K., **1984**, *Inorg. Chem.*, 23, 2453 -2459

Kleijn, J.M., and Lyklema, J., **1987**, *Colloid Polymer Sci.*, 265, 1105-1113

Kondo, A., Oku, S., and Higashitani, K., **1991**, *J. Colloid Interface Sci.* 143, 214-221

Koppenol, W.H., and Margoliash, E., **1982**, *J. Biol. Chem.*, 257, 4426-4437

Kozarac, Z., Dhathathreyan, N., and Möbius, D., **1988**, *FEBS Letters*, 229, 372-376

Lakowicz, J.R., **1983**, *"Principles of fluorescence spectroscopy"*, Plenum Press, New York, 496 pp

Lea, A.S., Pungor, A., Hlady, V., Andrade, J.D., Herron, J.N., and Voss Jr., E.W., **1992**, *Langmuir*, 8, 68-73

Lee, R.G., and Kim, S.W., **1974**, *J. Biomed. Mater. Res*, 8, 251

Levine, Y.K., **1979**, *"The molecular physics of membrane systems"*, Lecture Notes, Utrecht State University, Utrecht, The Netherlands

Lok, B.K., Cheng, Y.L., and Robertson, C.R., **1983a**, *J. Colloid Interface Sci.*, 91, 87-103

Lok, B.K., Cheng, Y.L., and Robertson, C.R., **1983b**, *J. Colloid Interface Sci.*, 91, 104-116

Lundström, I., and Elwing, H., **1990**, *J. Colloid Interface Sci.*, 136, 1, 68-84

Margalit, R., and Vasquez, R.P., **1990**, *J. Protein Chem.*, 9, 1, 105-108

Margoliash, E., and Schetjer, A., **1966**, *Advan. Prot. Chem.*, 21, 113

Martínez, M.A., Herrero, J., and Gutiérrez, M.T., **1992**, *Sol. Energy Mater. Sol. Cells*, 26, 309-321

Maruyama, T., and Fukui, K., **1991a**, *J. Appl. Phys.*, 70, 7, 3848-3851

Maruyama, T., and Fukui, K., **1991b**, *Thin Solid Films*, 203, 297-302

Matsumura, H., and Kleijn, J.M., **1993**, *Colloids Surfaces B: Biointeractions*, 1, 277-282

Mirabella, F.M., **1993**, *"Internal Reflection Spectroscopy", "Practical Spectroscopy Series"*, Vol. 15, Marcel Dekker Inc., New York, 374 pp

Morrissey, B.W., Smith, L.E., Stromberg, R.R., and Fenstermaker, C.A., **1976**, *J. Colloid Interface Sci.*, 56, 557-563

Mulvihill, J.N., Cazenave, J.P., Schmitt, A., Maisonneuve, P., and Pusineri, C., **1985**, *Colloids Surfaces*, 14, 317-324

Newton, I., **1717**, "*Opticks*", Dover Publications, New York, 1952, 2nd (English) ed.; Book III, part 1, query 29

Norde, W., **1985**, in *"Surface and interfacial aspects of biomedical polymers"*, J.D. Andrade, Editor, Vol. 2 "*Protein adsorption*", Plenum Press, New York, Ch. 8, 263-294

Norde, W., **1986**, *Adv. Colloid Interface Sci.*, 25, 267-340

Norde, W., MacRitchie, F., Nowicka, G., and Lyklema, J., **1986**, *J. Colloid Interface Sci.*, 112, 447-456

Norde, W., and Rouwendal, E., **1990**, *J. Colloid Interface Sci.*, 139, 169-176

Norde, W., Arai, T., and Shirahama, H., **1991**, *Biofouling*, 4, 37-51

Norde, W., and Lyklema, J., **1991**, *J. Biomater. Sci. Polymer Edn.*, 2, 183-202

Norde, W., **1992**, *Clinical Materials*, 11, 85-91

Norde, W., and Favier, J.P., **1992**, *Colloids Surfaces*, 64, 87-93

Norde,W., and Anusiem, A.C.I., **1992**, *Colloids Surfaces*, 66, 73-80

Pachence, J.M., Amador, S., Maniara, G., Vanderkooi, J.M., Dutton, P.L., and Blasie, J.K., **1990**, *Biophys. J.*, 58, 379-389

Peters, F., **1985**, *Adv. Protein Chem.*, 37, 161-245

Privalov, P.L., **1976**, *Pure Appl. Chem.*, 47, 293-304

Privalov, P.L., **1979**, *Adv. Protein Chem.*, 33, 167-241

Ramachandran, G.N., and Sasisekharan, V., **1968**, *Adv. Protein Chem.*, 23, 283

Ray, S., Banerjee, R., Basu, N., Batabyal, A.K., and Barua, A.K., **1983**, *J. Appl. Phys.*, 54, 3497

Rechnitz, G.A., **1988**, *Chem. Eng. News*, 24

Reichert, W.M., Suci, P.A., Ives, J.T., and Andrade, J.D., **1987**, *Appl. Spectrosc.*, 41, 503-508

Reipa, V., Gaigalas, A., and Abramowitz, S., **1993**, *J. Electroanal. Chem.*, 348, 413-428

Reynauld, J.A., Tavernier, I., Yu, L.T., and Cochet, J.M., **1986**, *Bioelectrochem. Bioenerg.*, 15, 103-112

Sagara, T., Niwa, K., Sone, A., Hinnen, C., and Nikki, K., **1990**, *Langmuir*, 6, 254

Schrijvers, R., van Dijk, M., Sanders, G.M., and Sudhölter, E.J.R., **1994**, submitted to Recueil

Sedlácek, B., Overberger, C.G., and Mark, H.F., **1979**, *J. Polymer Sci., Polymer Symposia*, No. 66

Shigesato, Y., Takaki, S., and Haranoh, T., **1991**, *Appl. Surface Sci.*, 48/49, 269-275

Shigesato, Y., Takaki, S., and Haranoh, T., **1992**, *J. Appl. Phys.*, 71, 7, 3356-3364

Shirahama, H., Lyklema, J., and Norde, W., **1990**, *J. Colloid Interface Sci.*, 139, 177-187

Sober, H.A., Editor, **1968**, "*Handbook of biochemistry. Selected data for molecular biology*", The Chemical Rubber Co., Cleveland, OH, USA, C-100

Suto, S., Uchida, W., Yashima, M., and Goto, T., **1987**, *Phys. Rev. B*, 35, 4393-4397

Suto, S., Uchida, W., Yashima, M., and Goto, T., **1988**, *Surface Sci.*, 205, 230-240

Suto, S., Ikehara, T., Koike, A., Uchida, W., and Goto, T., **1990**, *Solid State Commun.* , 73, 331-334

Tadros, Th.F., and Lyklema, J., **1968**, *J. Electroanal. Chem.*, 17, 267-275

Takano, T., Kallai, O.B., Swanson, R., and Dickerson, R.E., **1973**, *J. Biol. Chem.*, 248, 5234-5255

Takano, T., and Dickerson, R.E., **1981**, *J. Mol. Biol.*, 153, 95-115

Tanford, C., **1961**, *"Physical Chemistry of Macromolecules"*, John Wiley & Sons, New York, 710 pp

Taniguchi, I., and Spiro, T.G., *1986, J. Phys. Chem.*, 89, 5165

Timkovich, R., **1979**, in *"The Porphyrins"*, D. Dolphin, Editor, "*Physical Chemistry*" Part B, Vol. IV, Academic Press, New York, 241-294

Thompson, N.L., Burghardt, T.P., and Axelrod, D., **1981**, *Biophys. J.*, 33, 435-454

Thompson, N.L., McConnell, H.M., and Burghardt, T.P., **1984**, *Biophys. J.*, 46, 739-747

Thompson, N.L., and Burghardt, T.P., **1986**, *Biophys. Chem.*, 25, 91-97

Tweet, A.G., Gaines, G.L., and Bellamy, W.D., **1964**, *J. Chem. Phys.*, 40, 2596

Valdes, L.B., **1954**, *Proc. of the IRE.*, 104, 420

Vanderkooi, J.M., and Erecinska, M., **1975**, *Eur. J. Biochem.*, 60, 199-207

Vanderkooi, J.M., Adar, F., and Erecinska, M., **1976**, *Eur. J. Biochem.* 64, 381-387

Van Wagenen, R.A., Rockhold, S., and Andrade, J.D., **1982**, *Adv. Chem. Ser.*, 199, 351-370

Vasquez, R.P., and Margalit, R., **1990**, *Thin Solid Films*, 192, 173-180

Vos, K., Laane, C., Weyers, S.R., van Hoek, A., Veeger, C., and Visser, A.J.W.G., **1987**, *Eur. J. Biochem.*, 169, 259-268

Vroman, L., and Adams, A.L., **1969**, *Surface Sci.*, 16, 438-446

Vroman, L., and Leonard, E.F., **1991**, *Biofouling*, 4, 81

Ward, A.F.H., and Tordai, L., **1946**, *J. Chem. Phys.*, 14, 453-461

Watkins, R.W., and Robertson, C.R., **1977**, *J. Biomed. Mater. Res.*, 11, 915-938

Wei, A.P., **1991**, M.Sc.-thesis *"Surface tension kinetics of model proteins in relation to their structural properties"*, Department of Bioengineering, University of Utah, Salt Lake City, USA

Willit, J.L., and Bowden, E.F., **1990**, *J. Phys. Chem.*, 94, 8241-8246

White, D.J., **1991**, *Biofouling*, 4, 209

Willems, G.M., Hermans, W.Th., and Hemker, H.C., **1991**, *J. Biomaterials Sci.*, 2, 217

Wüthrich, K., **1986**, *"NMR of Proteins and Nucleic Acids"*, John Wiley & Sons, New York

Yamasaki, Y., Ueda, N., Nao, K., Sekiga, M., Kawamori, R., Shichiri, M., and Takenobu, K., **1989**, *Clin. Chim. Acta*, 180, 93-98

Yanagi, H., Ashida, M., Harima, Y., and Yamashita, K., **1990**, *Chem. Lett.*, 385-388

Samenvatting

Dit proefschrift behandelt de adsorptie van eiwitten aan vaste oppervlakken. Met name wordt aandacht besteed aan de oriëntatie van de geadsorbeerde eiwitmoleculen en de invloed van electrisch aangelegde velden op deze oriëntatie en op het adsorptieproces.

Adsorptie (hechting) van eiwitten is niets anders dan de ophoping van opgeloste eiwitmoleculen aan een oppervlak. Het is een verschijnsel dat op uitgebreide schaal voorkomt, zowel in de natuur als in kunstmatige systemen. In veel medische en technische toepassingen heeft de wisselwerking tussen een eiwit en een oppervlak grote gevolgen, die in sommige gevallen gewenst en in andere gevallen ongewenst zijn. Geadsorbeerde eiwitten worden bijvoorbeeld vaak gebruikt als stabilisatoren in farmaceutische en voedselprodukten. Ook in diagnostische testen, biosensoren en enzym-electroden wordt gebruik gemaakt van eiwitten die geadsorbeerd zijn aan oppervlakken. Aan de andere kant begint het ongewenste proces van vervuiling van apparatuur, bijvoorbeeld in de voedselverwerkende industrie, en van synthetische implantaten vaak met de adsorptie van eiwitten. Vervolgens kunnen bacterien zich op de eiwitlaag hechten. Een dergelijk proces ligt ook ten grondslag aan tandsteenvorming en aan het ontstaan van bloedstolsels aan implantaten.

Bij de hechting van eiwitten aan oppervlakken spelen vele factoren een rol. De drie belangrijkste zijn wel electrostatische en hydrofobe wisselwerkingen tussen eiwit en oppervlak en de structuurstabiliteit van het eiwit.

Electrostatische wisselwerkingen zijn het gevolg van de aanwezigheid van lading op het eiwit en op het oppervlak. De lading van een eiwitmolecuul wordt veroorzaakt door ionisatie van zwak zure en zwak basische zijgroepen van de aminozuren waaruit het eiwitmolecuul bestaat. Deze groepen zitten vooral aan de buitenkant van het eiwitmolecuul. Afhankelijk van de pH (zuurgraad) van de oplossing waarin het eiwit zich bevindt, zal het netto positief, negatief of ongeladen zijn. Een ongelijke verdeling van positief en negatief geladen groepen over het eiwitmolecuul kan een dipoolmoment tot gevolg hebben, dat ook een rol bij de adsorptie kan spelen. In het algemeen zal het oppervlak ook een lading dragen, afhankelijk van het materiaal waaruit het bestaat. Bij metalen of metaaloxiden ontstaan door contact met water OH-groepen op het oppervlak die een proton kunnen opnemen of

afstaan; de netto lading van dit type oppervlakken is dus ook afhankelijk van de pH. Het zal duidelijk zijn dat een positief geladen eiwitmolecuul eerder geneigd is te adsorberen aan een negatief dan aan een positief geladen oppervlak.

De factor hydrofobociteit (de mate waarin een molecuul waterminnend is) vindt zijn oorsprong in de bijzondere eigenschappen van water. Watermoleculen in de oplossing kunnen naar alle kanten waterstofbruggen vormen met andere watermoleculen. Ze kunnen daardoor gemakkelijk roteren. Met een apolaire stof zijn dergelijke interacties niet mogelijk, zodat watermoleculen in de buurt van een apolair molecuul een deel van hun rotatiemogelijkheden gaan missen, d.w.z. entropie verliezen. Een eiwit bestaat uit aminozuren met apolaire (hydrofoob = waterafstotend) en polaire (hydrofiel = waterminnend) zijgroepen. In een waterige oplossing zitten de waterafstotende aminozuren zoveel mogelijk bij elkaar in het binnenste van het eiwitmolecuul, waardoor het contact met water minimaal is. Deze zg. hydrofobe binding heeft een compacte, vaak bolvormige structuur van het eiwit tot gevolg. Wanneer er een hydrofoob oppervlak aanwezig is, zal het eiwit geneigd zijn om daaraan te adsorberen. Er treedt dan immers dehydratie op van zowel het oppervlak als van gedeelten van het eiwit. Entropietoename van het water dat hierbij vrijkomt, is dan een drijvende kracht voor adsorptie.

De derde factor, de structuurstabiliteit van het eiwit, wordt bepaald door wisselwerkingen binnen het eiwitmolecuul én wisselwerkingen van het molecuul met zijn omgeving (hydrofobe en electrostatische wisselwerkingen, H-bruggen, Van der Waalskrachten, S-bruggen). De stabiliteit van de natuurlijke (natieve) structuur van een eiwit is vaak thermodynamisch gezien marginaal, d.w.z. dat deze door kleine uitwendige invloeden verstoord kan worden. Het is daarom niet verwonderlijk dat het overbrengen van een eiwit vanuit een oplossing naar een grensvlak een conformatieverandering tot gevolg kan hebben. Hierbij neemt in het algemeen de entropie van het eiwitmolecuul toe (de gedeeltelijke afname van de compacte structuur leidt tot meer conformatie-mogelijkheden).

Een combinatie van deze factoren bepaalt vervolgens of een eiwit wel of niet adsorbeert. Norde en Arai [1991] formuleerden de volgende algemene regels:

☆ Eiwitten met een grote stabiliteit van de natieve structuur gedragen zich als "harde" deeltjes. Hun adsorptiegedrag wordt beheerst door hydrofobe en electrostatische wisselwerkingen met het oppervlak. Ze

adsorberen niet op hydrofiele oppervlakken, tenzij ze electrostatische attractie ondervinden.

☆ Bij eiwitten met een relatief lage interne samenhang speelt een extra factor mee die adsorptie bevordert. Deze hangt samen met structuuraanpassingen in het molecuul waarbij de conformatie-entropie toeneemt. Het gevolg is dat deze "zachte" eiwitten adsorberen aan alle typen oppervlakken, ongeacht de lading.

De adsorptie van eiwitten aan oppervlakken speelt een belangrijke rol bij de ontwikkeling van biosensoren. Een biosensor is een sensor waarmee de concentratie van een specifieke (biologische) stof in aanwezigheid van andere stoffen selectief kan worden bepaald, waarbij de sensor moet kunnen werken onder biologische omstandigheden. In onderstaande figuur is een zeer algemeen model van een biosensor weergegeven.

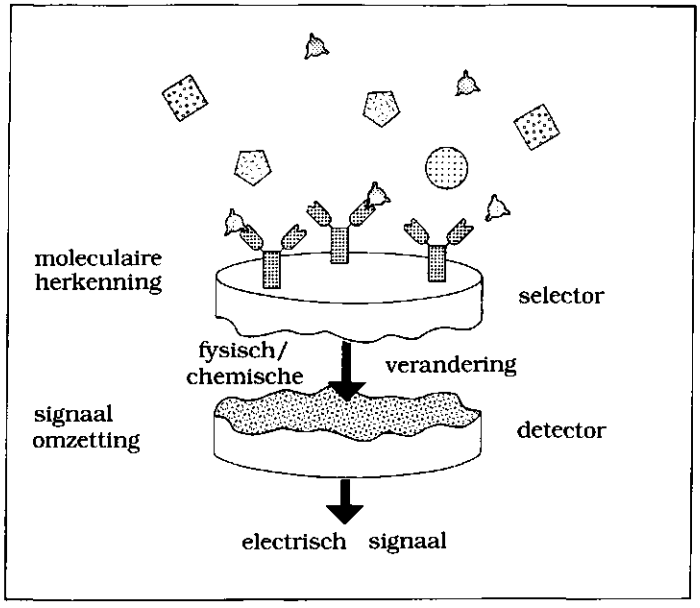

Figuur s1. *Een biosensor bestaat uit een (biologische) selector direct gekoppeld aan een detector.*

De selector bepaalt welke stof er gemeten wordt. Door binding van die stof aan de selector verandert er lokaal een bepaalde fysische parameter, bijvoorbeeld de brekingsindex of de lading. Deze verandering wordt gemeten

door de detector en omgezet in een electrisch signaal. Als selector worden vaak eiwitmoleculen gebonden aan een grensvlak gekozen; met name enzymen of antilichamen, waarmee selectief het betreffende substraat resp. de antistof kan worden gedetecteerd. Wanneer eiwitten niet als selector-moleculen worden gebruikt, kan adsorptie van eiwitten toch een rol spelen bij het functioneren van de sensor: de te detecteren stof zelf kan een eiwit zijn, of ongewenste adsorptie van eiwitten, die altijd aanwezig zijn in biologische monsters (bijv. bloed), kan de sensor vervuilen en daardoor de effectiviteit verminderen.

Een belangrijk aspect bij de adsorptie van eiwitten aan biosensoren is de oriëntatie van de geadsorbeerde eiwitmoleculen. Deze oriëntatie bepaalt voor een groot gedeelte de selectiviteit en effectiviteit van biosensoren. Men kan zich voorstellen dat aan een enzym dat met zijn actieve kant aan het oppervlak gebonden is geen substraat gebonden kan worden, zodat er geen enzymatische reactie zal plaatsvinden. Als de actieve kant naar de oplossing gericht is, kan er wel een reactie of herkenning van andere moleculen plaatsvinden.

De doelstelling van dit promotieonderzoek is nu het ontwikkelen van een methode om de oriëntatie van geadsorbeerde (eiwit)moleculen te bepalen. Daarnaast wordt nagegaan of het adsorptiegedrag van eiwitten, inclusief de oriëntatie in de geadsorbeerde toestand, te beïnvloeden is door een electrische potentiaal op het adsorbensoppervlak aan te brengen.

In dit promotieonderzoek hebben we gebruik gemaakt van een moderne techniek, bekend als totale interne reflectie fluorescentie, afgekort als TIRF. Het principe van deze optische techniek is als volgt. Wanneer men een lichtbundel door een kwartsprisma laat vallen op een kwarts/water grensvlak, wordt het licht volledig gereflecteerd als de hoek van inval groter is dan een bepaalde grenshoek (ca. 66°). Door interferentie van de invallende en teruggekaatste lichtstraal in het kwarts ontstaat er een electromagnetische golf, die een beetje "doorlekt" in het water. De amplitude van deze golf neemt aan de waterzijde van het grensvlak exponentiëel af. Deze "doorlekkende" golf wordt "evanescent wave" oftewel "verdwijnende" golf genoemd. Met TIRF wordt nu de fluorescentie gemeten van moleculen die zich in het water bevinden en zó dicht bij het grensvlak zijn (binnen 100 nanometer, d.w.z. één tiende van een miljoenste meter) dat ze door deze evanescent wave worden aangeslagen. Vooral moleculen die aan het kwarts geadsorbeerd zijn zullen bijdragen aan het fluorescentie-signaal. De meeste

eiwitten fluoresceren van nature, doordat ze de fluorescerende aminozuren tryptofaan en tyrosine bevatten. Deze moeten in het UV-licht worden aangeslagen. Het is ook mogelijk om een fluorescerende groep die met zichtbaar licht kan worden aangeslagen, aan eiwitmoleculen te hangen ("merken" of "labelen"). Het voordeel hiervan is dat de experimentele opstelling aan lagere eisen hoeft te voldoen, maar een nadeel is dat we niet weten wat voor invloed het label op het eiwit heeft; het kan de structuur en het adsorptiegedrag van het eiwit veranderen. In het onderzoek gepresenteerd in dit proefschrift is deze manier van merken daarom vermeden. Dit is bereikt door te werken met cytochroom *c*, waarvan de haemgroep fluorescent is gemaakt door er het centrale ijzeratoom uit te halen. Wil men uit de oriëntatie van de fluorescente groep conclusies trekken over de oriëntatie van het hele eiwit, dan is het noodzakelijk te weten hoe die groep in het eiwitmolecuul zit. Bovendien moet het eiwit natuurlijk zijn structuur niet veranderen bij adsorptie. Cytochroom *c* voldoet aan beide voorwaarden. Een bijkomende interessante eigenschap van cytochroom *c* is dat het een groot electrisch dipoolmoment heeft, waardoor de oriëntatie te beïnvloeden zou kunnen zijn door een electrische potentiaal op het oppervlak aan te leggen, hetgeen biologisch zeer interessant is.

Om de oriëntatie van geadsorbeerde moleculen te bepalen met behulp van TIRF was het nodig om de bestaande theorie uit te breiden. Uitgangspunt van deze theorie, die beschreven staat in hoofdstuk 2, is dat bij verandering van de polarisatie van het licht, het fluorescentie-signaal ook verandert op een manier die afhangt van de oriëntatie van de geadsorbeerde moleculen. Uit de theorie blijkt dat naast de intensiteit van het fluorescentie-licht, ook de polarisatie hiervan gemeten moet worden. Uit vier onafhankelijke fluorescentie-metingen worden vervolgens twee ordeparameters numeriek berekend. Met deze twee ordeparameters kan, met behulp van de zg. Maximum Entropie Methode, de meest waarschijnlijke en breedste oriëntatie-verdeling van de geadsorbeerde moleculen gereconstrueerd worden. Verder blijkt uit de theorie dat beweging van de geadsorbeerde moleculen op een tijdschaal veel sneller dan de fluorescentie levensduur (voor cytochroom *c* is dat 5 nanoseconden, d.w.z. 5 duizendsten van een miljoenste seconde), resulteert in het verlies van de polarisatie van het fluorescentie-licht.

Om de methode ter bepaling van de oriëntatie van geadsorbeerde moleculen te testen, zijn er metingen met tetramethypyridiniumporfyrine, afgekort als H_2TMPyP, uitgevoerd. Deze worden beschreven in hoofdstuk 4.

H_2TMPyP heeft dezelfde structuur en fluorescentie-eigenschappen als de haemgroep in het cytochroom *c* molecuul. Uit het adsorptiegedrag aan silica (glas) blijkt dat de geadsorbeerde hoeveelheden verschillen bij adsorptie vanuit water, fosfaatbuffer pH 7 en een zoutoplossing, terwijl desondanks de kinetiek van adsorptie gelijk is. Uit de oriëntatiemetingen blijkt dat de ontwikkelde methode werkt. Vanuit een oplossing met een lage concentratie (1 mg/l) blijken de moleculen in een tamelijk willekeurige oriëntatie te adsorberen, oftewel ze hebben geen bepaalde voorkeursoriëntatie. Echter, vanuit oplossingen met hogere concentraties (10 of 100 mg/l) adsorberen de moleculen wel in een voorkeursoriëntatie, namelijk met een hoek van 46° tussen het vlak van het molecuul en het oppervlak. Echter de verdeling rond deze hoek is vrij breed. De gevonden oriëntatieverdelingen blijken onafhankelijk van de pH te zijn. Experimenten met verschillende viscositeiten van de oplossing en het feit dat de fluorescentie gepolariseerd blijft, tonen aan dat de rotatiebeweging van de geadsorbeerde moleculen plaatsvindt op een tijdsschaal die veel langzamer is dan de fluorescentie-levensduur.

Om de invloed van de electrische potentiaal van het adsorptie-oppervlak op de oriëntatie van geadsorbeerde moleculen en op het adsorptiegedrag te bestuderen, hebben we gebruik gemaakt van een halfgeleideroppervlak. Deze halfgeleider is indium-tinoxide (ITO). Deze is in een zeer dunne laag (120 nanometer) aangebracht op glas of silicium als ondergrond. Via het ITO laagje is het mogelijk een potentiaal op het grensvlak aan te brengen om zo de electrostatische interacties te kunnen bestuderen. De ITO laagjes zijn gekarakteriseerd door middel van stromingspotentiaalmetingen, scanning electron microscopy, atomic force microscopy en door weerstandsmetingen, waarvan de resultaten beschreven staan in hoofdstuk 3. In dat hoofdstuk staan ook de experimentele technieken TIRF en reflectometrie beschreven die in dit promotieonderzoek gebruikt zijn.

Het adsorptiegedrag van verschillende eiwitten (zowel "harde" als "zachte") als functie van de extern aangelegde potentiaal staat beschreven in hoofdstuk 5. Deze resultaten zijn verkregen met behulp van reflectometrie. In een reflectometer wordt een linear gepolariseerde lichtbundel na reflectie op het (adsorberende) oppervlak gesplitst in zijn parallel en loodrecht gepolariseerde componenten. De intensiteitsverhouding tussen deze twee componenten wordt continu gemeten. Uit de verandering van deze verhouding door adsorptie kan na ijking de geadsorbeerde hoeveelheid

(massa/oppervlak) worden verkregen. Bij adsorptie zonder een aangelegde potentiaal, suggereren de resultaten dat electrostatische wisselwerkingen een belangrijke rol spelen in de adsorptie van structuur-stabiele eiwitten aan hydrofiele oppervlakken. Echter, het adsorptiegedrag van alle bestudeerde eiwitten wordt nauwelijks beïnvloed door de aangelegde potentiaal, onafhankelijk van hun structuurstabiliteit. Blijkbaar worden er, naast het veranderen van de electrostatische wisselwerkingen, ook andere eigenschappen van het bestudeerde systeem gevarieerd: bij variatie van de pH bijvoorbeeld ook de stuctuurstabiliteit en de netto lading van de eiwitten, bij variatie van de potentiaal de hydrofiliciteit van het oppervlak. Verder kunnen eiwitten hun lading aanpassen al naar gelang de lading of potentiaal van het oppervlak. Het is daarom moeilijk om hierover definitieve conclusies te trekken. Waarschijnlijk zijn in het verleden de resultaten van eiwitadsorptie als functie van de pH op een te simpele manier verklaard, waarbij de rol van de electrostatische interacties is overschat.

In hoofdstuk 6 staan de experimenten beschreven die met de natieve en de vrije-base vorm (ijzeratoom verwijderd) van cytochroom *c* zijn uitgevoerd. Via depletiemetingen en reflectometrie is het adsorptiegedrag van beide vormen bestudeerd. Hieruit is geconcludeerd dat de natieve vorm zich gedraagt als een structuurstabiel eiwit. De vrije-base vorm gedraagt zich in veel opzichten identiek aan de natieve vorm, echter de geadsorbeerde hoeveelheden bij pH 7 en 10 zijn veel hoger. Beide vormen vertonen hetzelfde gedrag waneer een potentiaal op het oppervlak wordt aangelegd: de invloed op het adsorptiegedrag is minimaal en vergelijkbaar met de invloed op het adsorptiegedrag van de structuurstabiele eiwitten lysozym en ribonuclease. Wat betreft de oriëntatiemetingen kan opgemerkt worden dat de resultaten niet in termen van oriëntatie-verdelingen te interpreteren waren. Dit komt door een te grote spreiding in de meetresultaten. Belangrijkste oorzaak daarvoor is de slechte signaal/ruis verhouding, waardoor de ordeparameters slecht te bepalen zijn. Wel blijkt uit de metingen dat de oriëntatie van vrije-base cytochroom c niet afhangt van de oppervlakte-bezetting en niet beïnvloed wordt door de potentiaal van het grensvlak. Het is moeilijk om de signaal/ruis verhouding te verbeteren, omdat bij hoge lichtintensiteiten of langer meten denaturatie van vrije-base cytochroom *c* aan het grensvlak op kan treden. Dit uit zich in veranderingen in het fluorescentiespectrum.

Samengevat blijkt uit dit promotieonderzoek dat de techniek TIRF geschikt is voor het uitvoeren van oriëntatiemetingen. Bovendien blijkt dat de adsorptie van eiwitten niet of nauwelijks te beïnvloeden is door een electrische potentiaal aan te leggen op het grensvlak. De ontwikkelde methode ter bepaling van de oriëntatie van geadsorbeerde moleculen is alleen toepasbaar op structuurstabiele, fluorescente (eiwit)moleculen, echter door het gebruik van labels en/of ultraviolet licht kunnen ook andere (eiwit)moleculen worden bestudeerd. In de toekomst zal deze methode worden gebruikt bij onderzoek naar structuurveranderingen en de doorlaatbaarheid van fosfolipide dubbellagen die model staan voor biologische membranen. Daarnaast wordt de methode gebruikt voor onderzoek naar de oriëntatie van verschillende porfyrines aan vaste oppervlakken. Deze porfyrines worden o.a. toegepast in de ontwikkeling van een speciaal type zonnecellen.

Curriculum Vitae

Martin Anton Bos werd op 18 maart 1965 geboren te Oldenzaal. In 1983 behaalde hij het Atheneum-B diploma aan het Thijcollege te Oldenzaal. Na een jaar Chemische Technologie te hebben gestudeerd aan de Technische Hoge School Twente begon hij in 1984 aan zijn studie Moleculaire Wetenschappen aan de Landbouwhogeschool Wageningen. In juni 1989 studeerde hij af in de fysisch-chemische oriëntatie als Moleculair Wetenschapper. De doctoraalstudie omvatte een afstudeervak Moleculaire Fysica, alsmede een praktijktijd die aan de Eidgenossische Technische Hochschule te Zürich werd doorgebracht. Van juni 1989 tot oktober 1993 werd het in dit proefschrift beschreven onderzoek uitgevoerd bij de vakgroep Fysische en Kolloïdchemie van de Landbouwuniversiteit Wageningen.